LETTER Communicated by Guillermo Cecchi

Effects of Multiplicative Power Law Neural Noise in Visual Information Processing

José M. Medina
jmanuel@fisica.uminho.pt
Center for Physics. University of Minho, Braga 4710–057, Portugal

The human visual system is intrinsically noisy. The benefits of internal noise as part of visual code are controversial. Here the information-theoretic properties of multiplicative (i.e. signal-dependent) neural noise are investigated. A quasi-linear communication channel model is presented. The model shows that multiplicative power law neural noise promotes the minimum information transfer after efficient coding. It is demonstrated that Weber's law and the human contrast sensitivity function arise on the basis of minimum transfer of information and power law neural noise. The implications of minimum information transfer in self-organized neural networks and weakly coupled neurons are discussed.

1 Introduction

Random fluctuations over time are a fundamental aspect of human vision as in other sensory systems. Examples can be found in photoreceptor transduction (Faisal, Selen, & Wolpert, 2008; Lamb, 1987; Torre, Ashmore, Lamb, & Menini, 1995), synaptic communication (Anderson, Lampl, Gillespie, & Ferster, 2000; Faisal et al., 2008, Moss, Ward, & Sannita, 2004), and visual-motor tasks (Gilden, 2001; Gilden, Thornton, & Mallon, 1995; Kello, Beltz, Holden, & Van Orden, 2007; Ward, 2002). Previous studies have shown that the visual system has exploited, in part, the inherent generated noise to its own benefit. Typical examples are the influence of internal noise in stochastic resonance (Aihara, Kitajo, Nozaki, & Yamamoto, 2008; Ward, 2004) and the role of membrane potential noise to maintain orientation selectivity in the primary visual cortex (Anderson et al., 2000; Finn, Priebe, & Ferster, 2007).

One means of classification of neural noise is on the basis of the external input signals. At least two different categories can be considered. The first is the standard additive noise. Additive noise is constant regardless of any external signal and is often uncorrelated. In this case, the signal-to-noise ratio (SNR) decreases as the signal strength decreases. The second is multiplicative noise and is a function of the mean signal strength (Coffey, Kalmykov, & Waldron, 2004; Fienberg, 1974; Harris & Wolpert, 1998; Legge, Kersten, & Burgess, 1987; Sperling, 1989). A large body of experimental data has concluded that the response variability of neurons increases with

the mean firing rate (Anzai, Bearse, Freeman, & Cai, 1995; Carandini, 2004; Dean, 1981; Geisler & Albrecht, 1995; Holt, Softky, Koch, & Douglas, 1996; Kasamatsu, Polat, Pettet, & Norcia, 2001; Lennie, 1981; Tolhurst, Movshon, & Dean, 1983; Vogels, Spileers, & Orban, 1989). Neural variability is also a function of stimulus strength such as the average light intensity or contrast (Cecchi et al., 2000; Finn et al., 2007; Geisler & Albrecht, 1995; Harris & Wolpert, 1998; Lennie, 1981; Stocker & Simoncelli, 2006; Tolhurst et al., 1983; Uzzell & Chichilnisky, 2004; Victor, Blessing, Forte, Buzas, & Martin, 2007). These findings are referred to as multiplicative neural noise and arise, at least in part, as a consequence of cortical activity (Carandini, 2004; Geisler & Albrecht, 1995; Kasamatsu et al., 2001; Ricciardi & Lansky, 2002).

A long-standing issue concerns the benefits of multiplicative neural noise in sensory processing. Multiplicative neural noise can carry information on the structure of the incoming signals and is often correlated. It is associated with nonlinear phenomena (Basalyga & Salinas, 2006; Fienberg, 1974; Lindner, Garcia-Ojalvo, Neiman, & Schimansky-Geier, 2004; Ricciardi & Lansky, 2002; Schieve, Bulsara, & Davis, 1991) and can maintain the SNR as the signal strength decreases. Multiplicative neural noise is important to control arm and saccadic eye movements (Harris & Wolpert, 1998), and to promote factorial codes (Gottschalk, Sexton, & Roschke, 2004). Computational models have examined the functional role of multiplicative neural noise in excitable and adaptive systems (Basalyga & Salinas, 2006; Buice & Cowan, 2009; Lindner et al., 2004; Ricciardi & Lansky, 2002; Schieve et al., 1991). In psychophysics, early models of visual performance did not consider multiplicative neural noise (Burgess, Wagner, Jennings, & Barlow, 1981; Hornstein, Pope, & Cohn, 1999; Legge et al., 1987; Pelli, 1985, 1990; Pelli & Farell, 1999; Rovamo, Kankaanpää, & Hukkonen, 1999; Sperling, 1989). Subsequent works, however (Kontsevich, Chen, & Tyler, 2002; Lu & Dosher, 1999; Meese, Challinor, & Summers, 2008; Tyler & Chen, 2000; Ward & Kitajo, 2005), have formally supported it.

Relatively little attention has been focused on multiplicative neural noise and the transmission of information. There are two possible strategies for maintaining the neural SNR. The first is to enhance signal power, increasing neural responses and thus demanding a significant amount of energy. The second is to reduce noise power, modulating response variability and concentrating energy resources. The existence of multiplicative neural noise could provide an empirical justification of the latter as part of an efficient internal code. The principle of efficient coding was initially formulated within the context of stimulus redundancy (Attneave, 1954; Barlow, 1961; Simoncelli & Olshausen, 2001) and has been generalized to other sensory neurons and their functions by maximizing information transmission (usually called Infomax) (Bialek, Scalettar, & Zee, 1989; Linsker, 1988, 1990, 1992, 1997; van Hateren, 1992; Zhaoping, 2006). In all Infomax procedures, Shannon's mutual information is maximized between a generic input (e.g., a stimulus) and the output (e.g., spike trains), in the

presence of neural noise. Infomax analysis has explained the receptive field properties of neurons in the primary visual cortex (Bell & Sejnowski, 1997; Olshausen & Field, 1996), and contrast-gain control mechanisms (Gottschalk, 2002; Laughlin, 1981). It also has been applied to many visual tasks, from motion detection (Lewen, Bialek, & de Ruyter van Steveninck, 2001; Strong, Koberle, de Ruyter van Steveninck, & Bialek, 1998), through visual discrimination (Bialek et al., 1989), to visual adaptation (Brenner, Bialek, & de Ruyter van Steveninck, 2000; Wainwright, 1999). However, the successful application of Infomax rules for early vision does not imply that neurons should follow the same procedure at the large scale of integration. It is less clear if Infomax can make testable predictions in the empirical laws of visual psychophysics and most cognitive tasks (Linsker, 1990; Zhaoping, 2002). Indeed, the use of Shannon's information theory assumes the existence of linear gaussian channels, an analysis that is mainly restricted to photoreceptors and retinal neurons (Borst & Theunissen, 1999; Cecchi et al., 2000; Laughlin, de Ruyter van Steveninck, & Anderson, 1998; de Ruyter van Steveninck & Laughlin, 1996). Based on the idea of optimization as an organizing principle, alternative approaches have been proposed. In neurophysiology, the principles of maximum entropy production (Jaynes, 1957; Yeh et al., 2010) and minimum mutual information (Globerson, Stark, Vaadiab, & Tishby, 2009) have been applied in the study of the spatial and temporal correlations from multielectrode data. In perception, Friston, Kilner, and Harrison (2006) have presented an information-theoretic measure of the free energy in the brain. This framework optimizes the free energy and has generalized the principle of efficient coding among others (Friston, 2010). Norwich has proposed a measurement of the internal uncertainty or information entropy in sensory systems (Norwich, 1977, 1981, 1982, 1993). The theory uses the methods of Boltzmann in statistical physics and claims that the optimization of the internal uncertainty as a function of time is important. The time evolution of perception is determined by the time evolution of this information entropy (Norwich, 1993).

Optimal information processing in visual psychophysics is part of a process that can be mediated by at least three mechanisms: oscillatory neural synchronization, self-organized criticality (SOC), and Bayesian decision theory. Oscillatory neural synchronization is a cooperative or binding mechanism that coordinates spike discharges between neurons (Singer, 1999). Among the factors that affect oscillatory neural synchronization, neural noise can induce and enhance synchrony (Ermentrout, Galán, & Urban, 2008; Lindner et al., 2004). SOC (Bak, 1996; Bak, Tang, & Wiesenfeld, 1987, 1988), is a popular theory in physics that has been applied to many dissipative systems out of thermodynamic equilibrium. In general, systems at SOC are in transition between stable states or phases. Phase transitions are often characterized by intrinsic perturbations of all sizes in the form of avalanches. In neural networks organized at SOC, the response of a single neuron to some external signal may induce responses in many neurons, generating neural activity in cascade. This neural activity often follows

characteristic power law distributions and may lead to optimal dynamic range and long-range correlations in space and time (Bak, 1996; Beggs, 2008; Kinouchi & Copelli, 2006; Kitzbichler, Smith, Christensen, & Bullmore, 2009). Computational models have shown that multiplicative noise is able to induce phase transitions in neural systems (Lindner et al., 2004). Alternatively, Bayesian analyses of visual performance have related the statistical properties of natural scenes and specific tasks by assigning probabilities in the presence of noise (Faisal et al., 2008; Geisler & Diehl, 2003). Bayesian models have been used to infer the properties of multiplicative neural noise from psychophysical data (Stocker & Simoncelli, 2006).

The aim of this work is to examine the information-theoretic properties of multiplicative neural noise and the benefits in the formation of psychophysical thresholds. The study of psychophysical thresholds in the context of noisy neurons and information theory is of great interest because multiplicative neural noise can modify the shape of the psychometric function and enhance the SNR monitoring few neurons (Tyler & Chen, 2000). In this study, we examine a particular class of multiplicative neural noise that shows power law scaling. Instead of using signal detection theory (Tyler & Chen, 2000), we present a simplified diffusion model based on statistical physics. The principle of efficient coding is redefined using the methods of the entropic theory of perception (Norwich, 1993). For a given input signal, the purpose is to examine how much information is transferred from the stimulus to the photoreceptors, and then to the cortex, in the presence of multiplicative neural noise. As shown later, multiplicative neural noise is defined as variability in the mean firing rate of the visual system. We focus on two classic examples: Weber's law and the human contrast sensitivity function (CSF). These two psychophysical examples capture representative nonlinear properties of neural arrays tuned to different mean intensities and frequencies of visual scenes. Although previous models have examined both cases (De Valois & De Valois, 1990; Norwich, 1993; Norwich & Wong, 1995, 1997; Rovamo et al., 1999; van Hateren, 1992), it is usually without consideration of internal noise and its efficiency of information transmission. Weber's law is probably one of the most sophisticated collective operations carried out by neurons. It states that the smallest perceived or differential intensity threshold (ΔI) is independent of the luminance background of the scene I at high illumination levels and for the Weber fraction, $\Delta I/I \cong$ constant (Fechner, 1966; Weber, 1834). The general form of the Weber fraction deviates at low illumination levels by a power function, sometimes described by the Rose–de Vries law ($\Delta I/I \cong I^{-1/2}$) (de Vries, 1943; Rose, 1946). At very high illumination levels, there is a second deviation. Saturation limits photoreceptor responses to the increment stimulus, and the Weber fraction rises slightly (Aguilar & Stiles, 1954; Nutting, 1907; Wyszecki & Stiles, 1982). The CSF represents the variation of the contrast threshold for both spatial and temporal sine wave gratings. The CSF normally presents a bandpass or low-pass shape as a function of the frequency

of waveforms. It depends on multiple visual factors including the optical quality of the eye, adapting background, and chromatic content (De Valois & De Valois, 1990; Mullen, 1985; Robson, 1966; Rovamo et al., 1999). The measurement of contrast sensitivity is considered a standard clinical test and is used in diagnosing neuro-ophthalmic disorders.

The organization of the letter is as follows. In section 2, we define the information entropy function as a measure of the average uncertainty in the visual system. Based on the above definition, the principle of efficient coding is redefined. Then the neural SNR is evaluated. We argue that neural noise is governed mainly by the interplay of two mechanisms: Brownian fluctuations over time and a form of background noise. This background noise can be beneficial in some cases and is assumed multiplicative neural noise. The estimated neural SNR gives the basis for analyzing the information entropy function. In section 3, we derive an analytical expression of the sensory threshold based on the neural SNR and the information entropy function. The average information capacity of the visual system at the threshold is also presented. We show that Weber's law and the CSF emerge from power law neural noise. It is demonstrated that contrary to the common assumption of an Infomax procedure, the visual system provides the minimum gain of information after efficient coding. In section 4, we discuss the model in relation to the possible spectral properties of the background noise and the information capacity of sensory systems. The conclusions are summarized in section 5.

2 Theoretical Background

2.1 Definition of the Information Entropy Function. Consider the visual system with photoreceptors at the retina as the source connected to the cortex as the receiver or the main center. The fundamental hypothesis is the existence of uncertainty during the sampling process. Uncertainty comes from fluctuations originating in part at the interface between the external visual stimulus and the photoreceptors. Initially the external input signal is added to an internally generated signal. In this approach, the information-theoretical entropy, or the H-function (see equation 2.1), describes the average uncertainty state (Norwich, 1993). Although the rate of photon absorption and the subsequent production of spikes can be modeled as being Poisson (Cecchi et al., 2000; Faisal et al., 2008; Lindner et al., 2004), there exists variability of neural responses that do not follow Poisson-like statistics (Uzzell & Chichilnisky, 2004; Victor et al., 2007). We have represented neural fluctuations by a gaussian process because gaussian distributions have the maximum possible information entropy for a given variance and provide an upper bound, that is, $H_{\text{Gaussian}} \geq H_{\text{Poisson}}$ (Cover & Thomas, 2006). The same approach has been considered before in the study of both neural (Borst & Theunissen, 1999), and perceptual (Norwich, 1993; Norwich & Wong, 1995) responses. The entropy function H is defined as

the difference between the differential entropies of two gaussian process before (H'_{before}) and after (H'_{after}) an external visual stimulus is applied, the former acting as the reference signal (Norwich, 1993), $H = H'_{\text{after}} - H'_{\text{before}}$. This difference can be greater or less than zero. The differential entropy of a gaussian channel depends on only the variance σ^2, $H' = (1/2)\ln(2\pi e\sigma^2)$ (Cover & Thomas, 2006). The convolution of the input and reference signal is also a gaussian distribution with variance, $\sigma^2_{\text{after}} + \sigma^2_{\text{before}}$. The H-function is therefore expressed as follows (Norwich, 1993; Norwich & Wong, 1995, 1997):

$$H = \frac{1}{2}\ln\left[1 + \left(\frac{\sigma^2_{\text{after}}}{\sigma^2_{\text{before}}}\right)\right] \text{(natural units)}, \tag{2.1}$$

where $\left(\sigma^2_{\text{after}}/\sigma^2_{\text{before}}\right)$ is the neural SNR to be evaluated. Equation 2.1 can be measured in bits divided by ln(2). It is assumed that the neural SNR will depend on some form of background noise and the visual latency. This background noise is not fixed but stimulus dependent and will represent multiplicative neural noise. The presence of time in the neural SNR will play a crucial role in the entropic function H and reflects that the visual system is not static; it takes time to acquire information. Visual reaction time is an example where time is usually less than 1 s (Luce, 1986). In comparison with Shannon's information entropy, the information entropy function H is a continuous time model in which the internal uncertainty is accumulated as a function of time (Norwich, 1993; Norwich & Wong, 1995, 1997). When time increases, if the H-function increases, it will represent high uncertainty, and vice versa. It is very important to note that the information content is related to the reduction of uncertainty over some finite interval of time. The presence of the reference signal refers in part to additive thermal noise, $H = H'_{\text{after}} - H'_{\text{before}}$. However, there are other internal sources of neural noise. We will apply equation 2.1 to those neural fluctuations that increase from additive noise by multiplicative power law noise.

2.2 Definition of an Information Threshold. We propose to extend the principle of efficient coding between photoreceptors and the cortex (Attneave, 1954; Barlow, 1961; Linsker, 1990; Simoncelli & Olshausen, 2001; van Hateren, 1992), using the entropic function H. The general scheme of the model is represented in Figure 1. The figure is a block diagram that describes the overall behavior but not the internal details of the visual system. It comprises a hypothetical source-channel encoder connected to an internal noisy channel together with a channel-source decoder. The encoder defines the transmission bandwidth and divides the temporal dynamics into those processes before and after the encoding time t_0. This is a constrained optimization problem and establishes the existence of an extreme criterion in

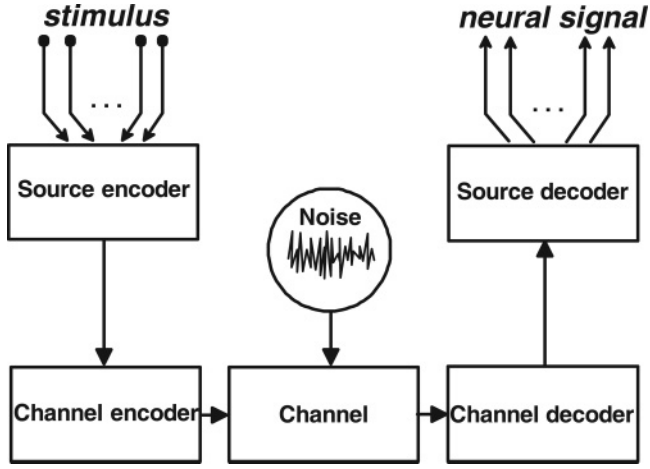

Figure 1: A multiple input-output noisy channel model. Each photoreceptor generates stochastic data from the input stimulus. This is represented by peripheral nodes. An efficient visual encoder processes the data in two steps. The source encoder provides an efficient representation of the stimulus. The channel encoder has a different purpose: it promotes the transfer of information in the channel with reliability. At the source-channel encoder, the information entropy function leads to the maximum uncertainty or minimum information from stimuli. The channel-source decoder or receiver makes the inverse operation by reconstructing the transmitted neural signal-to-noise ratio for further processing. There is a reduction of uncertainty and the visual system gathers ΔH bits of information.

the information entropy function (Medina, 2009; Norwich, 1993; Norwich & Wong, 1995):

$$\Delta H = H(t_0) - H(t) \geq 0. \tag{2.2}$$

The parameter t is the intrinsic or visual latency ($t \geq 0$). It is considered that the H-function is very close to zero or null at $t = 0$. Initially ($0 < t < t_0$), information does not accumulate over time. The encoding time t_0 establishes the information entropy state of maximum uncertainty or, equivalently, maximum loss of information from stimuli. The encoding time makes mention of neither particular neuronal codes nor sources of internal noise. It simply sets the origin of information, which is defined as the minimum quantity associated with an efficient encoder. Perception commences after this coding stage (Norwich, 1982) at the channel-source decoder. That is, after a long period of time ($t > t_0$), the visual system is adapted to the external stimulus and approaches the steady state. ΔH is the separation between

the entropic state of maximum uncertainty at t_0 and the entropic steady state at time t. There is a reduction of uncertainty and the system gathers $\Delta H \geq 0$ bits of information. Equation 2.2 indicates that visual perception has an accumulation of information after efficient coding. The quantity of information ΔH is required before the visual system can react or perceive. This is closely connected to the situation of crossing an effective threshold level but formulated in the information-theoretic domain. The onset of visual perception is therefore considered after the visual system reaches ΔH bits of information.

2.3 Langevin Approximation. Noise in the neural SNR (see equation 2.1) is modeled by a simplified diffusion process. Diffusion models usually assume the visual system as a single unit, without detailed consideration of individual neurons. There exist different diffusion models that depend on how noisy neural events are accumulated (Luce, 1986; Smith & Ratcliff, 2004). A representative model in many physical and self-organized biological systems is often established in the context of statistical physics and the microscopic description of Brownian motion (Coffey et al., 2004; Haken, 1977). The diffusion model of neural noise assumes a similar analogy. Fluctuations in spike timing (seconds per spike) are the encoding signal rather than the number of spikes (Lestienne, 2001; Sejnowski & Paulsen, 2006; Singer, 1999). Neural noise is defined as stochastic variability in the instantaneous firing rate of the visual system $m(t)$ (spikes per second). As shown later, this variability is related to the mean square displacement $\langle m^2 \rangle$. The instantaneous firing rate $m(t)$ is similar to the velocity of a large Brownian particle, and the mean square displacement $\langle m^2 \rangle$ will be similar to the average kinetic energy. Note that in this analogy, variations in $\langle m^2 \rangle$ will depend on the mechanisms of interactions between neurons. Stochastic dynamics in the firing rate $m(t)$ is summarized by a Langevin-type differential equation (Coffey et al., 2004; Haken, 1977):

$$\mathrm{d}m(t)/\mathrm{d}t = -C_{\mathrm{L}} m(t) + F(t), \tag{2.3}$$

C_{L} is the damping or response coefficient of the whole system that modulates the decay of the firing rate over time ($C_{\mathrm{L}} > 0$). As shown later, C_{L} represents the average information capacity of the visual system at the threshold (e. g., bits per second). The second additive term, $F(t)$,indicates the stochastic perturbation due to the interacting processes between neurons or background noise. Each excited neuron contributes to $F(t)$. Multiplicative neural noise is therefore represented within $F(t)$ and depends on the mean field of impulses in the network. This background noise contains excitatory or inhibitory impulses. They occur in a short-range interaction process that decays in time. The interaction process is sharply peaked around the time origin of stimulus presentation. The stochastic impulses

are assumed, on average, zero-mean gaussian delta correlated, $\langle F(t)\rangle \cong 0$, $\langle F(t)F(t')\rangle = 2D\delta(t-t')$ (Cecchi et al., 2000; Haken, 1977; Lindner et al., 2004), where $\langle ...\rangle$ represents the time average over the ensemble of impulses in the neural network. D is the diffusion parameter that indicates the average strength of interactions. It is also assumed that the accumulation of information ΔH in equation 2.2 is made at a constant rate. C_{L} is therefore approximately constant and does not undergo abrupt changes during the time t. The general solution of the differential equation 2.3 (Coffey et al., 2004):

$$m(t) = m(0)e^{-C_{\mathrm{L}}t} + e^{-C_{\mathrm{L}}t}\int_0^t e^{C_{\mathrm{L}}\tau}F(\tau)\,d\tau. \tag{2.4}$$

After a long period of time ($t > t_0$), the initial spike rate $m(0)$ decays exponentially and is not considered in the analysis. That is, the steady-state solution of equation 2.4 is mainly determined by the second term of the right-hand side. The term $m^2(t)$ can be expressed as follows:

$$m^2(t) = e^{-2C_{\mathrm{L}}t}\int_0^t d\tau \int_0^t d\tau' e^{C_{\mathrm{L}}(\tau+\tau')}F(\tau)F(\tau'). \tag{2.5}$$

The neural variance or the average noise power σ^2 is defined by $\sigma^2 = \langle m^2\rangle - \langle m\rangle^2$. Because the average over all the impulses $\langle F(t)\rangle$ has approximately zero mean, the mean firing rate is also very low $\langle m\rangle \cong 0$. Consequently, the neural variance is approximately equal to the mean square displacement, $\sigma^2 = \langle m^2\rangle - \langle m\rangle^2 \cong \langle m^2\rangle$. Using the autocorrelation function, $\langle F(t)F(t')\rangle = 2D\delta(t-t')$ and, after a few steps, the average noise power:

$$\sigma^2 = (D/C_{\mathrm{L}})\left(1 - \mathrm{e}^{-2C_{\mathrm{L}}t}\right). \tag{2.6}$$

The size of fluctuations D is rewritten proportional to the size of dissipation or the response of the visual system, C_{L}. That is, $D = \sigma_{\mathrm{ss}}^2 C_{\mathrm{L}}$, in a similar way as the fluctuation-dissipation theorem in nonequilibrium systems (Prost, Joanny, & Parrondo, 2009). The neural noise is now rewritten as

$$\sigma^2 = \sigma_{\mathrm{ss}}^2\left(1 - \mathrm{e}^{-2C_{\mathrm{L}}t}\right). \tag{2.7}$$

Equation 2.7 must be understood as an asymptotic result; it does not represent the exact temporal trajectory of any particular neuron. Equation 2.7 indicates that fluctuations grow with time and saturate in the steady state σ_{ss}^2 in the limit $t \to \infty$. The information capacity C_{L} reflects the timescale of evolution. High values of C_{L} indicate rapid saturation, and vice versa. To

complete the model, σ_{ss}^2 should be evaluated. It is proposed that the visual system will overcome the growth of fluctuations in time by modifying σ_{ss}^2. The steady-state variance σ_{ss}^2 is related to the mean energy of the background noise by a power function. Power laws are commonly defined in statistical physics to describe the variance-mean relationship of fluctuations when an external stimulus is present (Huang, 1987):

$$\sigma_{ss}^2 = (E/k_B T_b)^{-p} \leq 1. \tag{2.8}$$

The exponent p is a parameter that will be discussed later. K_B is the Bolztmann constant, and T_b is the body temperature. E is the mean energy of the background noise. This mean energy varies in multiples of thermal noise energy, $K_B T_b$, and is a function of the stimulus strength M or multiplicative neural noise: $E \cong \chi M$. The parameter χ is a constant. M indicates any physical variable that characterizes the input stimuli. For example, it was found that neural variability changes in the perception of stimuli with different contrast and speed (Cecchi et al., 2000; Stocker & Simoncelli, 2006). This notion is generalized, and M can also represent other physical attributes such us hue, orientation angle, or the spatial or temporal frequency of gratings. The presence of thermal noise $K_B T_b$ also indicates that neurons are in contact with an external random reservoir or heat bath. Equation 2.8 is reminiscent of the equipartition energy theorem in statistical physics (Coffey et al., 2004; Haken, 1977; Huang, 1987). Inserting equation 2.8 into 2.7 yields

$$\sigma^2 = (k_B T_b/E)^p \left(1 - e^{-2C_L t}\right). \tag{2.9}$$

The average noise power σ^2 in equation 2.9 contains the effects of three kinds of internal noise: multiplicative neural noise superimposed on an exponential noise from the Brownian transport of spikes over time together with thermal noise. The background noise is beneficial. If the mean energy E of the background noise increases, then the noise variance σ^2 decreases. Since $E \cong \chi M$, equation 2.9 is rewritten as

$$\sigma^2 = (1/\gamma M^p)\left(1 - e^{-2C_L t}\right), \tag{2.10}$$

where γ is a normalization constant that includes all previous constants such as the body temperature T_b. The neural noise σ^2 therefore contains a form of multiplicative (i.e., signal dependent) neural noise with $0 < \sigma_{ss}^2 \leq 1$ (see equation 2.8). When equation 2.10 is introduced into the neural SNR in equation 2.1, the entropy H-function is finally given by

$$H(M,t) = \frac{1}{2}\ln\left[1 + \frac{\gamma M^p}{\left(1 - e^{-2C_L t}\right)}\right], \tag{2.11}$$

where $\sigma^2_{\text{after}}/\sigma^2_{\text{before}} = \gamma M^p/(1 - e^{-2C_L t})$. Equation 2.11 is neither Shannon's information entropy nor thermodynamic entropy. Initially ($t \cong 0$) sensory receptors detect the external stimulus in a way similar to a linear channel with additive gaussian noise. As time advances ($t < t_0$), receptors' uncertainty about the external stimulus increases until they reach a maximum at time t_0. This process is driven by an efficient encoder at postreceptoral stages. After encoding ($t > t_0$), the sensory system accumulates evidence about the external stimulus modulating its own background noise. The H-function in equation 2.11 now enters in ΔH and describes the drop of uncertainty from the maximum value, or $\Delta H \geq 0$. The time evolution of the information entropy in equation 2.11 leads to the following mathematical condition: $dH(t)/dt \leq 0$; that is, after efficient coding, uncertainty always decreases due to the process of perception, in the same way as Boltzmann's theorem in statistical physics (Huang, 1987; Norwich, 1993). From stage to stage, all the internal sources of neural noise modify the original SNR at the sensory receptors. As a consequence, the H-function deviates from linearity by power law scaling. The mean energy of the background noise E is assumed not to deviate too much from the reference or thermal noise energy (see equation 2.8). That is, the effects of nonlinear propagation on the information entropy function are set close to zero. Weak nonlinearities result when the effective propagation distances of spikes along the nerve fibers are short. This is equivalent to the assertion that the mean energy of the background noise E, the visual latency t, or the product Et (the background noise strength) should be kept small.

The presence of multiplicative neural noise is beneficial to the visual system. The growth of the neural noise σ^2 as a function of time can be balanced by modulating the mean energy of the background noise E in σ^2_{ss} (see equation 2.9). Consequently, the neural SNR can be restored over time. The reduction of uncertainty after coding leads to: $\Delta H = H(t_0) - H(t) \geq 0$. However, multiplicative neural noise has the counterintuitive effect of increasing internal uncertainty (see equation 2.11). Therefore, the separation between the entropic state of maximum uncertainty at t_0 and the entropic steady state at time t tends to be a minimum. That is, ΔH does not increase but decreases or, equivalently, the gain of information tends to be a minimum. The information entropy function given in equation 2.11 has been derived previously but using different arguments and is included in a theoretical framework that has largely been validated with reference to sensory data (Norwich, 1993; Norwich & Wong, 1995, 1997).

3 Simulation Results

3.1 Weber Fraction and Visual Latency. A generic visual stimulus is modulated around the mean light intensity of the scene I. The principal issue is the estimation of the differential intensity threshold as a function

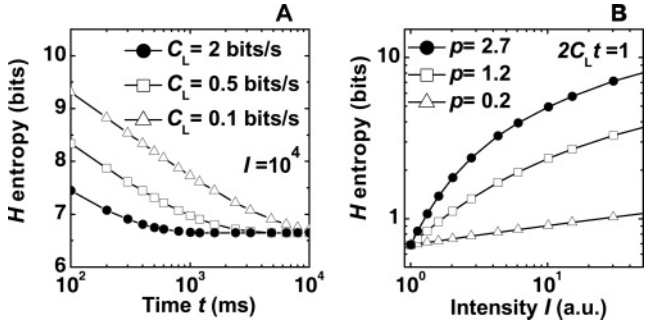

Figure 2: Simulation of information entropy. (A) Semilogarithmic plot of the H-function as a function of the intrinsic visual latency t for different values of C_{L}. Stimulus intensity I was fixed to 10^4 (arbitrary units). (B) Double logarithmic plot of the H-function as a function of stimulus intensity for different values of the exponent p. Time was fixed to the reciprocal of $2C_{\mathrm{L}}$. a.u. = arbitrary units.

of I. The stimulus strength $M = I$ and the rest of physical attributes are fixed. In this case, the mean energy of the background noise is $E = \chi I$ and $\sigma_{\mathrm{ss}}^2(I) = 1/\gamma I^p$. The dependency of the neural variance σ_{ss}^2 on I is consistent with previous physiological results results (Cecchi et al., 2000; Uzzell & Chichilnisky, 2004). The entropy H-function from the Langevin model is

$$H(I,t) = \frac{1}{2}\ln\left(1 + \frac{\gamma I^p}{1 - \mathrm{e}^{-2C_{\mathrm{L}}t}}\right). \tag{3.1}$$

Equation 3.1 represents a gaussian channel model with multiplicative neural noise. Figures 2A and 2B show the evolution of the information entropy as a function of time and stimulus intensity for different values of C_{L} and p, respectively. The entropy function decreases in time (a gain of information), but only after the light intensity I is encoded in accordance with equation 2.2. High-capacity values ($C_{\mathrm{L}} > 0.5$ bits/s) enhance this behavior (see Figure 2A). There is an improvement of the neural SNR as a function of I, but the entropy function increases (a gain of uncertainty, see Figure 2B). The exponent p modulates the rise of uncertainty($p < 1$). The increment of the H-function reflects that the visual system does not tolerate very high luminance or glare effects. In the same way, low luminance provides low neural SNR. However, there is a limited range of intensities where uncertainty does not grow much and the improvement of the neural SNR is moderate but significant (i.e., photopic vision). We consider this situation in the next section. From the definition of ΔH in equation 2.2 and the

information entropy function in equation 3.1

$$\Delta H \equiv H(t_0) - H(t) = \frac{1}{2}\left[\ln\left(1 + \frac{\gamma I^p}{1 - e^{-2C_L t_0}}\right) - \ln\left(1 + \frac{\gamma I^p}{1 - e^{-2C_L t}}\right)\right]. \tag{3.2}$$

The term γI^p can be expressed as follows:

$$\gamma I^p = \frac{\left(1 - e^{-2C_L t}\right)\left(e^{-2\Delta H} - 1\right)}{1 - \frac{e^{-2\Delta H}\left(1 - e^{-2C_L t}\right)}{\left(1 - e^{-2C_L t_0}\right)}}. \tag{3.3}$$

From equation 3.3, in the limit $t \to \infty$, the visual system estimates the differential intensity threshold or the Weber fraction $\left(\gamma I_0^p \equiv \Delta I / I\right)$. The visual threshold as a function of ΔH is

$$\gamma I_0^p = \frac{1 - e^{-2\Delta H}}{\frac{e^{-2\Delta H}}{\left(1 - e^{-2C_L t_0}\right)} - 1}. \tag{3.4}$$

Equation 3.4 is very important and connects the threshold γI_0^p with ΔH. The visual latency t, as a function of the intensity I, the information capacity C_L, and the encoding time t_0 can be written as

$$t = \frac{1}{2C_L} \ln\left\{\frac{\left[e^{2C_L t_0}\left(1 + \gamma I_0^p\right)\right] - \left(\frac{I_0}{I}\right)^p}{1 - \left(\frac{I_0}{I}\right)^p}\right\}, \tag{3.5}$$

Equation 3.5 is equivalent to the empirical Piéron's law in sensory psychophysics; that is, the visual latency t decreases as the intensity increases until an asymptotic value or plateau t_{RT_0} is reached at high intensities, $\lim_{I \to \infty}(t) \equiv t_{RT_0}$ (Lennie, 1981; Luce, 1986). This is shown in Figure 3A. Piéron's law is represented by the solid line. The full approach (see equation 3.5) is represented by open circles and captures the behavior at very low-intensity changes. Note that the time t in the Langevin model (see equation 2.7) cannot be related to a direct measurable property until ΔH is applied (see equation 3.1). The neural variance $\sigma_{ss}^2 = 1/\gamma I^p$ is represented in Figure 3A (see open circles, error bars) and gives a measure of neural variability at the steady state. This is in agreement with previous psychophysical results (Baird, 1997; Luce, 1986; Stocker & Simoncelli, 2006).

Figure 3B compares the term σ_{ss}^2 as a function of visual latency t for different values p. The variance increases linearly with t at low processing times and saturates at high times. High values of the exponent p diminish the growth of $\sigma_{ss}^2 (p > 1)$. These results are also in agreement with the empirical mean-variance relationship in human reaction times (Baird, 1997; Luce, 1986; Wagenmakers & Brown, 2007). It is interesting to note that the shape of Piéron's law remains invariant over different temporal scales. That

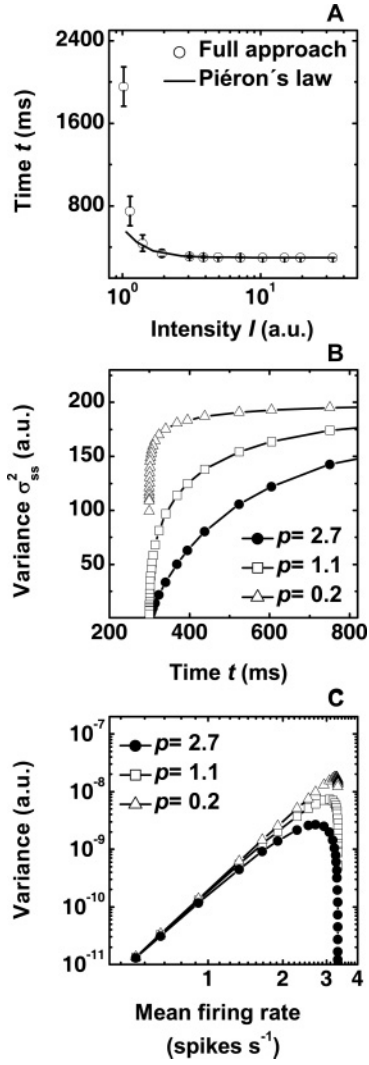

Figure 3: Visual latency and neural variance. (A). Semilogarithmic plot of the visual latency t as a function of stimulus intensity I. Open circles represent the full approach obtained from equation 3.5. Error bars simulate the dependence of the steady state σ^2_{SS} as a function of stimulus strength. The solid line indicates the numerical results from Piéron's law: $t = t_{RT_0}[1 + (I_0/I)^p]$ (Luce, 1986; Norwich et al., 1989). In both cases, data parameters are $t_{RT_0} = 300\,\text{ms}$, $p = 2.7$, $C_L = 0.5\,\text{bits/s}$. (B) Linear plot of the variance σ^2_{SS} (in normalized units) as a function of time t for different values of p. (C) Full logarithmic plot of σ^2_{SS}/t^4 as a function of the mean firing rate for different values of p. a.u. = arbitrary units.

is, the shape of Piéron's law repeats in time and is identical to the reciprocal of the Naka-Ruston equation in neurophysiology (Medina, 2009). From equation 3.5, the reciprocal of t is compared with the average spike rate (spikes per second) in the visual system: $\langle m \rangle \cong 1/t$. The error propagation method for indirect measurements was used (Squires, 2001) to estimate the variance associated with $1/t$. The estimated variance varies as σ_{SS}^2/t^4. Figure 3C represents σ_{SS}^2/t^4 as a function of the mean spike rate $\langle m \rangle$. At low rates, $\langle m \rangle < 1.5$, the variance increases linearly. As the mean firing rate increases, there are deviations from the linear behavior. High values of p diminish the rise of the neural variance ($p > 1$), and vice versa. At high rates, the model predicts that the neural variance no longer increases. It saturates and then drops until it reaches a minimum value. These numerical results are consistent with the previous physiological findings of multiplicative neural noise (Carandini, 2004; Holt et al., 1996; Tolhurst et al., 1983; Vogels et al., 1989).

3.2 Weber's Law. Photopic vision deals with regular bright conditions during daylight and foveal viewing mediated by cones. Under these circumstances, the differential visual threshold of the visual system γI_0^p should be small enough that the incoming signal can be easy detected (see equation 3.4). The reduction of the background noise strength Et leads the visual system close to a linear state and the subsequent threshold reduction. To meet the criteria, the product of $E \cong \chi I$ and t should be small. Figure 4A simulates this condition taking t from Figure 3A (open circles). The background noise strength decreases and reaches a minimum. The arrow indicates the expected quasi-ideal regime. This minimum remains approximately constant over a finite range of intensities, a condition that resembles Bloch's law in psychophysics (Norwich, 1993). After this minimum, the background noise strength diverges. Figure 4B represents ΔH as a function of I(t is taken from Figure 3A). There is a minimum at low intensities that matches the range close to the ideal performance (see Figure 4A). ΔH minimum applies only when the mean energy of the background noise E increases and the neural SNR maximizes (see equations 2.9 and 3.1). Far from the ideal performance, ΔH increases, but the neural SNR decreases too. The threshold γI_0^p can be rewritten as a function of the visual latency t and the intensity I:

$$\gamma I_0^p = \frac{e^{2C_L t} - e^{2C_L t_0}}{e^{2C_L t_0} + \left[\left(\frac{1}{\gamma I^p}\right)\left(e^{2C_L t} - 1\right)\right]}. \tag{3.6}$$

From equation 3.6, Figure 4C gives the final result and simulates the Weber fraction $\left(\Delta I/I \equiv \gamma I_0^p\right)$ as a function of I. At very low and high intensities, the underlying quasi-linear communication channel in the entropic function H does not hold up, and nonlinearities start to dominate (see equation 3.1

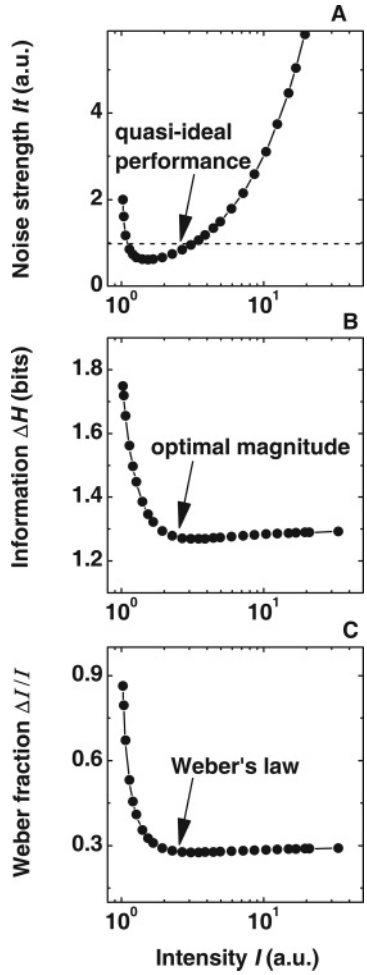

Figure 4: Simulation of Weber's law. (A) Semilogarithmic plot of the product $(I \times t)$ as a function of stimulus intensity. (B) ΔH (see equation 2.2) as a function of $I(t_0 = 44\,\text{ms}, p = 1.1, C_\text{L} = 0.5\,\text{bits/s})$. (C) Simulation of the Weber fraction. The plateau corresponds to Weber's law. The parameters are the same as in B. a.u. = arbitrary units.

and Figure 4A). At very low intensity levels, the visual threshold γI_0^p decreases as ΔH decreases. The reduction of the visual threshold captures the power function dependency, but the drop was simulated steeper (-2.4) than the Rose–de Vries law. The plateau or Weber's law is located in the same place as ΔH minimum (see Figure 4B). At high intensities, there is

a slight but gradual rise of the differential visual threshold, indicating the second departure from Weber's law.

3.3 Information Capacity. From equation 3.5, the asymptotic limit on the visual latency t_{RT_0} and the encoding time t_0 define the bandwidth at the threshold: $B_0 = 1/[2(t_{RT_0} - t_0)]$. Inserting t_{RT_0} into equation 3.4 and using logarithms to base 2, the information capacity C_L of the Langevin approach at the threshold is

$$C_L = B_0 \log_2 \left(1 + \gamma I_0^p\right) \text{(bits per s)}. \tag{3.7}$$

The logarithmic term in equation 3.7 represents the spectral efficiency in bits. Note that the analytical form of C_L is similar to Shannon's channel capacity, $C = B' \log_2 [1 + \text{SNR}]$. B' is the bandwidth. However, it is important to note that C_L no longer represents a linear channel. The estimated capacity C_L does not increase logarithmically as the input signal strength I increases. It depends on the visual threshold γI_0^p or, equivalently, on the exponent p and ΔH (see equation 3.4).

3.4 Contrast Sensitivity. A visual stimulus is modulated as a function of the frequency of the sine wave gratings f'(spatial or temporal). The visual system now calculates the contrast threshold C_0 as a function of f'. The stimulus strength M depends on only the reciprocal of f', $M = 1/f'$. Frequency-selective cells balance the mean energy of the background noise E against Brownian fluctuations over time: $E = \chi f'_{max}/f'$. f'_{max} indicates the maximum frequency supported before nonlinear effects start to dominate. The neural variance at the steady state is rewritten as $\sigma_{ss}^2 = \gamma (f'/f'_{max})^p$. σ_{ss}^2 increases as the normalized spatial frequency increases. High values of the exponent p modulate the rise of variability ($p > 1$). The dependency of σ_{ss}^2 with f' is in agreement with previous physiological results at low spatial frequencies (Dean, 1981; Geisler & Albrecht, 1995). The entropy H-function is now given by

$$H(f', t) = \frac{1}{2} \ln \left[1 + \frac{f'^p_{max}}{\gamma f'^p \left(1 - e^{-2C_L t}\right)} \right], \tag{3.8}$$

Figure 5A represents the evolution of the information entropy as a function of the normalized frequency for different values of p. Far from the maximum frequency (i.e., a ratio f'/f'_{max} close to zero), the mean energy of the background noise E increases the SNR at the expense of increased uncertainty. High values of p control the rise of uncertainty at low frequencies ($p > 1$).

Equation 3.8 is the reciprocal of the H function as a function of the stimulus intensity (see equation 3.1). Solving equations 2.2 and 3.8 therefore

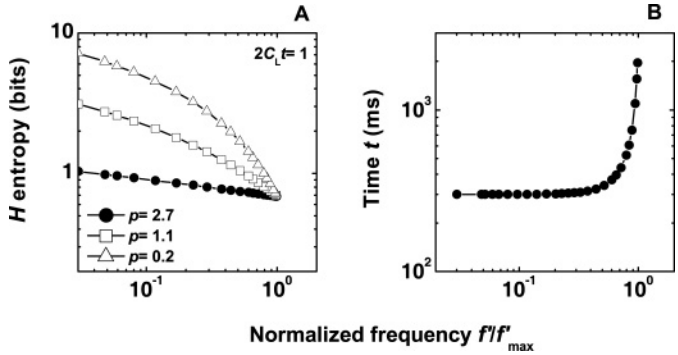

Figure 5: Simulation of the information entropy. (A) Full logarithmic plot of the H-function as a function of stimulus frequency f' (in normalized units) for different values of the coupling strength p. Time was fixed to the reciprocal of $2C_{\mathrm{L}}$. (B) Full logarithmic plot of the neural conduction-time as a function of stimulus frequency ($t_{\mathrm{RT}_0} = 300$ ms, $p = 2.7$, $C_{\mathrm{L}} = 0.5$ bits/s).

represents the inverse problem from equations 3.1 to 3.6. The visual latency t in equation 3.5 is now a function of stimulus frequency f'. Figure 5B indicates that t increases as the spatial frequency of gratings increases. This is in agreement with previous psychophysical observations in human reaction times (Felipe, Buades, & Artigas, 1993).

Quasi-ideal performance applies only when nonlinear effects are restricted close to zero. The background noise strength Et or the product of the reciprocal of the frequency f' and the time t are represented in Figure 6A. The arrow indicates the quasi-ideal regime. Figure 6B gives an example of ΔH as a function of the normalized stimulus frequency f'. At low to medium-frequency values, ΔH is restricted to low values. It reaches the minimum only close to the ideal performance (see Figure 6A).

In visual psychophysics, contrast sensitivity is related to the reciprocal of the contrast threshold, $C_0 \equiv \gamma I_0^p$. After resolving equations 2.2 and 3.8, Figures 7A and 7B give two classical examples of the CSF. Figure 7A represents the CSF for binocular and monocular vision. Here, only the exponent p varies and differences in $f'_{\max}$ are ignored. Close to the ideal regime (see Figure 6A), the mean energy of the background noise E balance better Brownian fluctuations over time. The neural SNR increases and minimizes ΔH. That is, the contrast sensitivity of the binocular system increases over a narrow ($p = 1.1$) or wider frequency bandwidth ($p = 0.2$). The simulation results are in agreement with previous psychophysical and physiological results on binocular contrast summation (Anzai et al., 1995; Campbell & Green, 1965). Figure 7B represents the CSF for achromatic (De Valois & De Valois, 1990; Robson, 1966; Rovamo et al., 1999) and chromatic gratings (Mullen, 1985; Rovamo et al., 1999). In general, high-capacity values ($C_{\mathrm{L}} > 0.5$ bits/s)

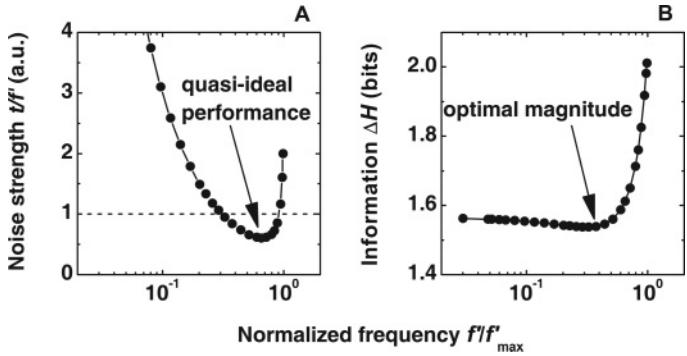

Figure 6: (A) Semilogarithmic plot of the product (t/f') as a function of stimulus frequency. (B) Semilogarithmic plot of ΔH (see equation 2.2) as a function of stimulus frequency ($t_0 = 30$ ms, $p = 1.1$, $C_L = 0.5$ bits/s). a.u. = arbitrary units.

diminish contrast sensitivity at low to medium frequencies. This effect is opposed to the encoding time t_0: contrast sensitivity increases as t_0 increases. However, only the enhancement of the mean energy E by the exponent p at the appropriate frequency of gratings (see Figure 6A) changes the CSF from low-pass to bandpass. That is, low exponents' values ($p < 1$) improve multiplicative neural noise and maintain the SNR over time better. Uncertainty increases but below the maximum value. ΔH therefore minimizes and enhances contrast sensitivity in the same way as in Weber's law. The final results, presented in Figures 7A and 7B, show in part why two eyes are better than one and why those pure chromatic signals are less effective than achromatic ones.

4 Discussion

This study shows that after efficient coding, multiplicative neural noise is beneficial. It restores the SNR as a function of time but at the expense of increased uncertainty. Uncertainty is measured by the entropic function H. Because information is related to a reduction of uncertainty, maximization of the neural SNR inevitably leads to maximization of uncertainty and optimal information processing approaches the minimum value. This study has analyzed two possible forms of multiplicative neural noise. The first case takes into account that neural noise can decrease as the average stimulus intensity I increases, that is, $\sigma_{ss}^2 = 1/\gamma I^p$(Baird, 1997; Cecchi et al., 2000; Stocker & Simoncelli, 2006; Uzzell & Chichilnisky, 2004). In the second case, multiplicative neural noise increases as a function of the stimulus frequency, $\sigma_{SS}^2 = \gamma\,(f'/f'_{max})^p$ (Dean, 1981; Geisler & Albrecht, 1995). The entropic model is consistent with previous experimental findings of multiplicative neural noise, in which variability increases linearly as the mean

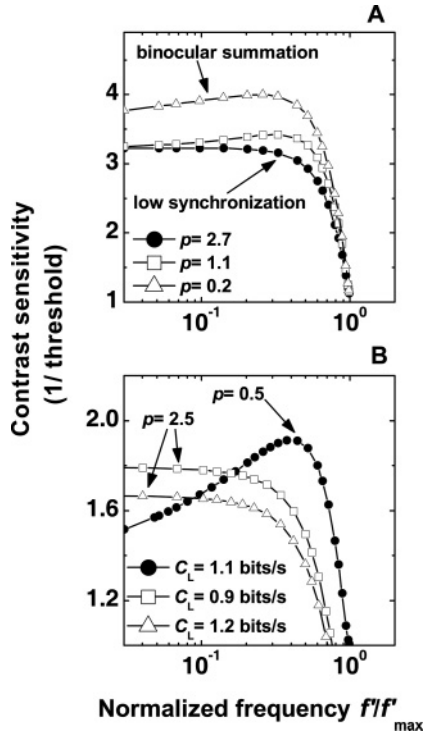

Figure 7: The contrast sensitivity function (1/threshold) in visual psychophysics. (A) Semilogarithmic plot of the binocular-monocular CSF as a function of stimulus frequency for different values of the exponent p, ($t_0 = 30$ ms,$C_L = 0.5$ bits/s). (B) Semilogarithmic plot of the spatial CSF in human color vision. Solid circles, open squares, and triangles represent achromatic stimuli and red-green and blue-yellow stimuli at isoluminance, respectively. The encoding time t_0 was 44 ms, 67 ms, and 96 ms, respectively.

firing rate increases (see Figure 3C); (Carandini, 2004; Dean, 1981; Tolhurst et al., 1983). The entropic model also describes the empirical Piéron's law in psychophysics (see Figure 3A); (Baird, 1997; Lennie, 1981; Luce, 1986), and the experimental findings that relate the visual latency as a function of the stimulus frequency (see Figure 5B) (Felipe et al., 1993). It describes the relationship between the mean and the standard deviation of the visual latency (see Figure 3B) (Baird, 1997; Luce, 1986; Wagenmakers & Brown, 2007)—both Weber's fraction and Weber's law (see Figure 4C); (Aguilar & Stiles, 1954; de Vries, 1943; Fechner, 1966; Nutting, 1907; Rose, 1946; Weber, 1834)—binocular contrast summation at the threshold (see Figure 7A) (Anzai et al., 1995; Campbell & Green, 1965), and the CSF for both achromatic

and chromatic gratings (see Figure 7B); (De Valois & De Valois, 1990; Mullen, 1985; Robson, 1966; Rovamo et al., 1999). Therefore, the simulation results suggest that multiplicative neural noise is not a nuisance but valuable to human vision (Kontsevich et al., 2002; Lu & Dosher, 1999; Tyler & Chen, 2000). They promote the minimum transfer of information after coding and reinforce the idea that internal noise shapes emerging phenomena in visual psychophysics (Hornstein et al., 1999; Rovamo et al., 1999).

4.1 Plausibility of the Assumptions. The information-theoretic model contains two important assumptions. First, in any biological system, the acquisition of information is not instantaneous (see equation 2.2), and second, the presence of multiplicative neural noise shows power law scaling (see equation 2.8). Power laws in psychophysics assume a general form of symmetry called scale invariance (Chater & Brown, 1999). Scale invariance preserves identical copies of the observed quantities over transformations of scale. They look similar, and their resemblance is often restricted over lower and upper cut-offs (Chater & Brown, 1999; Gisiger, 2001; Huang, 1987; Kello et al., 2010).

In comparison with previous information-theoretic analyses, the reduction of uncertainty or, equivalently, the gain of information, is measured by entropic function H, which is a continuous time function. The H-function depends on the intrinsic or visual latency t and leads to qualitatively new phenomena. The information entropy of a gaussian process is adopted because for a given variance, gaussian distributions have the maximum associated entropy (Cover & Thomas, 2006). Therefore, the entropic model shows that the time evolution of gaussian channels will favor the minimum transfer of information after coding and thus provide an upper bound to the transmission of information in real neurons. The effects of neural noise are modeled by a one-dimensional diffusion process on the instantaneous firing rate $m(t)$ of the visual system (i.e., the Langevin approximation). The time evolution of σ^2 (see equation 2.7) does not represent the fine details of individual neurons but a coarsely grained or time-smoothed picture of the entire neural network. It should be remembered that the Langevin model takes into account only those processes from encoding time t_0 to time t. No analysis is made from $t = 0$ to encoding time t_0. Therefore, the model does not avoid the presence of skewed distributions. The Langevin model defines multiplicative neural noise from the mean energy E of the background noise or, equivalently, from the diffusion coefficient D and takes into account the presence of excitatory and inhibitory impulses in the network. The existence of background noise that modifies neural responses may be compatible in part with synaptic noise in network interactions (Faisal et al., 2008; Fellous, Rudolph, Destexhe, & Sejnowski, 2003).

It is assumed that the average information capacity of the visual system C_L is nearly constant from encoding time t_0 to time t. Our results do not exclude that C_L might fluctuate over time around a reference value. When

C_L does not remain approximately constant, the Langevin model is not applicable, and other approaches may be suitable (Coffey et al., 2004). Finally, it is interesting to note that the entropic model explains both Weber's law and the CSF as a function of the exponent p. Regarding the CSF, the entropic model is not able to describe the presence of selective filters or multiple neural units tuning to different narrow-bandwidths as previous physiological studies have reported (De Valois & De Valois, 1990).

4.2 Spectral Efficiency. The cost of multiplicative neural noise means that C_L is degraded as compared with Shannon's capacity. For a fixed bandwidth B_0, weak nonlinearities set the visual system close to the ideal case but also give low spectral efficiencies. The values of B_0 are unknown, and the hypothesis that C_L remains approximately constant merits further investigation. However, it is possible to estimate spectral efficiency (see equation 3.7).

Figures 8A and 8B give an example of the spectral efficiency as a function of the signal strength—the intensity background I and the normalized frequency $(f'/f'_{max}) \leq 1$, respectively. The spectral efficiency decreases if ΔH decreases too. Nonlinear mechanisms do not always impair the capacity of the visual system. Figure 8B indicates that the spectral efficiency increases if ΔH increases, in the same way as the perceived visual threshold does (see equation 3.4 and Figures 4B and 6B). Low values of spectral efficiency may be compatible with the high metabolic cost per bit of neuronal communications (Laughlin & Sejnowski, 2003; Laughlin et al., 1998).

4.3 Oscillatory Neural Synchronization, Self-Organized Criticality, and Bayesian Decision Theory. It has been argued (Baird, 1997; Bonnet, 1992; Norwich, 1993; Norwich, Seburn, & Axelrad, 1989) that the exponent p of equation 2.8 shares a common origin with Steven's exponent (Stevens, 1970). Stevens's power law of sensation has been related to some form of gain control in oscillatory neural synchronization (Billock & Tsou, 2005) and is a critical exponent in branching processes (Copelli, Roque, Oliveira, & Kinouchi, 2002; Kinouchi & Copelli, 2006). In the former view, p is related to the degree of coupling. Low values of p $(p < 1)$ will represent strong coupling strength between neurons, and vice versa (Billock & Tsou, 2005). In the latter, low values of p $(p < 1)$ are associated with neurons' operating close to critical states, whereas high values $(p \cong 1)$ represent subcritical activity (Kinouchi & Copelli, 2006). Both views may not be mutually exclusive. Indeed, the theoretical work presented by Billock and Tsou (2005) is similar to an extension of the Kuramoto model for synchronization at SOC (Acebron, Bonilla, Vicente, Ritort, & Spigler, 2005; Kitzbichler et al., 2009).

Figures 4A and 6A showed that nonlinear propagation effects are set close to zero when the background noise strength Et is small. Mathematically, there is a constant $\varepsilon_0$where the spectral content of the mean energy $E(f)$ can be expressed as follows: $\forall \varepsilon_0 > 0, \varepsilon \to 0$, $E(f)t \cong \varepsilon, (\varepsilon \geq \varepsilon_0)$. The

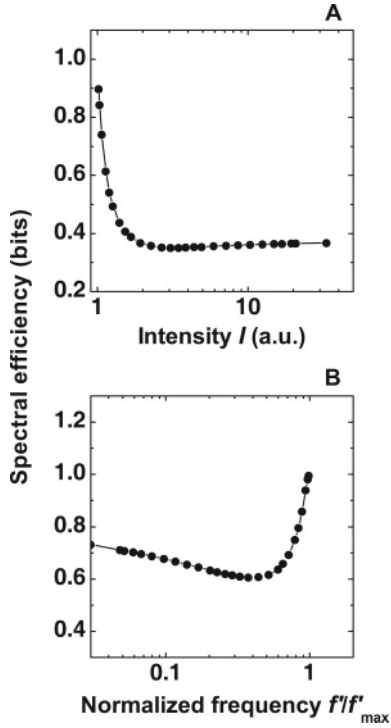

Figure 8: Spectral efficiency. (A). Semilogarithmic plot of spectral efficiency (see equation 3.7) as a function of stimulus intensity I. Threshold values were taken from Weber's law in Figure 4C ($p = 1.1$). (B) Semilogarithmic plot of spectral efficiency as a function of the normalized frequency. Threshold values were taken from Figure 7B (solid circles) ($p = 0.5$). a.u. = arbitrary units.

linear frequency f is the reciprocal of the visual latency t. ε_0 can be rewritten as a function of the encoding time t_0, $\varepsilon_0 = E_0 t_0$, where E_0 is a reference value. In the limit, $\varepsilon = \varepsilon_0$, and taking the frequency in normalized units, $(\tilde{f} = f/f_{\min}) \equiv (t/t_0) > 1$, where $(f = 1/t_0)$ and $(f_{\min} = 1/t)$, the normalized mean energy, $\tilde{E}(\tilde{f}) = [E(\tilde{f})/E_0] > 1$ is

$$\tilde{E}(\tilde{f}) \cong 1/\tilde{f}. \tag{4.1}$$

Equation 4.1 suggests that the optimal transfer of information (ΔH minimum) may apply if the spectral content of background noise involves $1/f$ noise over a limited low-frequency range, a result that is in agreement with SOC (Bak, 1996). Figures 7A and 7B also suggest that ΔH tends to be a minimum when p takes low values ($p < 1$) or, equivalently, from moderate to strong coupling between neurons (Billock & Tsou, 2005). The presence of

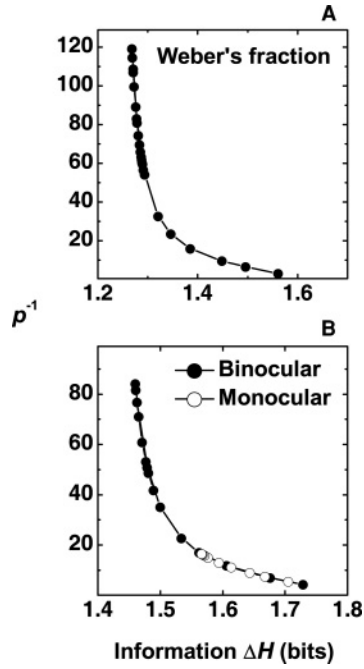

Figure 9: The exponent p. (A) Linear plot of the reciprocal of the exponent p as a function of ΔH (see equation 4.2). ΔH values were taken from Weber's law in Figure 4B ($t_0 = 44$ ms, $C_L = 0.5$ bits/s). (B) Linear plot of the reciprocal of the exponent p as a function of the binocular-monocular information threshold ΔH (solid and open circles, respectively) ($t_0 = 30$ ms, $C_L = 0.5$ bits/s). Binocular and monocular ΔH values were taken from Figure 7A (solid circles and open triangles, respectively).

a power function in equation 2.8 may indicate that the steady-state σ_{ss}^2 has self-organized close to a critical state and the reciprocal of the exponent p should increase ($1/p > 1$) close to the optimal regime (Kinouchi & Copelli, 2006). Therefore, ΔH should minimize when p takes an optimal value. To test this hypothesis, from equation 3.4, it is possible to solve the reciprocal of p as a function of ΔH:

$$\frac{1}{p} = \frac{\ln\left(E_0/k_B T_b\right)}{\ln\left(1 - e^{-2\Delta H}\right) - \ln\left[\left(e^{-2\Delta H}/1 - e^{-2C_L t_0}\right) - 1\right]}. \tag{4.2}$$

The numerator in equation 4.2 is a scaling factor related to the energy expense. The ratio $(E_0/k_B T_b)$ can be fixed to 10^5 (Laughlin et al., 1998). Figures 9A and 9B represent equation 4.2 for Weber's law and the CSF (both

binocular and monocular vision), respectively. Input values are taken from Figures 4C and 7A, respectively. Although the simulations do not reproduce the same numerical values as in previous computational studies (Kinouchi & Copelli, 2006), these two examples show that the reciprocal of the exponent p reaches the maximum value when ΔH minimizes. In Figure 9B, binocular vision enhances ΔH minimum and promotes lower values of the exponent p. This is in agreement with previous psychophysical estimates of p under dark adapting conditions (Ueno, 1977). The modulation of the exponent p is also compatible with previous studies of magnetoencephalograph recordings for weak subthreshold visual signals (Shimono, Owaki, Amano, Kitajo, & Takeda, 2007). Finally, the existence of an optimal Bayesian encoder remains unknown. One possibility might be the state of maximum uncertainty defined by the encoding time (i.e., the maximum loss of information). The encoding time includes those stages for early processing and could provide the prior probabilities (i.e., the prior knowledge) of the different stimulus categories (Geisler & Diehl, 2003).

5 Conclusion

Multiplicative neural noise is beneficial in human vision. It restores the neural SNR over time and shapes certain emerging processes in visual psychophysics. The fundamental insight is that the information entropy or the H-function describes the average uncertainty state of the visual system as a function of intrinsic visual latency. Multiplicative neural noise increases internal uncertainty and leads to the minimum information transfer after efficient coding. The existence of multiplicative noise may be compatible with a computational design that maintains the neural SNR and re allocates the limited energy resources at the same time. Although this analysis has been restricted to Weber's law and contrast sensitivity, there are certain predictions in sensory psychophysics, such as Piéron's law. A promising experimental approach to multiplicative noise and power laws in sensory psychophysics might be the study of temporal variability as a function of the mean value as well as the different stimulus parameters. The minimum transfer of information may constitute a fundamental factor in detection and discrimination tasks under the presence of externally added noise (Aihara et al., 2008; Moss et al., 2004; Ward, 2004), as well as in the functional organization of complex networks.

Acknowledgments

I thank Kenneth H. Norwich (University of Toronto) for helping me clarify the text and the discussion of the issues, and José A. Díaz (University of Granada) and David H. Foster (University of Manchester) for helpful comments and early discussion of the issues. This work was supported by

the Fundação para a Ciência e Tecnologia and by the Center for Physics, University of Minho, Portugal.

References

Acebron, J. A., Bonilla, L. L., Vicente, C. J. P., Ritort, F., & Spigler, R. (2005). The Kuramoto model: A simple paradigm for synchronization phenomena. *Reviews of Modern Physics, 77*(1), 137–185.

Aguilar, M., & Stiles, W. S. (1954). Saturation of the rod mechanism of the retina at high levels of stimulation. *Optica Acta, 1*, 59–65.

Aihara, T., Kitajo, K., Nozaki, D., & Yamamoto, Y. (2008). Internal noise determines external stochastic resonance in visual perception. *Vision Research, 48*(14), 1569–1573.

Anderson, J. S., Lampl, I., Gillespie, D. C., & Ferster, D. (2000). The contribution of noise to contrast invariance of orientation tuning in cat visual cortex. *Science, 290*(5498), 1968–1972.

Anzai, A., Bearse, M. A., Freeman, R. D., & Cai, D. Q. (1995). Contrast coding by cells in the cat's striate cortex: Monocular vs. binocular detection. *Visual Neuroscience, 12*(1), 77–93.

Attneave, F. (1954). Some informational aspects of visual information. *Psychological Review, 61*(3), 183–193.

Baird, J. C. (1997). *Sensation and judgement*. Mahwah, NJ: Erlbaum.

Bak, P. (1996). *How nature works*. New York: Springer-Verlag.

Bak, P., Tang, C., & Wiesenfeld, K. (1987). Self-organized criticality: An explanation of 1/f noise. *Physical Review Letters, 59*(4), 381–384.

Bak, P., Tang, C., & Wiesenfeld, K. (1988). Self-organized criticality. *Physical Review A, 38*(1), 364–374.

Barlow, H. B. (1961). Possible principles underlying the transformation of sensory messages. In W. A. Rosenblith (Ed.), *Sensory communication* (pp. 217–234). Cambridge, MA: MIT Press.

Basalyga, G., & Salinas, E. (2006). When response variability increases neural network robustness to synaptic noise. *Neural Computation, 18*(6), 1349–1379.

Beggs, J. M. (2008). The criticality hypothesis: How local cortical networks might optimize information processing. *Philosophical Transactions of the Royal Society A—Mathematical Physical and Engineering Sciences, 366*(1864), 329–343.

Bell, A. J., & Sejnowski, T. J. (1997). The "independent components" of natural scenes are edge filters. *Vision Research, 37*(23), 3327–3338.

Bialek, W., Scalettar, R., & Zee, A. (1989). Optimal performance of a feedforward network at statistical discrimination tasks. *Journal of Statistical Physics, 57*(1–2), 141–156.

Billock, V. A., & Tsou, B. H. (2005). Sensory recoding via neural synchronization: Integrating hue and luminance into chromatic brightness and saturation. *Journal of the Optical Society of America A, 22*(10), 2289–2298.

Bonnet, C. (1992). Psychophysical scaling within an information-processing approach. *Behavioral and Brain Sciences, 15*(3), 560–561.

Borst, A., & Theunissen, F. E. (1999). Information theory and neural coding. *Nature Neuroscience, 2*(11), 947–957.

Brenner, N., Bialek, W., & de Ruyter van Steveninck, R. (2000). Adaptive rescaling maximizes information transmission. *Neuron, 26*, 695–702.

Buice, M. A., & Cowan, J. D. (2009). Statistical mechanics of the neocortex. *Progress in Biophysics and Molecular Biology, 99*(2–3), 53–86.

Burgess, A. E., Wagner, R. F., Jennings, R. J., & Barlow, H. B. (1981). Efficiency of human visual signal discrimination. *Science, 214*(4516), 93–94.

Campbell, F. W., & Green, D. G. (1965). Monocular versus binocular visual acuity. *Nature, 208*(5006), 191–192.

Carandini, M. (2004). Amplification of trial-to-trial response variability by neurons in visual cortex. *Plos Biology, 2*(9), 1483–1493.

Cecchi, G. A., Sigman, M., Alonso, J. M., Martinez, L., Chialvo, D. R., & Magnasco, M. O. (2000). Noise in neurons is message dependent. *Proceedings of the National Academy of Sciences of the United States of America, 97*(10), 5557–5561.

Chater, N., & Brown, G. D. A. (1999). Scale-invariance as a unifying psychological principle. *Cognition, 69*(3), B17–B24.

Coffey, W. T., Kalmykov, Y. P., & Waldron, J. T. (2004). *The Langevin equation* (2nd ed.). Singapore: World Scientific.

Copelli, M., Roque, A. C., Oliveira, R. F., & Kinouchi, O. (2002). Physics of psychophysics: Stevens and Weber-Fechner laws are transfer functions of excitable media. *Physical Review E, 65*(6), 060901(R).

Cover, T. H., & Thomas, J. A. (2006). *Elements of information theory* (2nd ed.). Hoboken, NJ: Wiley.

de Ruyter van Steveninck, R., & Laughlin, S. B. (1996). The rate of information transfer at graded-potential synapses. *Nature, 379*(6566), 642–645.

De Valois, R. L., & De Valois, K. K. (1990). *Spatial vision*. New York: Oxford University Press.

de Vries, H. L. (1943). The quantum character of light and its bearing upon threshold of vision, the differential sensitivity and visual acuity of the eye. *Physica, 10*, 553–564.

Dean, A. F. (1981). The variability of discharge of simple cells in the cat striate cortex. *Experimental Brain Research, 44*(4), 437–440.

Ermentrout, G. B., Galán, R. F., & Urban, N. N. (2008). Reliability, synchrony and noise. *Trends in Neurosciences, 31*(8), 428–434.

Faisal, A. A., Selen, L. P. J., & Wolpert, D. M. (2008). Noise in the nervous system. *Nature Reviews Neuroscience, 9*(4), 292–303.

Fechner, G. T. (1966). *Elements of psychophysics* (H. E. Adler, trans.). New York: Holt. Reinhart and Winston.

Felipe, A., Buades, M. J., & Artigas, J. M. (1993). Influence of the contrast sensitivity function on the reaction-time. *Vision Research, 33*(17), 2461–2466.

Fellous, J. M., Rudolph, M., Destexhe, A., & Sejnowski, T. J. (2003). Synaptic background noise controls the input/output characteristics of single cells in an in vitro model of in vivo activity. *Neuroscience, 122*(3), 811–829.

Fienberg, S. E. (1974). Stochastic models for single neuron firing trains: A survey. *Biometrics, 30*(3), 399–427.

Finn, I. M., Priebe, N. J., & Ferster, D. (2007). The emergence of contrast-invariant orientation tuning in simple cells of cat visual cortex. *Neuron, 54*(5), 137–152.

Friston, K. (2010). The free-energy principle: A unified brain theory? *Nature Reviews Neuroscience, 11*(2), 127–138.

Friston, K., Kilner, J., & Harrison, L. (2006). A free energy principle for the brain. *Journal of Physiology–Paris, 100*(1–3), 70–87.

Geisler, W. S., & Albrecht, D. G. (1995). Bayesian analysis of identification performance in monkey visual cortex: Nonlinear mechanisms and stimulus certainty. *Vision Research, 35*(19), 2723–2730.

Geisler, W. S., & Diehl, R. L. (2003). A Bayesian approach to the evolution of perceptual and cognitive systems. *Cognitive Science, 27*, 379–402.

Gilden, D. L. (2001). Cognitive emissions of 1/f noise. *Psychological Review, 108*(1), 33–56.

Gilden, D. L., Thornton, T., & Mallon, M. W. (1995). 1/f noise in human cognition. *Science, 267*(5205), 1837–1839.

Gisiger, T. (2001). Scale invariance in biology: Coincidence or footprint of a universal mechanism? *Biological Reviews, 76*(2), 161–209.

Globerson, A., Stark, E., Vaadiab, E., & Tishby, N. (2009). The minimum information principle and its application to neural code analysis. *Proceedings of the National Academy of Sciences of the United States of America, 106*(9), 3490–3495.

Gottschalk, A. (2002). Derivation of the visual contrast response function by maximizing information rate. *Neural Computation, 14*(3), 527–542.

Gottschalk, A., Sexton, M. G., & Roschke, G. (2004). Multiplicative neural noise can favor an independent components representation of sensory input. *Network-Computation in Neural Systems, 15*(4), 291–311.

Haken, H. (1977). *Synergetics*. Berlin: Springer-Verlag.

Harris, C. M., & Wolpert, D. M. (1998). Signal-dependent noise determines motor planning. *Nature, 394*(6695), 780–784.

Holt, G. R., Softky, W. R., Koch, C., & Douglas, R. J. (1996). Comparison of discharge variability in vitro and in vivo in cat visual cortex neurons. *Journal of Neurophysiology, 75*(5), 1806–1814.

Hornstein, E. P., Pope, D. R., & Cohn, T. E. (1999). Noise and its effects on photoreceptor temporal contrast sensitivity at low light levels. *Journal of the Optical Society of America A, 16*(3), 705–717.

Huang, K. (1987). *Statistical Physics* (2nd ed.). Hoboken, NJ: Wiley.

Jaynes, E. T. (1957). Information theory and statistical mechanics. *Physical Review, 106*(4), 620–630.

Kasamatsu, T., Polat, U., Pettet, M. W., & Norcia, A. M. (2001). Colinear facilitation promotes reliability of single-cell responses in cat striate cortex. *Experimental Brain Research, 138*(2), 163–172.

Kello, C. T., Beltz, B. C., Holden, J. G., & Van Orden, G. C. (2007). The emergent coordination of cognitive function. *Journal of Experimental Psychology–General, 136*(4), 551–568.

Kello, C. T., Brown, G. D. A., Ferrer-i-Cancho, R., Holden, J. G., Linkenkaer-Hansen, K., Rhodes, T., et al. (2010). Scaling laws in cognitive sciences. *Trends in Cognitive Sciences, 14*(5), 223–232.

Kinouchi, O., & Copelli, M. (2006). Optimal dynamical range of excitable networks at criticality. *Nature Physics, 2*(5), 348–352.

Kitzbichler, M. G., Smith, M. L., Christensen, S. R., & Bullmore, E. (2009). Broadband criticality of human brain network synchronization. *Plos Computational Biology, 5*(3), 13.

Kontsevich, L. L., Chen, C. C., & Tyler, C. W. (2002). Separating the effects of response nonlinearity and internal noise psychophysically. *Vision Research, 42*(14), 1771–1784.

Lamb, T. D. (1987). Sources of noise in photoreceptor transduction. *Journal of the Optical Society of America A, 4*(12), 2295–2300.

Laughlin, S. (1981). A simple coding procedure enhances a neuron's information capacity. *Zeitschrift Fur Naturforschung C—Journal of Biosciences, 36*(9–10), 910–912.

Laughlin, S. B., & Sejnowski, T. J. (2003). Communication in neuronal networks. *Science, 301*(5641), 1870–1874.

Laughlin, S. B., de Ruyter van Steveninck, R., & Anderson, J. C. (1998). The metabolic cost of neural information. *Nature Neuroscience, 1*(1), 36–41.

Legge, G. E., Kersten, D., & Burgess, A. E. (1987). Contrast discrimination in noise. *Journal of the Optical Society of America A, 4*(2), 391–404.

Lennie, P. (1981). The physiological-basis of variations in visual latency. *Vision Research, 21*(6), 815–824.

Lestienne, R. (2001). Spike timing, synchronization and information processing on the sensory side of the central nervous system. *Progress in Neurobiology, 65*(6), 545–591.

Lewen, G. D., Bialek, W., & de Ruyter van Steveninck, R. (2001). Neural coding of naturalistic motion stimuli. *Network-Computation in Neural Systems, 12*(3), 317–329.

Lindner, B., Garcia-Ojalvo, J., Neiman, A., & Schimansky-Geier, L. (2004). Effects of noise in excitable systems. *Physics Reports—Review Section of Physics Letters, 392*(6), 321–424.

Linsker, R. (1988). Self-organization in a perceptual network. *Computer, 21*(3), 105—117.

Linsker, R. (1990). Perceptual neural organization: Some approaches based on network models and information theory. *Annual Review of Neuroscience, 13*, 257–281.

Linsker, R. (1992). Local synaptic learning rules suffice to maximize mutual information in a linear network. *Neural Computation, 4*(5), 691–702.

Linsker, R. (1997). A local learning rule that enables information maximization for arbitrary input distributions. *Neural Computation, 9*(8), 1661–1665.

Lu, Z. L., & Dosher, B. A. (1999). Characterizing human perceptual inefficiencies with equivalent internal noise. *Journal of the Optical Society of America A, 16*(3), 764–771.

Luce, R. D. (1986). *Response times*. New York: Oxford University Press.

Medina, J. M. (2009). $1/f^{\alpha}$ noise in reaction times: A proposed model based on Piéron's law and information processing. *Physical Review E, 79*(1), 011902.

Meese, T. S., Challinor, K. L., & Summers, R. J. (2008). A common contrast pooling rule for suppression within and between the eyes. *Visual Neuroscience, 25*(4), 585–601.

Moss, F., Ward, L. M., & Sannita, W. G. (2004). Stochastic resonance and sensory information processing: A tutorial and review of application. *Clinical Neurophysiology, 115*(2), 267–281.

Mullen, K. T. (1985). The contrast sensitivity of human color vision to red-green and blue-yellow chromatic gratings. *Journal of Physiology–London, 359*, 381–400.

Norwich, K. H. (1977). Information received by sensory receptors. *Bulletin of Mathematical Biology, 39*(4), 453–461.

Norwich, K. H. (1981). Uncertainty in physiology and physics. *Bulletin of Mathematical Biology, 43*(2), 141–149.

Norwich, K. H. (1982). Perception as an active process. *Mathematics and Computers in Simulation, 24*(6), 535–539.

Norwich, K. H. (1993). *Information, sensation, and perception*. San Diego: Academic Press.

Norwich, K. H., Seburn, C. N. L., & Axelrad, E. (1989). An informational approach to reaction times. *Bulletin of Mathematical Biology, 51*(3), 347–358.

Norwich, K. H., & Wong, W. (1995). A universal model of single-unit sensory receptor action. *Mathematical Biosciences, 125*(1), 83–108.

Norwich, K. H., & Wong, W. (1997). Unification of psychophysical phenomena: The complete form of Fechner's law. *Perception and Psychophysics, 59*(6), 929–940.

Nutting, P. G. (1907). The complete form of Fechner's law. *Bulletin of the Bureau of Standards, 3*, 59–64.

Olshausen, B. A., & Field, D. J. (1996). Emergence of simple-cell receptive field properties by learning a sparse code for natural images. *Nature, 381*(6583), 607–609.

Pelli, D. G. (1985). Uncertainty explains many aspects of visual contrast detection and discrimination. *Journal of the Optical Society of America A, 2*(9), 1508–1532.

Pelli, D. G. (1990). The quantum efficiency of vision. In C. Blakemore (Ed.), *Vision: Coding and efficiency* (pp. 3–24). Cambridge: Cambridge University Press.

Pelli, D. G., & Farell, B. (1999). Why use noise? *Journal of the Optical Society of America A, 16*(3), 647–653.

Prost, J., Joanny, J. F., & Parrondo, J. M. R. (2009). Generalized fluctuation-dissipation theorem for steady-state systems. *Physical Review Letters, 103*(9), 4.

Ricciardi, L. M., & Lansky, P. (2002). Diffusion models of neural activity. In M. A. Arbib (Ed.), *The handbook of brain theory and neural networks: The second edition* (pp. 343–348). Cambridge, MA: MIT Press.

Robson, J. G. (1966). Spatial and temporal contrast-sensitivity functions of visual system. *Journal of the Optical Society of America, 56*(8), 1141–1142.

Rose, A. (1946). The sensitivity performance of the human eye on an absolute scale. *Journal of the Optical Society of America, 38*, 196–208.

Rovamo, J. M., Kankaanpää, M. I., & Hukkonen, H. (1999). Modelling spatial contrast sensitivity functions for chromatic and luminance-modulated gratings. *Vision Research, 39*, 2387–2398.

Schieve, W. C., Bulsara, A. R., & Davis, G. M. (1991). Single effective neuron. *Physical Review A, 43*(6), 2613–2623.

Sejnowski, T. J., & Paulsen, O. (2006). Network oscillations: Emerging computational principles. *Journal of Neuroscience, 26*(6), 1673–1676.

Shimono, M., Owaki, T., Amano, K., Kitajo, K., & Takeda, T. (2007). Functional modulation of power-law distribution in visual perception. *Physical Review E, 75*(5), 5.

Simoncelli, E. P., & Olshausen, B. A. (2001). Natural image statistics and neural representation. *Annual Review of Neuroscience, 24*, 1193–1216.

Singer, W. (1999). Neuronal synchrony: A versatile code for the definition of relations? *Neuron, 24*(1), 49–65.

Smith, P. L., & Ratcliff, R. (2004). Psychology and neurobiology of simple decisions. *Trends in Neurosciences, 27*(3), 161–168.

Sperling, G. (1989). Three stages and two systems of visual processing. *Spatial Vision, 4*(2/3), 183–207.

Squires, G. L. (2001). *Practical physics*. Cambridge: Cambridge University Press.

Stevens, S. S. (1970). Neural events and the psychophysical law. *Science, 170*(3962), 1043–1050.

Stocker, A. A., & Simoncelli, E. P. (2006). Noise characteristics and prior expectations in human visual speed perception. *Nature Neuroscience, 9*(4), 578–585.

Strong, S. P., Koberle, R., de Ruyter van Steveninck, R., & Bialek, W. (1998). Entropy and information in neural spike trains. *Physical Review Letters, 80*(1), 197–200.

Tolhurst, D. J., Movshon, J. A., & Dean, A. F. (1983). The statistical reliability of signals in single neurons in cat and monkey visual cortex. *Vision Research, 23*, 775–785.

Torre, V., Ashmore, J. F., Lamb, T. D., & Menini, A. (1995). Transduction and adaptation in sensory receptor cells. *Journal of Neuroscience, 15*(12), 7757–7768.

Tyler, C. W., & Chen, C. C. (2000). Signal detection theory in the 2AFC paradigm: Attention, channel uncertainty and probability summation. *Vision Research, 40*(22), 3121–3144.

Ueno, T. (1977). Reaction time as a measure of temporal summation at suprathreshold levels. *Vision Research, 17*(2), 227–232.

Uzzell, V. J., & Chichilnisky, E. J. (2004). Precision of spike trains in primate retinal ganglion cells. *Journal of Neurophysiology, 92*(2), 780–789.

Van Hateren, J. H. (1992). A theory of maximizing sensory information. *Biological Cybernetics, 68*(1), 23–29.

Victor, J. D., Blessing, E. M., Forte, J. D., Buzas, P., & Martin, P. R. (2007). Response variability of marmoset parvocellular neurons. *Journal of Physiology–London, 579*(1), 29–51.

Vogels, R., Spileers, W., & Orban, G. A. (1989). The response variability of striate cortical neurons in the behaving monkey. *Experimental Brain Research, 77*(2), 432–436.

Wagenmakers, E. J., & Brown, S. (2007). On the linear relation between the mean and the standard deviation of a response time distribution. *Psychological Review, 114*(3), 830–841.

Wainwright, M. (1999). Visual adaptation as optimal information transmission. *Vision Research, 39*, 3960–3974.

Ward, L. M. (2002). *Dynamical cognitive science*. Cambridge, MA: MIT Press.

Ward, L. M. (2004). Psychophysics of stochastic resonance. *Fluctuation and Noise Letters, 4*(1), L11–L21.

Ward, L. M., & Kitajo, K. (2005). *Attention excludes noise. Does it exclude stochastic resonance?* Paper presented at the Fourth International Conference on Unsolved Problems of Noise and Fluctuations in Physics, Biology and High Technology. College Park, MD: American Institute of Physics.

Weber, E. H. (1834). *De pulsu, resorptione, audita et tactu, Annotationes anatomicae et physiologicae*. Leipzig: Koehler.

Wyszecki, G., & Stiles, W. S. (1982). *Color science: Concepts and methods, quantitative data and formulae* (2nd ed.). Hoboken, NJ: Wiley.

Yeh, F. C., Tang, A. N., Hobbs, J. P., Hottowy, P., Dabrowski, W., Sher, A., et al. (2010). Maximum entropy approaches to living neural networks. *Entropy, 12*(1), 89–106.

Zhaoping, L. (2002). Optimal sensory encoding. In M. A. Arbib (Ed.), *The handbook of brain theory and neural networks: The second edition* (pp. 815–919). Cambridge, MA: MIT Press.

Zhaoping, L. (2006). Theoretical understanding of the early visual processes by data compression and data selection. *Network: Computation in Neural Systems, 17*, 301–334.

Received October 12, 2009; accepted September 15, 2010.

1/*f* noise in human color vision: the role of S-cone signals

José M. Medina,[1,*] and José A. Díaz[2]

[1]*Center for Physics, University of Minho, Campus de Gualtar, 4710-057 Braga, Portugal*
[2]*Departamento de Optica, Universidad de Granada, 18071 Granada, Spain*
**Corresponding author: jmanuel@fisica.uminho.pt*

Received September 1, 2011; revised November 15, 2011; accepted November 16, 2011; posted November 28, 2011 (Doc. ID 153875); published January 13, 2012

We examine the functional role of S-cone signals on reaction time (RT) variability in human color vision. Stimuli were selected along red–green and blue–yellow cardinal directions and at random directions in the isoluminant plane of the color space. Trial-to-trial RT variability was not statistically independent but correlated across experimental conditions and exhibited 1/*f* noise spectra with an exponent close to unity in most of the cases. Regarding contrast coding, 1/*f* noise for random chromatic stimuli at isoluminance was similar to that for achromatic stimuli, thus suggesting that S-cone signals reduce variability of higher order color mechanisms. If we regard spatial coding, the effect of S-cone density in the retina on RT variability was investigated. The magnitude of 1/*f* noise at 16 min of arc (S-cone free zone) was higher than at 90 min of arc in the blue–yellow channel, and it was similar for the red–green channel. The results suggest that S-cone signals are beneficial and they modulate 1/*f* noise spectra at postreceptoral stages. The implications related to random multiplicative processes as a possible source of 1/*f* noise and the optimal information processing in color vision are discussed.

OCIS codes: 330.1720, 330.5310, 330.1880, 330.1800, 330.4060.

1. INTRODUCTION

Human color processing is intrinsically noisy in the same way as in other sensory processes [1]. Noise is early produced at the level of photoreceptor transduction [1–4]. Moreover, it is also present at postreceptoral stages as well as at multiple levels from cortical neurons to visual perception [1,2,5–7]. Internal noise is commonly assumed as a disadvantage; however, it could play a constructive role such as in synaptic communication [6], motor planning [8], or the design and organization of neural circuits [1]. How internal noise affects trichromatic color vision at each stage is an issue that remains to be determined. Current color vision models assert that long (L)- and middle (M)-wavelength-sensitive cone signals are combined into a subcortical nonopponent luminance channel (L + M cone axis), and a red–green chromatic-opponent channel (L–M cone axis). There is a second subcortical chromatic-opponent mechanism that supports blue–yellow vision, and it is mediated by short (S)-wavelength-sensitive cone signals [S – (L + M) cone axis] [9–12]. S cones mainly project to blue-on ganglion cells and are segregated in the koniocellular (*K*) pathway [11–17]. *K* cells have the smallest size [14–16] and a sluggish component in the cortex in relation to the parvocellular (*P*) pathway [18], which mediates red–green opponency [11,12,14,15,17].

Although photoreceptor noise influences the formation of color discrimination thresholds [19], postreceptoral noise is often assumed uncorrelated, stimulus-independent, and separated for each chromatic-opponent mechanism [20–22]. However, irregular variability from simple reaction times (RTs) at suprathreshold conditions, which we will refer to as a part of internal noise manifestation [1], can be considered as stochastic [23], although it does not need to be considered totally random [1,7]. RT variability increases as the mean response level increases [23–27], and it can depend on basic stimulus features such as its contrast [23,25,27,28] and spatial frequency [29].

Any stochastic time signal with a Fourier power spectrum proportional to $1/f^{\alpha}(\alpha > 0)$, where f denotes the frequency, can maintain long-range correlations over multiple time scales. Low and high frequencies correspond to coarse and fine resolution, respectively, and thus the $1/f^{\alpha}$ Fourier spectrum is a measure of how much a noisy signal resembles itself at different frequency bands. When $\alpha = 0$ no correlation between the samples exists; hence, the spectrum is flat and all the frequencies contribute equally, i.e., "white noise." When $\alpha = 2$ the noise power spectrum is dominated by low frequencies and the expected form of the Fourier spectrum is similar to the time series created by a random walk, such as the Brownian motion or "Brown noise" (i.e., strong long-term correlations). Besides these noises, many different stochastic processes have a Fourier spectrum with $\alpha \cong 1$ and it was called "1/*f* noise," "flicker noise," "pink noise," or "1/*f* scaling." The discovery of 1/*f* noise was a pioneer in the irregular electron fluctuations in vacuum tubes (coined the "flicker effect") [30]. 1/*f* scaling has been a common feature in different electronic and photonic devices as well as in a wide range of diverse biological and social phenomena [31–33], suggesting perhaps a common underlying principle. 1/*f* noise in the nervous system has been observed at multiple levels of analysis. For instance, 1/*f* noise has been found in the voltage fluctuations in the nerve membrane [34], in the squid giant axon [35], in the autonomic nervous system (e.g., pupil light reflex and focal accommodation) [36], electroencephalogram recordings [37,38], and functional magnetic resonant imaging (fMRI) signals [39,40]. In human cognition, 1/*f* noises are found in music and speech [41] or in the estimation of time [5]. In motor behavior, 1/*f* noises appear in sensorimotor coordination [42] and in body movements (e.g., human sway and gait) [35,43]. 1/*f* noise is considered a signature of complex behavior because it often appears in stochastic processes that they resemble themselves across multiple

scales or random fractals. For a review of $1/f$ noise in human behavior, see [32,43–45].

Trial-to-trial RT fluctuations also exhibit $1/f^{\alpha}$ Fourier spectra with the exponent α close to unity in normal color vision [25,46]. The existence of $1/f$ noise in RTs is not an artifact from instrument noise, and it is thought to be caused from neural activity [46–50] and modulated by task difficulty [45,47,48,51]. Taking into account the three cardinal directions of the color space, the magnitude of $1/f$ noise was lower for achromatic than for red–green isoluminant stimuli and both were lower than for blue–yellow stimuli at isoluminance [25]. A miniaturization effect was suggested across different subcortical pathways: the smaller the axon diameter of neurons that transport color signals such as in K cells, the higher $1/f$ noise will be [25], in the same way as electrons moving through thin resistors in solid-state physics [30,31]. S-cone signals therefore can raise a substantial amount of $1/f$ noise in blue–yellow vision and they could be an important limiting factor in higher order color mechanisms where chromatic-opponent signals are transformed [10–12,17,52–54]. Further, the efficient adaptation of cortical neurons to $1/f$ scaling [33,55] could modulate color processing in an optimal way. However, the potential benefits of S-cone signals in $1/f$ noise are largely unknown.

In the present study, we investigate the functional role of S-cone vision in $1/f$ noise derived from RTs taking into account the effects of chromatic contrast and the spatial processing of the retinal image. Although the dependence of RT to chromatic contrast and spatial summation has been widely studied [56–64], previous RT studies have taken the average mean response from a few static experimental conditions. This has ignored the presence of correlations or memory effects. The research on RT variability is important for revealing the correlation structure at different time scales, and it adds new information on understanding the role of stochastic latency mechanisms in color coding, their nontrivial statistical properties, and complex dynamics. In this work, two different sets of experiments were designed. In the first set, the trial-to-trial variability of RTs was measured for random chromatic variations at isoluminance (simultaneous L-, M- and S-cone variations). Achromatic signals were used as the test control condition. Thus, we extend previous works on RTs and noise by comparing $1/f$ noise for higher order color mechanisms tuned at intermediate directions in the isoluminant plane [10,52–54], to the superior performance of RTs for achromatic stimuli [25]. In the second set of experiments, the effect that the S-cone density in the human retina has on RT variability was investigated. S cones are absent over 20 min of arc in the central fovea or *foveola*. Beyond this region, the density of S cones increases up to a maximum around 1° eccentricity, and then it decreases toward the retinal periphery, reaching an asymptotic value around 5° eccentricity [16,65]. Blue–yellow isoluminant stimuli were selected for two different stimulus sizes: 16 min of arc (S-cone free zone) and 90 min of arc. Red–green isoluminant signals were also selected as the test control condition for the same stimulus sizes. This affords us the possibility to examine the absence or not of S-cone signals on RT variability, i.e., foveal tritanopia [16,65], and to compare them to the superior performance of RTs for red–green signals [25,62].

Among the multiple mathematical models that can explain the production of $1/f$ noise in human cognition [5,26,38,44–48,66,67], those corresponding to multiplicative processes, or the product of stochastic variables in cascade, are of particular interest in RTs. Multiplicative process can generate heavy-tailed distributions in the form of log–normal, power laws or a mixture of both [26], and they often implicate scaling laws in psychophysics [26,67,68]. A classic example of scaling law in RTs is Piéron's law, where the mean RT, t_{RT}, decreases by the power law as a function of the stimulus strength [23,69]:

$$t_{\mathrm{RT}} = t_{\mathrm{RT}_0} + \mu S^{-p}, \tag{1}$$

where S is the stimulus strength (e.g., stimulus contrast), p and μ are parameters, and t_{RT_0} is the asymptotic plateau reached at very high stimulus strength. Piéron's law is shape-invariant across temporal scales, and it can be better explained as the result of a multiplicative noise process [67,70].

One common way to study the stochastic latency mechanisms that generate RT variability deals with the analysis of the hazard functions $h(t)$ [23,26,27,63,71]. The hazard function is defined as the quotient between the probability density function (pdf) $f(t)$, and the reciprocal of the cumulative distribution function $F(t)$, i.e., $h(t) = f(t)/[1 - F(t)]$ (measured in units of events per millisecond). It represents the probability of an event occurring at time t, given that it has not occurred yet [23,26,72]. Here, the term "event" refers to the response or the completion of the visual task, i.e., chromatic detection at suprathreshold conditions and motor execution. The hazard function has the same information as the pdf or the cumulative distribution function, and it is possible to derive $h(t)$ from the pdf or the $F(t)$ by integration and vice versa [23]. However, the analysis of the hazard functions offers distinctive information in the right tails of the RT distributions, and it can discriminate between experimental pdfs that have very similar shapes [23]. The hazard functions are more useful than the simplified method of taking mean values to examine the structure of RT distributions at different stimulus strength [23,27,63,71,73], to distinguish models of RTs [23,71], and to model the capacity or the total completion stage in binocular color processing [74,75].

At least two type of multiplicative process have been identified in the hazard functions. At suprathreshold levels, hazard functions of typical RT distributions exhibits a high-tailed peaked form—that is, they first increase up to reaching a maximum, following a decrease toward a nonzero value, and then they reach an asymptotic level that remains constant. Therefore, signals well above the threshold level present hazard functions that have been interpreted as evidence of transient or log–normal dominant dynamics [23,26]. On the contrary, at near-threshold level conditions, the peak is absent or attenuated and the visual system will show evidence of quasi-sustained or power-law dominant dynamics [23,26]. In previous works, the hazard functions were estimated for chromatic-opponent responses at isoluminance [27,63]. Comparisons between red–green hazard functions at different chromatic-contrast increments and stimulus size were compatible with the existence of power-law dominant activity at low chromatic-contrasts [27,63], and low stimulus size [27]. In the present work, we expand previous results on the hazard functions to blue–yellow signals at different chromatic-contrast levels and stimulus size.

2. GENERAL METHODS

The methods reported in this study have been presented elsewhere [58–60,63,74]. All RT data analyzed correspond to original time series collected across multiple experimental conditions and observers over years [76,77]. The complete description of the experimental device, color-calibration method, stimuli and procedure has also been described elsewhere [56,58,59,63,74,78,79]. Consequently, only a brief summary of them will be presented here.

A. Observers

The two authors (JM and JA) and two additional observers were used (JR and MC). All had normal color vision according to the Ishihara and Farnswoth–Munsell 100-hue tests. All had experience in RT experiments except observer MC, who was naïve. Observers JA, JM, and JR wore corrective lenses. JM, JA, and JR participated in the RT experiments on random chromatic variations at isoluminance [74]. JA and MC participated in the experiments on spatial summation at isoluminance [58]. All the experiments were performed in accordance with the Declaration of Helsinki [80].

B. Experimental Device

The display system consisted of a cathode ray tube (CRT) color monitor (Sony Trinitron GDM 2038) connected to a graphics card (8 bits) in a computer. The monitor had a resolution of 1024×768 with a frame rate of 74 Hz. The chromaticity and luminance of stimuli were controlled by periodic calibrations using a SpectraScan PR-704 Photo Research spectroradiometer. A CRT color-calibration method was used [78,79] to produce stimuli with accurate CIE 1931 (x, y) coordinates and luminance. Observers were seated 70 cm from the CRT in an isolated dark room, and a chin rest was used for head stabilization.

C. Procedure

RTs at isoluminance were determined following the standard procedure. That is, isoluminant variations were presented over a spatially coincident steady reference stimulus on a dark background. This prevented any transient luminance changes and, thus, only pure hue changes were observed by the subject [58,59,63,73,74,81]. The goodness of isolation to luminance intrusions has been tested previously [58,59,63,74].

At the beginning of each experimental session, the subject was allowed to adapt for 3 min to darkness and 3 additional min for adapting to the reference stimulus. At this point, a tone followed by a 7 s pause signaled the start of a trial. After a random delay (3–7 s, uniform sampling distribution) to avoid anticipation, the reference stimulus was changed to the test stimulus, the change being synchronized with the beginning of the video refresh cycle. The test stimulus that replaced the reference remained on until the subject responded by pressing the button on the mouse connected to the computer, thus indicating that a stimulus change had been detected. Immediately following a response, the test stimulus was replaced by the reference stimulus. Observers did not know which stimulus was the next in the sequence and their task consisted only of responding as soon as possible. Each test stimulus was randomly presented a total of 8 times during a session. A number of sessions were performed until reaching a distribution of no less than 80 RTs in each test. An MS-DOS application was developed to run the RT experiments and as well as to program the 8253 clock timer by using assembler language instructions providing a 1 ms accuracy in RT measurements [58–60,63,74].

D. Data Analysis

False alarms were established as those below 110 ms [63,74]. Those RTs exceeding the minimum interstimulus time interval of 3000 ms were rejected as misses. Isoluminant stimuli were scaled using the root mean square cone contrast, $[(L_C^2 + M_C^2 + S_C^2)]^{1/2}$, where L_C, M_C, and S_C, represent the L-, M-, and S-cone signal difference between the test and the reference stimulus divided by the L-, M-, and S-cone values of the reference one, respectively [82]. Cone excitations inputs for the L-, M-, and S-cone values were calculated by using the (x', y', z') Judd-modified chromaticity coordinates and the Smith and Pokorny cone fundamentals [2,83].

1. Power Spectra

We have followed the spectral estimation method proposed in previous studies on RTs and $1/f$ noise based on Welch's method [5,47,84]. The standard raw periodogram based on the fast Fourier transform does not provide a reliable estimation of the power spectrum because the variance in each data point does not decrease as the data length increases [84]. Welch's method is an improved version of the periodogram. It splits the data into overlapped window segments at half their length. Then it computes the periodogram over the overlapping windows and averages to obtain an estimation of the power spectral density. This gives a better reduction of the variance in each data point than without overlapping [84]. To reduce distortion from spectral leakage in the periodogram estimation [84], data windowing was done by using the Bartlett window [49,84]. In Welch's method there is a trade-off between variance reduction and resolution. The lowest frequency that can be resolved depends on the window size, and thus, small and large windows are often assigned for high and low frequencies, respectively [5,47]. In this work, the power spectrum was generated for each observer separately from the original RT series at window sizes of 4, 8, 16, 32, 64, 128, 256, and 512. The final composite spectrum was the result of the lowest eight frequencies that can be resolved at the different window sizes, and it was normalized to these sizes in order to preserve the frequency order [5,47]. If necessary, zero padding was added at the end of the original RT series to complete 1024 data points [84]. In some cases, a seven-point power spectrum was generated from 512 data points at window sizes of 4, 8, 16, 32, 64, 128, and 256. In all cases, the power spectrum was fitted to a power function by means of a nonlinear least-square fitting procedure based on the minimization of the Chi-square statistics [84]. Parameter fitting was done by applying the Levenberg–Marquardt algorithm [84]. The regression coefficient R square or R^2 adjusted to the different degrees of freedom evaluated the goodness of fit.

2. Hazard Functions

For each observer and for each experimental configuration, hazard functions were calculated by using a common procedure in RTs and visual perception—that is, the "random smoothing method" with a degree of smoothing $j = 20$ [23,27,63,72,73]. The random smoothing method is

nonparametric, and it divides the time axis in intervals defined as the difference between ordered RTs from the original RT series. Each time interval has assigned a constant hazard rate that is the result of some form of averaging over the previous j intervals, i.e., by using equal sample sizes [23,72,73].

3. EXPERIMENT 1

A. Stimuli

A set of 12 chromatic stimuli was selected in the isoluminance plane, having a luminance level of 15 cd/m^2. They correspond to random chromatic variations in the isoluminant plane and therefore activating simultaneously both red–green and blue–yellow chromatic channels (simultaneous L-, M-, and S-cone variations) [74]. For each observer, the isoluminance condition was reached by using the method of heterochromatic flicker photometry at the frequency of 12.3 Hz and at 15 cd/m^2 [58,59,63,74,81]. Figure 1(a) represents their CIE (x, y) values selected in the CIE 1931 chromaticity diagram.

We also used 12 achromatic stimuli as the control condition on the luminance axis, i.e., perpendicular to the CIE 1931 chromaticity diagram. They were chosen with chromaticity coordinates equal to those of the equal-energy white ($x = 0.333$, $y = 0.333$) and with luminance values between 3 and 27 cd/m^2 at steps of 2 cd/m^2 [60]. For both chromatic and achromatic stimuli, the reference stimulus was an achromatic one, having a luminance of 15 cd/m^2, with chromaticity coordinates also identical to the equal-energy white [see Fig. 1(a)]. The reference stimulus was also the adapting one. All stimuli including the reference stimulus had an angular size of 90 min of arc in diameter at the viewing distance of 70 cm, as depicted in Fig. 1(b). They were uniform circular patches presented on a dark background, and they were observed on fovea with natural pupils by using the right eye. The nontested eye was covered with a black patch. Observers were instructed to maintain their central fixation and to minimize their involuntary eye movements. This was improved for naïve as well as for experienced observers by making several training RT sessions. When there were no significant differences in their mean and in their standard deviation (SD) between training sessions, the observers were ready to begin the main experiments. This was particularly checked in Experiment 2 when using the smaller stimulus size. The same training sessions were also used to minimize learning effects. All the RTs measured during the training sessions were discarded in the subsequent analyses. In Experiment 1, the total number of RTs analyzed was 5825.

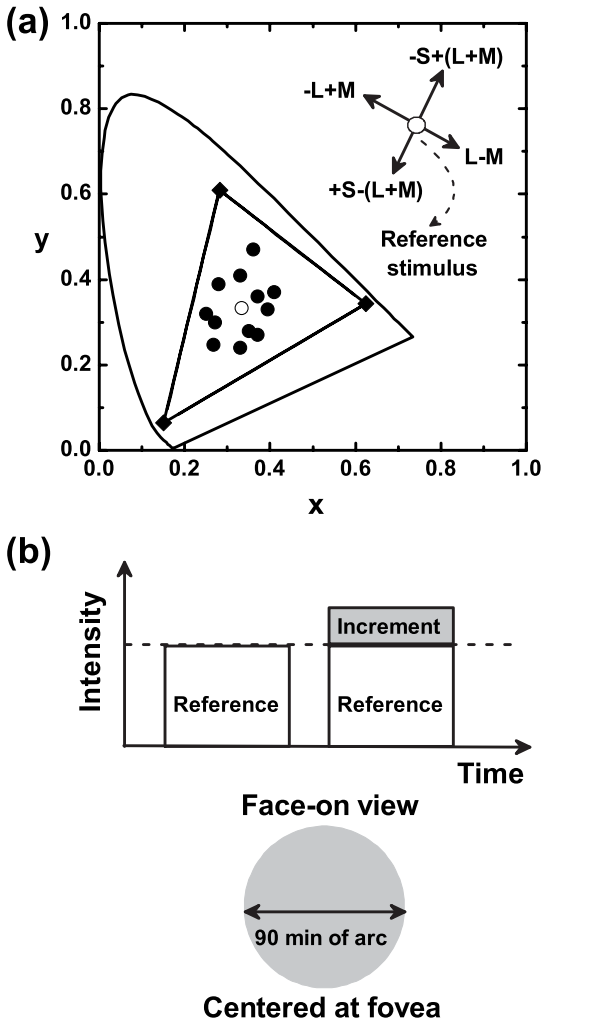

Fig. 1. (a) Random chromatic stimuli at isoluminance (black circles) represented in the CIE 1931 chromaticity diagram. The empty circle indicates the reference adapting stimuli. The triangle indicates the monitor color gamut delimited by the coordinates of the red, green, and blue phosphor primaries (black diamonds). For the fixed reference stimuli, the schematic diagram at the top-right border indicates the corresponding L–M- and S-cone axis variations. Level of reference luminance: 15 cd/m^2. (b) Temporal and spatial configuration of the stimuli selected.

B. Results

Figure 2 represents, for three observers (JA, JM, and JR) and for each signal type (chromatic and achromatic), the RT series in a linear plot ordered in the time axis as a function of the trial number (raw data). Both chromatic and achromatic RT series exhibit characteristic waves running through them, suggesting the presence of correlations in the same way as in previous RT studies [46].

The mean RT for random chromatic variations at isoluminance was higher (JA, 385.1 ms; JM, 367.8 ms; JR, 385.6 ms) than for achromatic variations (JA, 351.2 ms; JM, 330.3 ms; JR, 358.5 ms). Mean RT differences between chromatic and achromatic stimuli are less than 38 ms. RT raw data were grouped as a function of the stimulus contrast for each observer and for each signal class (chromatic or achromatic). The trial order in Fig. 2 was neglected, and the SD and the mean RT values were calculated at each experimental condition (12 chromatic and 12 achromatic variations). Figure 3 shows, in a double logarithmic plot, the RT variability in each stimulus contrast condition as measured by the SD as a function of the mean RT. As the SD is measured over longer RT responses, more variability is included. Although other measures of spread are more conservative, they provide similar results [27]. Figure 3 indicates that RT variability is not bounded but correlated across achromatic variations and increases monotonically, similar to a Weber-like function [23–27]. This is reminiscent of scale invariance, a general form of symmetry that preserves the shape of the analyzed function across multiple scales by a power-law relationship and is usually found in random fractals [44,68,85]. The coefficient of variation, defined as the ratio between the SD and the

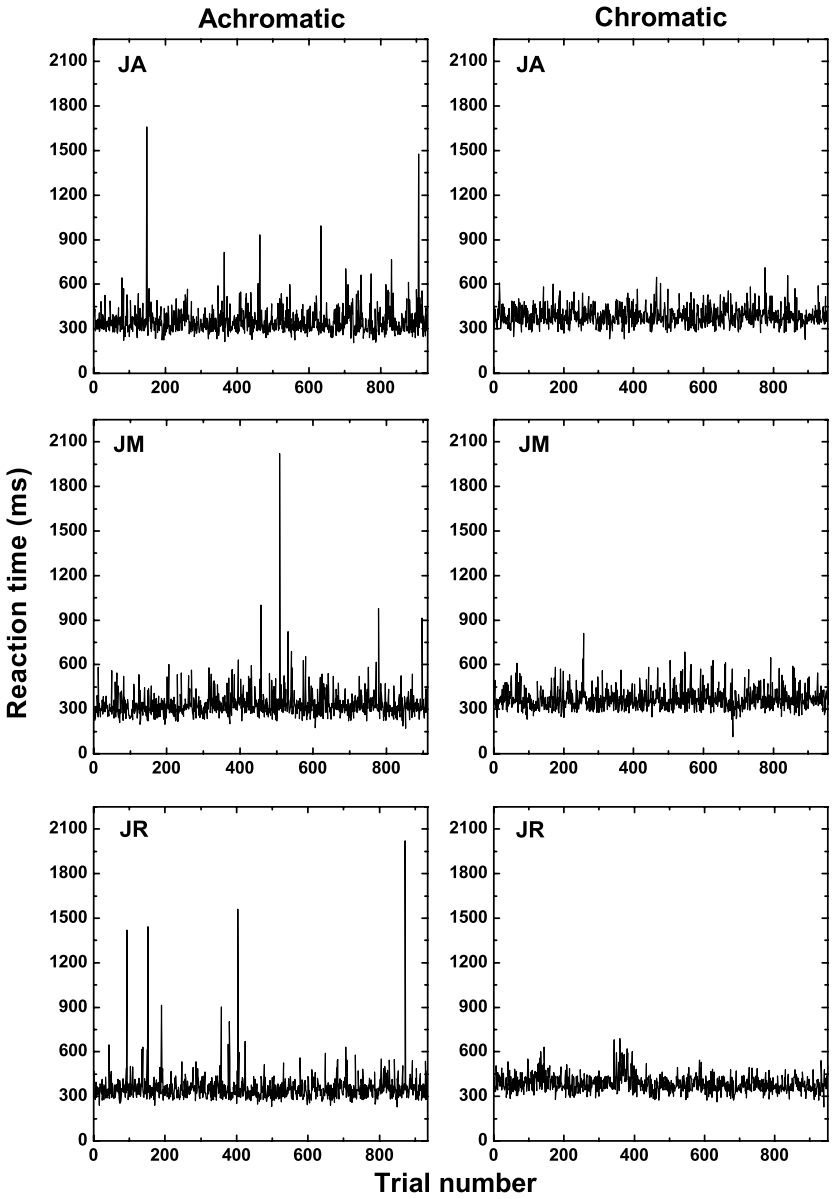

Fig. 2. Plot of RT series (in ms) for random chromatic variations at isoluminance (right column) and those for achromatic variations (left column). Data are presented to observers JA, JM, and JR separately.

mean, gives an estimation of the slope in Fig. 3 and was on average lower than unity (JA, 0.24; JM, 0.26; JR, 0.20), indicating that RT dynamics does not follow a Poisson process (a ratio equal to unity).

However, if we regard random chromatic variations at isoluminance, the mean RT at each experimental condition is higher but the range spanned by the SD was unexpectedly lower and similar to achromatic variations. The coefficient of variation averaged over all isoluminant conditions was also sub-Poisson and lower than achromatic variations (JA, 0.16; JM, 0.19; JR, 0.14). Figure 4 represents, in a double logarithmic plot, the estimated eight-point power spectra from RT series. Note that frequency is not expressed in hertz here but in cycles per trial [5,46,47].

The results confirm the presence of $1/f$ noise for achromatic variations [25]. The estimated exponent was very close to unity (black lines, in all cases $R^2 > 0.99$). There is also some contribution of white noise (i.e., flat spectrum) at high frequencies [5,46,47]. This issue will be discussed below. The results show the existence of $1/f$ noise (gray lines, in all cases $R^2 > 0.99$) for random chromatic variations at isoluminance. Power spectra were similar or slightly higher than for achromatic stimuli, whereas the exponent was close to unity for JA (1.02) and slightly lower for JM (0.98) and JR (0.97).

C. Discussion

Previous works have concluded the existence of $1/f$ noise along the cardinal directions in the color space. The magnitude of $1/f$ noise was higher for blue–yellow than for red–green signals at isoluminance, and both were higher than for achromatic variations [25]. The results in Figs. 3 and 4 extend these results and clearly demonstrate that S-cone signals are not detrimental but they can contribute positively by reducing the magnitude of $1/f$ noise when both L, M, and S

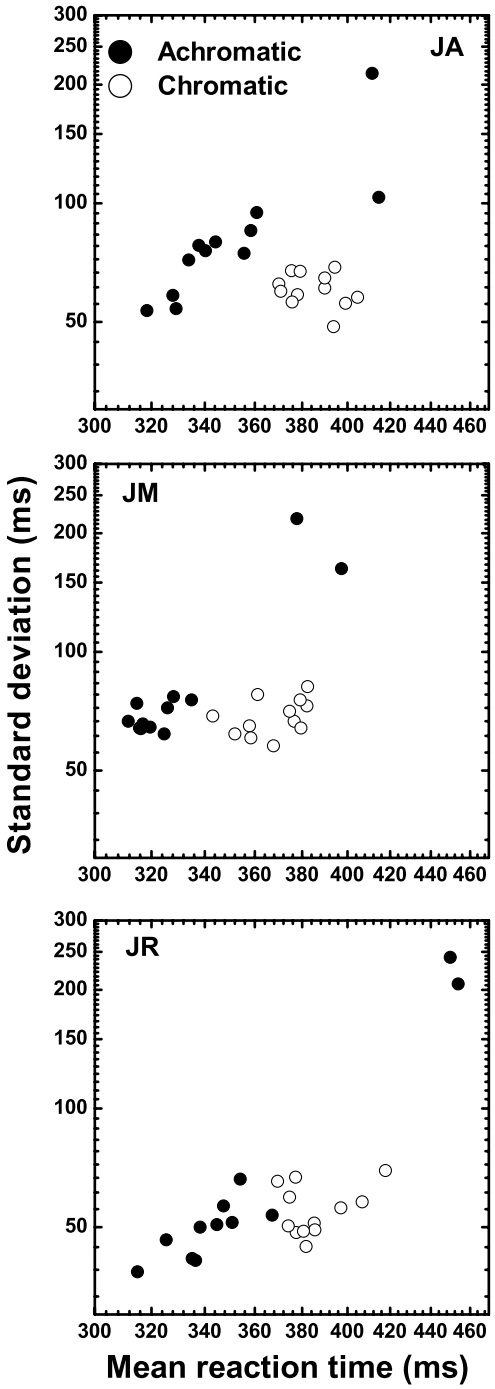

Fig. 3. Plot of the SD (in ms) as a function of the mean RT (in ms) in logarithmic axes. Open and black circles indicate random chromatic variations at isoluminance and achromatic variations, respectively. Data correspond to observers JA, JM, and JR, separately.

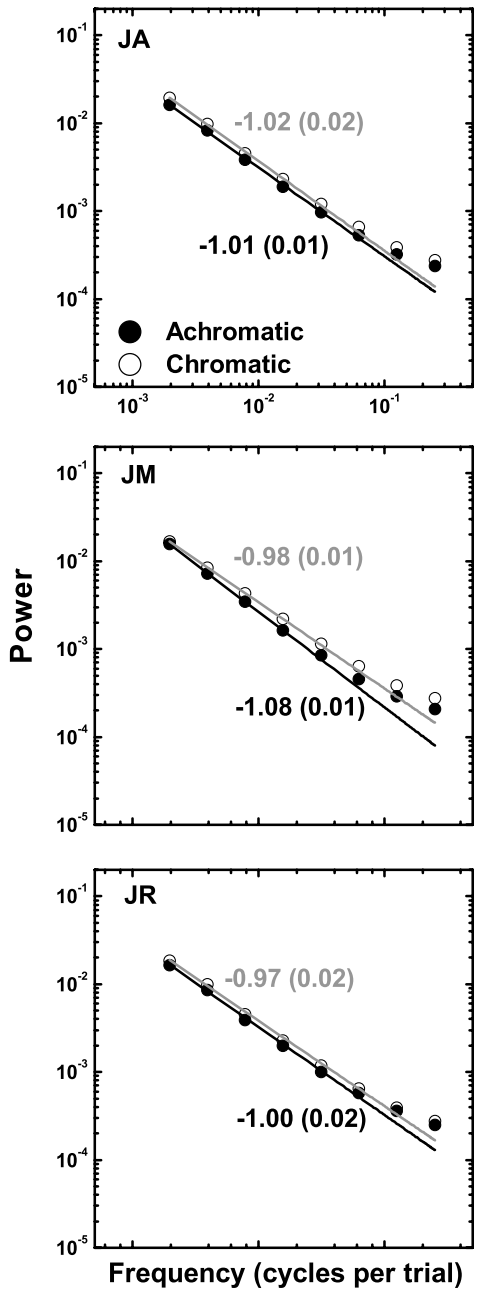

Fig. 4. Full logarithmic plot of the power spectrum generated from the RT series for random chromatic variations at isoluminance (open circles) and that for achromatic variations (black circles). Gray and black solid straight lines correspond to those fits taking chromatic and achromatic data, respectively. Gray and black numbers are their resulting slope, respectively. Numbers in parentheses are their associated standard errors. Data correspond to observers JA, JM, and JR, separately.

cones are activated simultaneously at isoluminance. These findings suggest that higher order color mechanisms tuned to noncardinal directions in the color space have access to the same amount of internal noise as in luminance processing. This result may be important in the optimization of the cortical signal-to-noise ratio (SNR), and it could have a direct impact on the overall integration of different color attributes such as hue, saturation, and brightness by means of neural synchronization [86].

4. EXPERIMENT 2

A. Stimuli

A set consisting of 10 blue–yellow stimuli (L&M-constant cone or S-cone axis) was chosen, being selected along a tritan confusion line originated at the CIE 1931 point ($x = 0.175$, $y = 0.0$) [2,9]. Figure 5(a) presents these stimuli plotted in the CIE 1931 (x, y) chromaticity diagram.

Another set of seven red–green stimuli was also selected as a control condition. These stimuli were along a red–green

confusion line (S-constant or L–M-cone axis). This red–green line originates at the point ($x = 1.0$, $y = 0.0$) [2,9], as shown in Fig. 5(a). Isolation of both blue–yellow and red–green stimuli was done by heterochromatic flicker photometry at the frequency of 12.3 Hz and at 12 cd/m^2 [58,59,63]. The reference stimulus was the same for both blue–yellow and red–green variations and was a chromatic one with chromaticity coordinates ($x = 0.442$, $y = 0.290$), as depicted in Fig. 5(a). The two spatial stimulus sizes selected are also shown in Fig. 5(b). All stimuli, including the reference stimulus, had an angular size of 16 and 90 min of arc in diameter at the viewing distance of 70 cm, and they were presented on fovea in a dark background. The first stimulus size (16 min of arc) enabled us to stimulate the S-cone free zone over 20 min of arc in the central fovea or *foveola* [16,65] and, thus, to test the lack of S-cone signals in chromatic-opponent coding. S-cone density increases beyond this central fovea up to 1.5° eccentricity [16,65]. Therefore, the second stimulus size includes S-cone

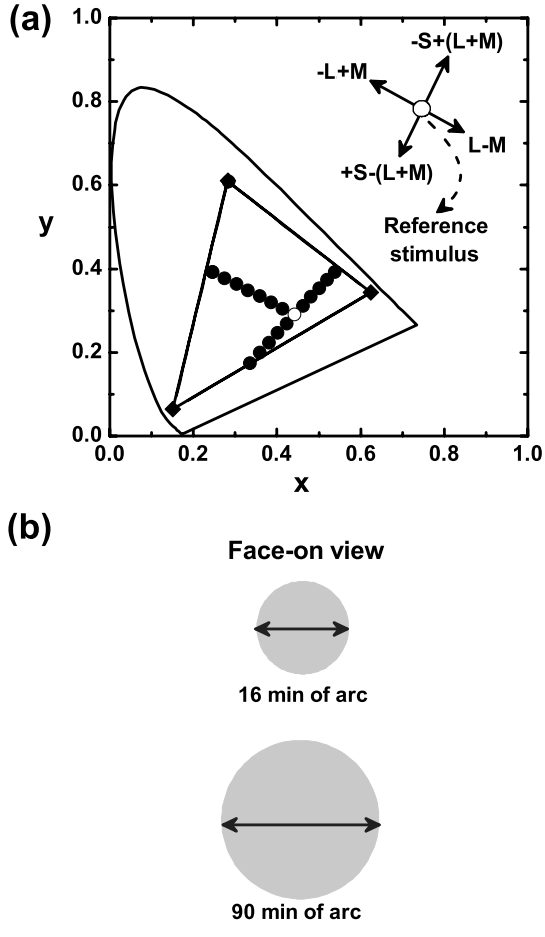

Fig. 5. Plot of red–green and blue–yellow stimuli at isoluminance (black circles) in the CIE 1931 chromaticity diagram. The empty circle indicates the reference adapting stimulus. The triangle indicates the monitor color gamut delimited by the coordinates of the red, green, and blue phosphor primaries (black diamonds). For the fixed reference stimuli, the schematic diagram at the top-right border indicates the corresponding L–M and S-cone axis variations. Level of reference luminance: 12 cd/m^2. (b) Spatial configuration of the stimuli selected at 16 and 90 min of arc.

responses in the same way as in Experiment 1. Again, the RT variability was measured using natural pupils with the right eye. The nontested eye was also covered with a black patch. The total number of RTs analyzed in the Experiment 2 was 5473.

B. Results

Figure 6 shows, for two observers (JA and MC), the RT series in a linear plot ordered chronologically by the trial number for red–green variations at isoluminance (L–M cone axis). The results confirm the presence of waves in the RT series [25,46]. Red–green RTs at 16 min of arc are, when averaged across all stimulus contrasts (see Fig. 5), slightly higher (JA 437.3 ms, MC 547.4 ms) than 90 min of arc (JA 409.7 ms, MC 531.8 ms). Mean RT differences between stimulus sizes are less than 28 ms, this suggesting that S-cone signals have some residual effect along the red–green axis in spatial summation [9,10,12].

The corresponding RT series for blue–yellow variations at isoluminance are represented in Fig. 7. These RT series corroborate that blue–yellow signals have longer RTs than red–green variations [59–63] for the same adapting stimulus. Strikingly, RTs at 16 min of arc are, on average, much longer and variable (JA, 915.2 ms; MC, 912.7 ms), than at 90 min of arc (JA, 441.1 ms; MC, 600.6 ms). Mean RT differences between stimulus sizes can be as high as 475 ms.

Following the same procedure as in the Experiment 1, for each stimulus size (16 or 90 min of arc), the corresponding RT series was grouped as a function of the stimulus contrast. The trial order in Fig. 7 was neglected, and the SD and the mean RT values were calculated at each experimental condition. Figure 8 shows, in a double logarithmic plot, the SD as a function of the mean RT for each observer and for each experimental condition. As expected, RT variability increases as the mean response level of the visual system increases similar to Weber's law [23,24,26,85] in L–M cone axis [25,27], in the S-cone axis [25] and, now, with spatial summation.

The coefficient of variation averaged over all the experimental conditions in spatial summation was sub-Poisson, and it was very similar in the L–M cone axis (JA, 0.19 both 16 and 90 min of arc; MC, 0.40 and 0.42 at 16 and 90 min of arc, respectively). In the S-cone axis, although it was higher at a small stimulus size for observer JA (0.33 and 0.22 at 16 and 90 min of arc, respectively), it was similar for observer MC (0.39 and 0.40 at 16 and 90 min of arc, respectively). A bilinear regime has been found for the red–green isoluminant stimuli, and therefore, RTs below and above 16 min of arc RTs follow different tendencies [27]. A similar behavior is also found in Fig. 8 in the S-cone axis. This effect is more pronounced in observer MC with the separation of the two regimes of variability located between 800 and 1000 ms.

The calculated power spectra (seven points) in both L–M cone and S-cone axis are represented in a double logarithmic plot in Fig. 9. In the former, flicker noise was confirmed with some contribution of white noise at high frequencies, in the same way as in the achromatic case (see Fig. 4) [25]. Although there are individual differences, the magnitude of the power spectra and the scaling exponent were very similar at 16 and 90 min of arc (JA, −0.97; MC, −0.90). Regarding the S-cone axis, the results show evidence for flicker noise in spatial summation. For both observers, the magnitude of the power

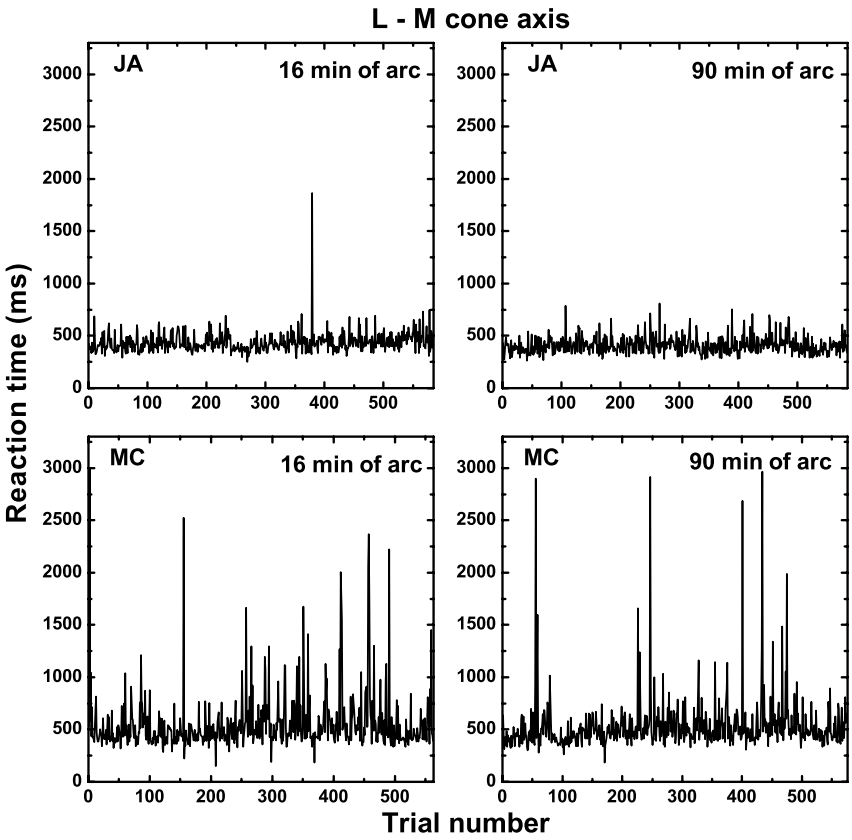

Fig. 6. Plot of the RT series (in ms) series for red–green variations at isoluminance (L–M cone axis) at 16 and 90 min of arc. Data correspond to observers JA, JM, and JR, separately.

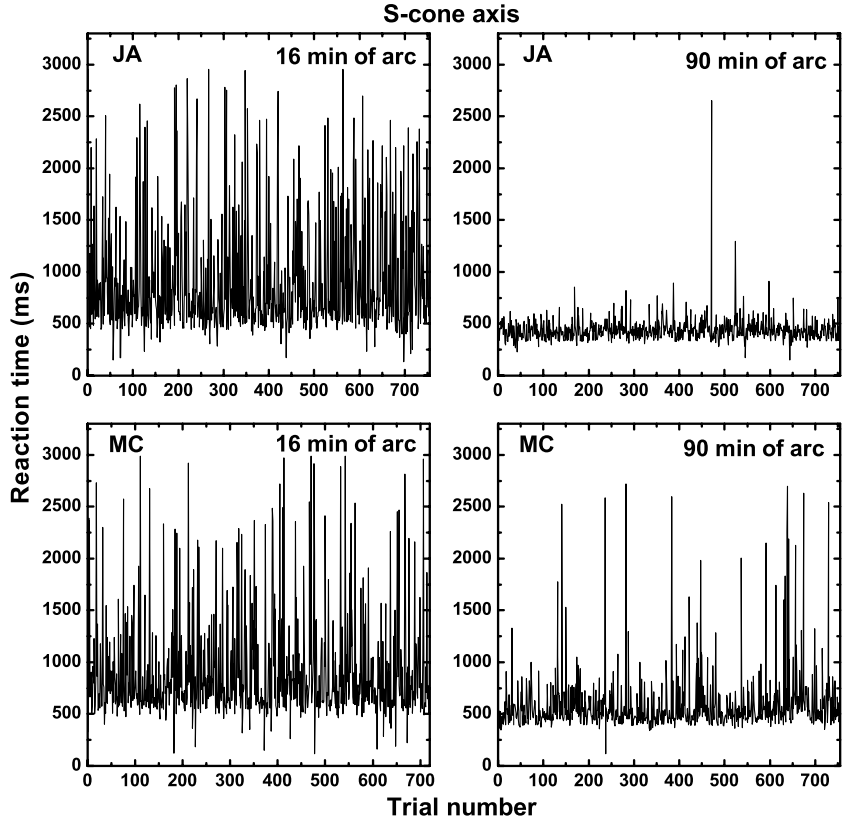

Fig. 7. Plot of the RT series (in ms) series for blue–yellow variations at isoluminance (S-cone axis) at 16 and 90 min of arc. Data are presented for observers JA and MC, separately.

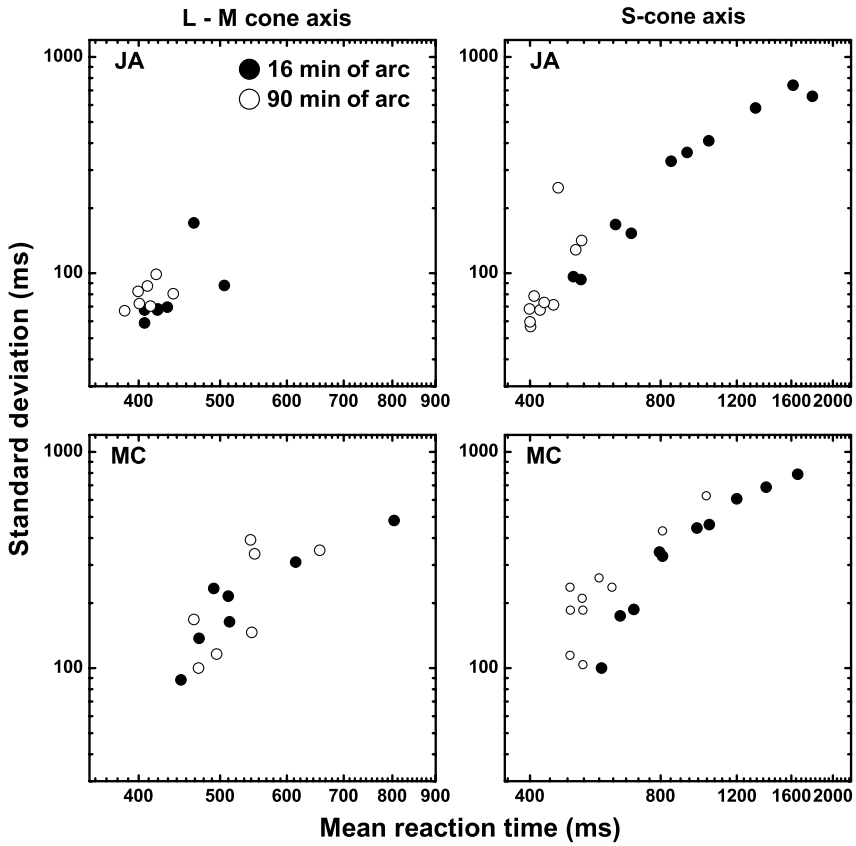

Fig. 8. Plot of the SD (in ms) as a function of the mean RT (in ms) for blue–yellow variations (S-cone axis, right column) and red–green variations at isoluminance (L–M cone axis, left column) in logarithmic axes. Open and black circles indicate those stimuli selected at 16 and 90 min of arc. Data correspond to observers JA and MC, separately.

spectra is higher at 16 min of arc, and it drops at 90 min of arc. The scaling exponent was lower at 16 min of arc (JA, −0.85; MC −0.91) and approximates to unity at 90 min of arc (JA, −0.95; MC, −0.97). This suggests that foveal tritanopia could favor $1/f$ scaling ($\alpha \cong 1$) over weaker ($0 < \alpha < 1$) or stronger ($\alpha > 1$) long-term correlations. It is worth noting that the comparisons between chromatic-opponent signals reveal that the magnitude of the power spectra in the S-cone axis at 90 min of arc was similar to the power spectra in the L–M cone axis.

Figure 10 shows the influence of the cone-contrast level and stimulus size in the hazard functions for red–green variations in a linear plot. The analysis of the hazard functions in the L–M cone axis reproduces the standard effects. They behave like a quasi-sustained mechanism—that is, they are weakly peaked at short time intervals, rising to the nonzero asymptotic level at near-threshold contrasts [23,63,71] and small stimulus size (16 min of arc) [27]. However, at well above threshold cone-contrast conditions, a clearly peaked form is revealed: the RT-hazard functions first increase to a maximum at short time intervals, and then they decrease to the asymptotic level at longer time intervals [63]. No distinction between small and large stimulus size is found [27].

The behavior of the hazard functions in the S-cone axis as a function of the cone-contrast level and stimulus size is similar to the L–M cone axis as indicated in Fig. 11 and extend previous results on spatial summation [27]. The S-cone hazard functions confirm the existence of sustained-based activity at low stimulus size and moderate contrast and a transient-sustained activity at high cone-contrast values.

C. Discussion

Previous works have demonstrated that the mean RT decreases as the product of the stimulus size by its luminance or by local intensity factors (retinal contrast and grating period) increases [57,87–89]. Mean RTs almost collapse into a single Piéron's function [87–89]. This effect has been explained assuming the existence of a probability summation effect in the neural activity for achromatic nonperiodic stimuli [87] and a linear spatial summation for gratings [88,89]. The effect of foveal tritanopia has been also examined using mean RTs and the parameter μ in Piéron's law (see Eq. 2) [62], which is related with the formation of visual thresholds [67]. In all these studies, the internal noise is usually assumed constant and spatial summation is modeled as a discrimination task between signal and noise within a critical area in accordance with Ricco's law for complete summation and Pipper's law for partial summation [90,91]. The new results in Fig. 8 show that the analysis of RT variability provides important properties on the intrinsic noise that were simplified in previous RT models based on the mean response. Figure 8 clearly demonstrates that RT variability is not bounded and increases as the mean RT increases at different stimulus size. This suggests the existence of scale invariance in spatial summation and contrast processing in the red–green channel [85] as well as in the blue–yellow channel that could be related to how

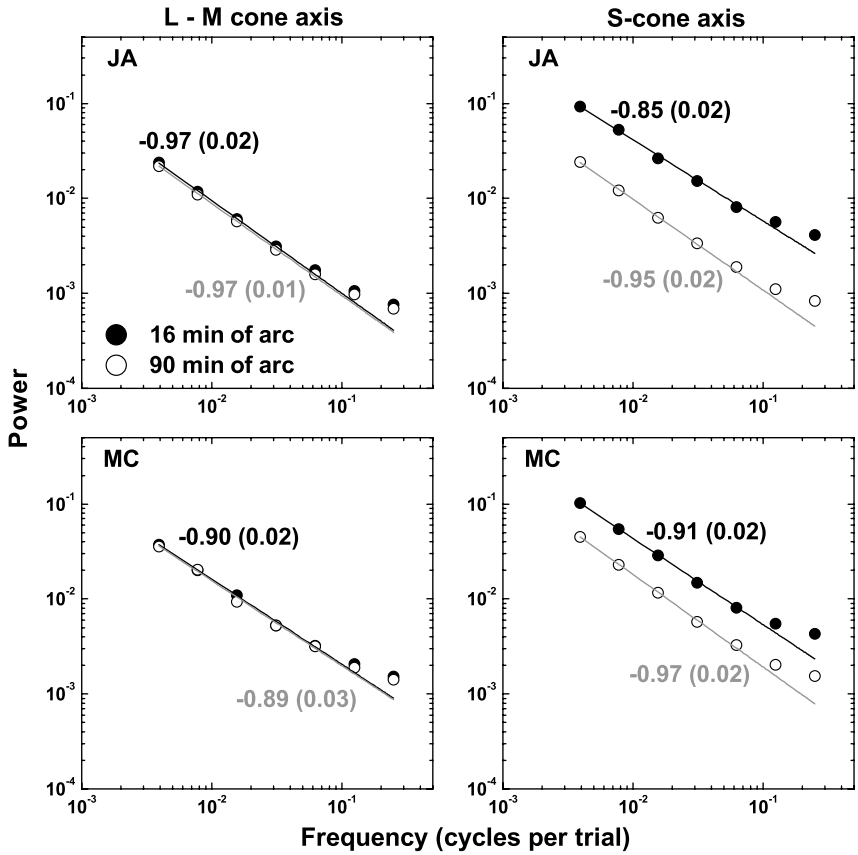

Fig. 9. Full logarithmic plot of the power spectrum generated from RT series for blue–yellow variations (S-cone axis, right column) and red–green variations at isoluminance (L–M cone axis, left column). Black and gray solid straight lines indicate those fits at 16 and 90 min of arc, respectively. Black and gray and numbers are their obtained slope, respectively. Numbers in parentheses are their associated standard errors. Data correspond to observers JA and MC, separately.

photoreceptor noise is managed during the first stages at the retina [3,4,12,15–17]. In Fig. 9 the existence of $1/f$ noise as a function of the stimulus size clearly demonstrates that the noise power in the blue–yellow channel is related directly with the S-cone density distribution in the human retina. Because the magnitude of $1/f$ noise was lower at 90 min of arc than at 16 min of arc, spatial summation of S-cone noise could support a possible benefit in the computation of the SNR and it could help in the discrimination of signal from noise in contrast detection [91]. Figure 9 also shows that the power spectrum in the S-cone axis at 90 min of arc is also similar to the L–M cone axis, this suggesting the same level of neural noise at later stages possibly in the visual cortex.

The experimental results on RT variability in Figs. 8 and 9 do not validate the multichannel stochastic models of the hazard functions [71,92]. In these models, the transient-sustained activity has been interpreted in terms of probability summation and neural summation where some kind of response pooling is considered [23,71,73,92]. However, these models do not include explicitly $1/f$ noise and they have only assumed white noise into a later decision stage [71]. Therefore, we suggest that the RT-hazard functions shown in Figs. 10–11 could support better the notion of multiplicative correlations in cascade [26]. The RT-hazard functions support sustained activity at low contrasts and small stimulus size that is compatible a multiplicative process that exhibits power-law dominant dynamics [26]. The transient-based activity at high contrast values could be derived from a multiplicative process with log–normal dominant dynamics [26].

5. GENERAL DISCUSSION

We have shown that trial-to-trial RT variability contains complex dynamical processes with long-term correlations (“memory”), and it provides valuable information on how the stochastic latency mechanisms control color vision. The scaling relationship between the SD and the mean RT (Figs. 3 and 8) indicates that the RT variability is compatible with scale invariance [44,68,85]. There exists RT variations of all sizes, and, therefore, large variations near the threshold are also important and are correlated with small variations at suprathreshold conditions. This agrees with the existence of long-term correlations in the subcortical pathways [93] and in the visual cortex [94,95]. The relation between the SD and the mean RTs also implies that the RT variability depends on the stimulus size and on the stimulus contrast [27,28]. This suggests the existence of signal-dependent internal noise from retina to motor planning [1,8,27,96].

The persistence of $1/f$ noise with an exponent α close to unity in most of the experiments except at 16 min of arc in the blue–yellow channel (S-cone free zone) indicates that S-cone signals have the counterintuitive effect of modulating

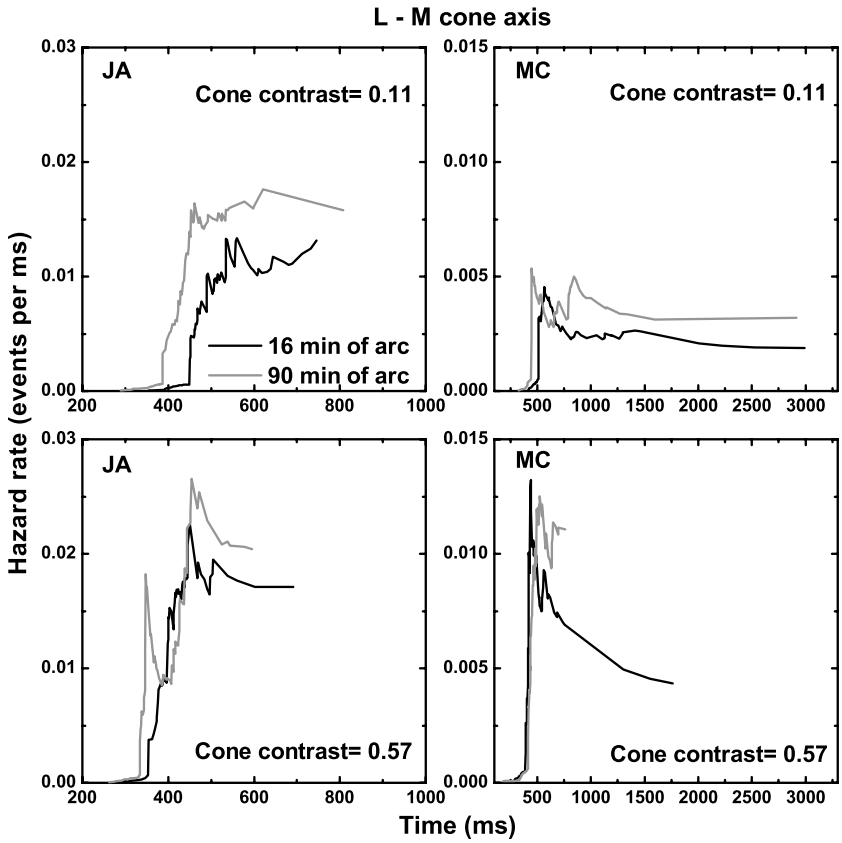

Fig. 10. Linear plot of the hazard functions (in events per ms) as a function of the cone contrast for red–green variations at isoluminance (L–M cone axis). Black and gray lines correspond to a stimulus size of 16 and 90 min of arc, respectively. Data for observer JA and MC are shown separately.

the noise power spectra. The results in Fig. 4 demonstrate that S-cone signals are beneficial because they reduce the magnitude of $1/f$ noise in higher order color mechanisms to almost the same level as in luminance processing. The results in Fig. 9 show that the reduction of the power spectrum was markedly stronger in the blue–yellow channel and clearly demonstrate the dependency of $1/f$ noise on the S-cone density in the human retina.

There are two different strategies to maintain the SNR over time—a brute force strategy that consists of increasing the signal power at the expense of increase the energy costs and a second strategy that may allocate the energy resources modulating the noise power as a function of the external experimental conditions (i.e., a signal-dependent noise). The control of $1/f$ noise spectra by the S cones in human color vision may support this second strategy in everyday tasks. The ubiquitous presence of $1/f$ noise may also reflect an efficient communication mechanism within the visual–motor system [33]. It has been argued that habituation to externally added $1/f$ noise optimizes the transfer of information in the visual cortex [55]. In human visual perception, a stochastic diffusion model driven by thermal noise has been the first to suggest a relationship between RTs, $1/f$ noise, and the optimal transfer of information [67,70,97,98]. In this model, the information entropy function H, or the H function, gives a measure of the internal uncertainty in the visual system. High values of H imply high uncertainty and vice versa. The model asserts that neural processing is not instantaneous and the neurons always take time to acquire information. Accordingly, the visual system must gather $\Delta H \geq 0$ bits of information before reacting [67,70,97]. The quantity ΔH is the minimum gain of information, and it is related with the formation of an internal threshold S_0 [67,70,97]. The parameter μ in Eq. 2 can be expressed by $\mu = t_{\mathrm{RT}_0} S_0^p$, and Piéron's law is rewritten as follows [67,97]:

$$t_{\mathrm{RT}} = t_{\mathrm{RT}_0}[1 + (S_0/S)^p]. \tag{2}$$

The asymptotic plateau t_{RT_0} also contains those processes at the threshold [67,70], and the RT model is constructed from a multiplicative process, that is, those processes in t_{RT} multiplied from the previous one t_{RT_0} by the factor indicated in the brackets in Eq. 2 and so on [67,70]. Higher values of S_0 imply higher RTs and vice versa. The RT series can be mapped in the fluctuations generated by S_0 over time:

$$\text{RT observations} \Rightarrow \text{Piéron's law} + \text{threshold fluctuations}. \tag{3}$$

The origin of threshold fluctuations in S_0 is based upon a situation in which the total neural SNR is controlled by a signal-dependent background noise that undergoes a modification from thermal noise to become $1/f$ noise [67,70]. Finally, it has been proposed that RT variability that arises from white noise (see Figs. 4 and 9) could be originated from the

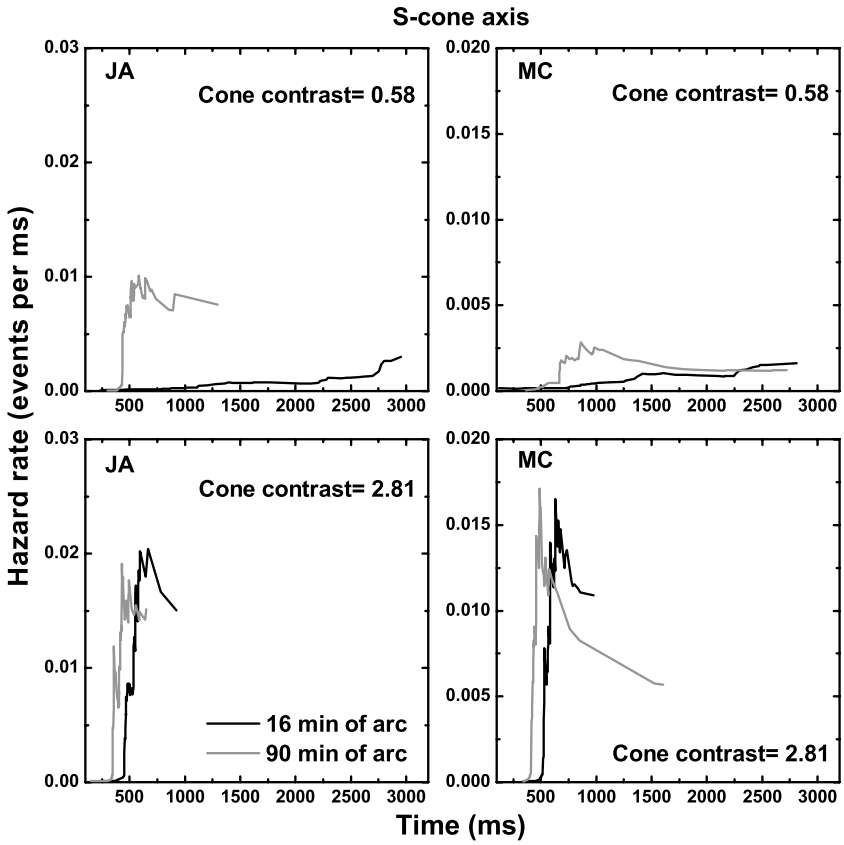

Fig. 11. Linear plot of the hazard functions (in events per ms) as a function of the cone contrast for blue–yellow variations at isoluminance (S-cone axis). Black and gray lines indicate a stimulus size of 16 and 90 min of arc, respectively. Data for observer JA and MC are shown separately.

motor mechanisms [5,46]. However, the information-based RT model discussed in Eqs. 2–3 claims that motor variability also follows $1/f$-type scaling and the white noise content could be originated, at least in part, from thermal noise controlled by body temperature [67,70]. This model prediction is in agreement with the existence of $1/f$ noise in the motor cortex derived from spontaneous fluctuations of fMRI signals [39,40] and may explain the dependency of mean RTs on the changes in thermoregulation [99].

6. CONCLUSION

We have found that S-cone signals modulate RT variability in higher order color mechanisms by reducing $1/f$ noise spectra for random chromatic variations at isoluminance, and they are also beneficial in spatial summation, where their presence drops the magnitude of $1/f$ noise in the blue–yellow chromatic-opponent channel. This may be related to threshold fluctuations through Piéron's law and could confer neural variability in the form of $1/f$ scaling an efficient form of communication by promoting the optimal transfer of information in color vision and in the visual–motor system [33,55]. These results on $1/f$ noise should be incorporated into dynamical RT models of human vision that seek to explain RT variability using the hazard functions. The research on RT variability in the human color space may offer new perspectives in the study of stochastic latency mechanisms that mediate color vision with age and diseases.

ACKNOWLEDGMENTS

This work was supported by the Center for Physics, University of Minho, Portugal.

REFERENCES

1. A. A. Faisal, L. P. J. Selen, and D. M. Wolpert, "Noise in the nervous system," Nat. Rev. Neurosci. **9**, 292–303 (2008).
2. G. Wyszecki and W. S. Stiles, *Color Science: Concepts and Methods, Quantitative Data and Formulae*, 2nd ed. (Wiley, 1982).
3. T. D. Lamb, "Sources of noise in photoreceptor transduction," J. Opt. Soc. Am. A **4**, 2295–2300 (1987).
4. V. Torre, J. F. Ashmore, T. D. Lamb, and A. Menini, "Transduction and adaptation in sensory receptor cells," J. Neurosci. **15**, 7757–7768 (1995).
5. D. L. Gilden, T. Thornton, and M. W. Mallon, "$1/f$ Noise in human cognition," Science **267**, 1837–1839 (1995).
6. J. S. Anderson, I. Lampl, D. C. Gillespie, and D. Ferster, "The contribution of noise to contrast invariance of orientation tuning in cat visual cortex," Science **290**, 1968–1972 (2000).
7. R. B. Stein, E. R. Gossen, and K. E. Jones, "Neuronal variability: noise or part of the signal?" Nat. Rev. Neurosci. **6**, 389–397 (2005).
8. C. M. Harris and D. M. Wolpert, "Signal-dependent noise determines motor planning," Nature **394**, 780–784 (1998).
9. D. I. A. Macleod and R. M. Boynton, "Chromaticity diagram showing cone excitation by stimuli of equal luminance," J. Opt. Soc. Am. **69**, 1183–1186 (1979).
10. R. L. De Valois and K. K. De Valois, "A multistage color model," Vis. Res. **33**, 1053–1065 (1993).
11. K. R. Gegenfurtner and D. C. Kiper, "Color vision," Annu. Rev. Neurosci. **26**, 181–206 (2003).

12. S. G. Solomon and P. Lennie, "The machinery of colour vision," Nat. Rev. Neurosci. **8**, 276–286 (2007).
13. P. R. Martin, A. J. R. White, A. K. Goodchild, H. D. Wilder, and A. E. Sefton, "Evidence that blue-on cells are part of the third geniculocortical pathway in primates," Eur. J. Neurosci. **9**, 1536–1541 (1997).
14. S. H. C. Hendry and R. C. Reid, "The koniocellular pathway in primate vision," Annu. Rev. Neurosci. **23**, 127–153 (2000).
15. D. M. Dacey, "Parallel pathways for spectral coding in primate retina," Annu. Rev. Neurosci. **23**, 743–775 (2000).
16. D. J. Calkins, "Seeing with S cones," Prog. Retin. Eye Res. **20**, 255–287 (2001).
17. J. J. Nassi and E. M. Callaway, "Parallel processing strategies of the primate visual system," Nat. Rev. Neurosci. **10**, 360–372 (2009).
18. N. P. Cottaris and R. L. De Valois, "Temporal dynamics of chromatic tuning in macaque primary visual cortex," Nature **395**, 896–900 (1998).
19. M. Vorobyev and D. Osorio, "Receptor noise as a determinant of colour thresholds," Proc. R. Soc. Lond. B **265**, 351–358 (1998).
20. K. R. Gegenfurtner and D. C. Kiper, "Contrast detection in luminance and chromatic noise," J. Opt. Soc. Am. A **9**, 1880–1888 (1992).
21. M. J. Sankeralli and K. T. Mullen, "Postreceptoral chromatic detection mechanisms revealed by noise masking in three-dimensional cone contrast space," J. Opt. Soc. Am. A **14**, 2633–2646 (1997).
22. K. T. Mullen, W. H. A. Beaudot, and W. H. McIlhagga, "Contour integration in color vision: a common process for the blue–yellow, red–green and luminance mechanisms?" Vis. Res. **40**, 639–655 (2000).
23. R. D. Luce, *Response Times* (Oxford University, 1986).
24. E. J. Wagenmakers and S. Brown, "On the linear relation between the mean and the standard deviation of a response time distribution," Psychol. Rev. **114**, 830–841 (2007).
25. J. M. Medina and J. A. Díaz, "$1/f$ Noise through retino-cortical pathways assessed by reaction times," in *Noise and Fluctuations*, *AIP Conference Proceedings* (AIP, 2009), Vol. 1129, 553–556.
26. J. G. Holden, G. C. Van Orden, and M. T. Turvey, "Dispersion of response times reveals cognitive dynamics," Psychol. Rev. **116**, 318–342 (2009).
27. J. M. Medina and J. A. Díaz, "Response variability of the red-green color vision system using reaction times," Proc. SPIE **8001**, 80013B (2011).
28. P. Lennie, "The physiological basis of variations in visual latency," Vis. Res. **21**, 815–824 (1981).
29. D. Mitov and T. Totev, "How many pathways determine the speed of grating detection?" Vis. Res. **45**, 821–825 (2005).
30. W. Schottky, "Small-shot effect and flicker effect," Phys. Rev. **28**, 74–103 (1926).
31. W. H. Press, "Flicker noises in astronomy and elsewhere," Comments Astrophys. **7**, 103–119 (1978).
32. C. M. Anderson and A. J. Mandell, "Fractal time and the foundations of consciousness," in *Fractals of Brain*, *Fractals of Mind: In Search of a Symmetry Bond*, E. A. Mac Cormac and M. I. Stamenov, eds. (John Benjamins, 1996), pp. 75–126.
33. B. J. West, E. L. Geneston, and P. Grigolini, "Maximizing information exchange between complex networks," Phys. Rep. **468**, 1–99 (2008).
34. A. A. Verveen and H. E. Derksen, "Fluctuation phenomena in nerve membrane," Proc. IEEE **56**, 906–916 (1968).
35. T. Musha, Y. Kosugi, G. Matsumoto, and M. Suzuki, "$1/f$ fluctuations in biological systems," IEEE Trans. Biomed. Eng. **BME-28**, 616–623 (1981).
36. T. Musha and M. Yamamoto, "$1/f$ fluctuations in biological systems," in *Engineering in Medicine and Biology Society, 1997. Proceedings of the 19th Annual International Conference of the IEEE* (IEEE, 1997), Vol. 6, pp. 2692–2697.
37. W. J. Freeman and B. W. Vandijk, "Spatial patterns of visual cortical fast EEG during conditioned reflex in a rhesus monkey," Brain Res. **422**, 267–276 (1987).
38. P. Allegrini, D. Menicucci, R. Bedini, L. Fronzoni, A. Gemignani, P. Grigolini, B. J. West, and P. Paradisi, "Spontaneous brain activity as a source of ideal $1/f$ noise," Phys. Rev. E **80**, 061914 (2009).
39. M. D. Fox, A. Z. Snyder, J. L. Vincent, and M. E. Raichle, "Intrinsic fluctuations within cortical systems account for intertrial variability in human behavior," Neuron **56**, 171–184 (2007).
40. B. Y. J. He, J. M. Zempel, A. Z. Snyder, and M. E. Raichle, "The temporal structures and functional significance of scale-free brain activity," Neuron **66**, 353–369 (2010).
41. R. F. Voss and J. Clarke, "$1/f$ noise in music and speech," Nature **258**, 317–318 (1975).
42. Y. Q. Chen, M. Z. Ding, and J. A. S. Kelso, "Long memory processes ($1/f^{\alpha}$ type) in human coordination," Phys. Rev. Lett. **79**, 4501–4504 (1997).
43. K. Torre and E.-J. Wagenmakers, "Theories and models for $1/f^{\beta}$ noise in human movement science," Hum. Mov. Sci. **28**, 297–318 (2009).
44. T. Gisiger, "Scale invariance in biology: coincidence or footprint of a universal mechanism?" Biol. Rev. **76**, 161–209 (2001).
45. L. M. Ward, *Dynamical Cognitive Science* (MIT Press, 2002).
46. D. L. Gilden, "Cognitive emissions of $1/f$ noise," Psychol. Rev. **108**, 33–56 (2001).
47. T. L. Thornton and D. L. Gilden, "Provenance of correlations in psychological data," Psychon. Bull. Rev. **12**, 409–441 (2005).
48. P. Grigolini, G. Aquino, M. Bologna, M. Lukovic, and B. J. West, "A theory of $1/f$ noise in human cognition," Physica A **388**, 4192–4204 (2009).
49. D. L. Gilden, "Fluctuations in the time required for elementary decisions," Psychol. Sci. **8**, 296–301 (1997).
50. C. T. Kello, B. C. Beltz, J. G. Holden, and G. C. Van Orden, "The emergent coordination of cognitive function," J. Exp. Psychol. Gen. **136**, 551–568 (2007).
51. J. Correll, "Order from chaos? $1/f$ noise predicts performance on reaction time measures," J. Exp. Soc. Psychol. **47**, 830–835 (2011).
52. J. Krauskopf, "Higher order color mechanisms," in *Color Vision: From Genes to Perception*, K. R. Gegenfurther and L. T. Sharpe, eds. (Cambridge University, 1999), pp. 303–317.
53. R. L. De Valois, N. P. Cottaris, S. D. Elfar, L. E. Mahon, and J. A. Wilson, "Some transformations of color information from lateral geniculate nucleus to striate cortex," Proc. Natl. Acad. Sci. USA **97**, 4997–5002 (2000).
54. R. L. De Valois, K. K. De Valois, and L. E. Mahon, "Contribution of S opponent cells to color appearance," Proc. Natl. Acad. Sci. USA **97**, 512–517 (2000).
55. Y. G. Yu, R. Romero, and T. S. Lee, "Preference of sensory neural coding for $1/f$ signals," Phys. Rev. Lett. **94**, 108103 (2005).
56. M. A. Webster and J. D. Mollon, "The influence of contrast adaptation on color appearance," Vis. Res. **34**, 1993–2020 (1994).
57. B. G. Breitmeyer and J. I. Breier, "Effects of background color on reaction time to stimuli varying in size and contrast: inferences about human M channels," Vis. Res. **34**, 1039–1045 (1994).
58. J. A. Díaz, L. del Jiménez Barco, J. R. Jiménez, and F. Perez-Ocón, "Chromatic spatial summation at equiluminance," Opt. Rev. **8**, 388–396 (2001).
59. J. A. Díaz, L. del Jiménez Barco, J. R. Jiménez, and E. Hita, "Simple reaction time to chromatic changes along L&M-constant and S-constant cone axes," Color Res. Appl. **26**, 223–233 (2001).
60. J. R. Jiménez, J. M. Medina, L. del Jiménez Barco, and J. A. Díaz, "Binocular summation of chromatic changes as measured by visual reaction time," Atten. Percept. Psychophys. **64**, 140–147 (2002).
61. D. J. McKeefry, N. R. A. Parry, and I. J. Murray, "Simple reaction times in color space: the influence of chromaticity, contrast, and cone opponency," Investig. Ophthalmol. Vis. Sci. **44**, 2267–2276 (2003).
62. N. R. A. Parry, S. Plainis, I. J. Murray, and D. J. McKeefry, "Effect of foveal tritanopia on reaction times to chromatic stimuli," Vis. Neurosci. **21**, 237–242 (2004).
63. J. M. Medina and J. A. Díaz, "Postreceptoral chromatic-adaptation mechanisms in the red-green and blue-yellow systems using simple reaction times," J. Opt. Soc. Am. A **23**, 993–1007 (2006).
64. B. M. O'Donell, J. F. Barraza, and E. M. Colombo, "The effect of chromatic and luminance information on reaction times," Vis. Neurosci. **27**, 1–11 (2010).

65. C. A. Curcio, K. A. Allen, K. R. Sloan, C. I. Lerea, J. B. Hurley, I. B. Klock, and A. H. Millam, "Distribution and morphology of human cone photoreceptors stained with anti-blue opsin," J. Comp. Neurol. **312**, 610–624 (1991).
66. P. Bak, C. Tang, and K. Wiesenfeld, "Self-organized criticality: an explanation of $1/f$ noise," Phys. Rev. Lett. **59**, 381–384 (1987).
67. J. M. Medina, "$1/f^{\alpha}$ noise in reaction times: a proposed model based on Pieron's law and information processing," Phys. Rev. E **79**, 011902 (2009).
68. C. T. Kello, G. D. A. Brown, R. Ferrer-i-Cancho, J. G. Holden, K. Linkenkaer-Hansen, T. Rhodes, and G. C. Van Orden, "Scaling laws in cognitive sciences," Trends Cogn. Sci. **14**, 223–232 (2010).
69. H. Piéron, *The Sensations* (Yale University, 1952).
70. J. M. Medina, "Effects of multiplicative power law neural noise in visual information processing," Neural Comput. **23**, 1015–1046 (2011).
71. P. L. Smith, "Psychophysically principled models of visual simple reaction time," Psychol. Rev. **102**, 567–593 (1991).
72. N. D. Singpurwalla and M. Y. Wong, "Estimation of the failure rate: a survey of nonparametric methods. 1 Non-Bayesian methods," Commun. Stat. Theory Methods **12**, 559–588 (1983).
73. T. Ueno, "Sustained and transient properties of chromatic and luminance systems," Vis. Res. **32**, 1055–1065 (1992).
74. J. M. Medina, "Binocular interactions in random chromatic changes at isoluminance," J. Opt. Soc. Am. A **23**, 239–246 (2006).
75. H. C. Hughes and J. T. Townsend, "Varieties of binocular interaction in human vision," Psychol. Sci. **9**, 53–60 (1998).
76. J. A. Díaz, "Estudio de los efectos de la integración espacio-temporal en los fenónemos de detección cromática en visión central y periférica," Ph.D. thesis (University of Granada, 1997).
77. J. M. Medina, "Estudio de las propiedades y modelos del tiempo de reaccion binocular simple con relacion al color," Ph.D. thesis (University of Granada, 2002).
78. L. del Jiménez Barco, J. A. Díaz, J. R. Jiménez, and M. Rubino, "Considerations on the calibration of color displays assuming constant channel chromaticity," Color Res. Appl. **20**, 377–387 (1995).
79. J. A. Díaz, J. R. Jiménez, E. Hita, and L. del Jiménez Barco, "Optimizing the constant-channel chromaticity and color gamut of CRT color displays by control of brightness and contrast levels," Appl. Opt. **35**, 1711–1718 (1996).
80. "Declaration of Helsinki: ethical principles for medical research involving human subjects," (World Medical Association, 2008), www.wma.net/en/30publications/10policies/b3/.
81. M. J. Nissen and J. Pokorny, "Wavelength effects on simple reaction time," Atten. Percept. Psychophys. **22**, 457–462 (1977).
82. G. R. Cole, T. Hine, and W. McIlhagga, "Detection mechanisms in L-, M-, and S-formula contrast space," J. Opt. Soc. Am. A **10**, 38–51 (1993).
83. V. C. Smith and J. Pokorny, "Spectral sensitivity of foveal cone photopigments between 400 and 500 nm," Vis. Res. **15**, 161–171 (1975).
84. W. Press, S. Teukolsky, W. Vetterling, and B. Flannery, *Numerical Recipes in C* (Cambridge University, 1992).
85. N. Chater and G. D. A. Brown, "Scale-invariance as a unifying psychological principle," Cognition **69**, B17–B24 (1999).
86. V. A. Billock and B. H. Tsou, "Sensory recoding via neural synchronization: integrating hue and luminance into chromatic brightness and saturation," J. Opt. Soc. Am. A **22**, 2289–2298 (2005).
87. C. Bonnet, J. Gurlekian, and P. Harris, "Reaction time and visual area: searching for determinants," Bull. Psychon. Soc. **30**, 396–398 (1992).
88. A. Vassilev, M. Mihaylova, and C. Bonnet, "On the delay in processing high spatial frequency visual information: reaction time and VEP latency study of the effect of local intensity of stimulation," Vis. Res. **42**, 851–864 (2002).
89. K. Donner and P. Fagerholm, "Visual reaction time: neural conditions for the equivalence of stimulus area and contrast," Vis. Res. **43**, 2937–2940 (2003).
90. H. B. Barlow, "Temporal and spatial summation in human vision at different background intensities," J. Physiol. **141**, 337–350 (1958).
91. H. B. Barlow, "Increment thresholds at low intensities considered as signal/noise discriminations," J. Physiol. **136** 469–488 (1957).
92. J. Miller and R. Ulrich, "Simple reaction time and statistical facilitation: a parallel grains model," Cogn. Psychol. **46**, 101–151 (2003).
93. J. D. Victor, E. M. Blessing, J. D. Forte, P. Buzas, and P. R. Martin, "Response variability of marmoset parvocellular neurons," J. Physiol. **579**, 29–51 (2007).
94. D. J. Tolhurst, J. A. Movshon, and A. F. Dean, "The statistical reliability of signals in single neurons in cat and monkey visual cortex," Vis. Res. **23**, 775–785 (1983).
95. R. Vogels, W. Spileers, and G. A. Orban, "The response variability of striate cortical neurons in the behaving monkey," Exp. Brain Res. **77**, 432–436 (1989).
96. G. A. Cecchi, M. Sigman, J. M. Alonso, L. Martinez, D. R. Chialvo, and M. O. Magnasco, "Noise in neurons is message dependent," Proc. Natl. Acad. Sci. USA **97**, 5557–5561 (2000).
97. K. H. Norwich, C. N. L. Seburn, and E. Axelrad, "An informational approach to reaction times," Bull. Math. Biol. **51**, 347–358 (1989).
98. K. H. Norwich, *Information, Sensation, and Perception* (Academic, 1993).
99. T. M. Makinen, L. A. Palinkas, D. L. Reeves, T. Paakkonen, H. Rintamaki, J. Leppaluoto, and J. Hassi, "Effect of repeated exposures to cold on cognitive performance in humans," Physiol. Behav. **87**, 166–176 (2006).

Physics Letters A 376 (2012) 1617–1623

Contents lists available at SciVerse ScienceDirect

Physics Letters A

www.elsevier.com/locate/pla

Multiplicative processes and power laws in human reaction times derived from hyperbolic functions

José M. Medina *

Center for Physics, University of Minho, Campus de Gualtar, 4710-057 Braga, Portugal

ARTICLE INFO

Article history:
Received 2 January 2012
Received in revised form 8 March 2012
Accepted 9 March 2012
Available online 13 March 2012
Communicated by C.R. Doering

Keywords:
Human reaction time
Decision making
Multiplicative process
Power law
Information transfer
$1/f$-noise

ABSTRACT

In sensory psychophysics reaction time is a measure of the stochastic latency elapsed from stimulus presentation until a sensory response occurs as soon as possible. A random multiplicative model of reaction time variability is investigated for generating the reaction time probability density functions. The model describes a generic class of hyperbolic functions by Piéron's law. The results demonstrate that reaction time distributions are the combination of log-normal with power law density functions. A transition from log-normal to power law behavior is found and depends on the transfer of information in neurons. The conditions to obtain Zipf's law are analyzed.

1. Introduction

Multiple biochemical and physiological processes can be described by hyperbolic functions written as:

$$R = \frac{R_{\max}}{1 + (\frac{S_0}{S})^{\alpha}}, \tag{1}$$

where S and R are the input and output variables, respectively, $R_{\max}$ is the maximum R-value, S_0 is a reference input value and α is a parameter that controls the steepness of the sigmoidal growth ($\alpha > 0$). Classical examples of hyperbolic functions are the Michaelis–Menten equation in enzyme reactions [1], the Hill equation in the control of human ventilation by blood carbon dioxide [2], and the Naka–Rushton response function in neurophysiology [3]. In the Naka–Rushton equation, the input variable S indicates the stimulus strength or intensity such as the contrast level in vision [4], the odorant concentration in olfaction [5], etc. The output variable R refers to the neural response or firing rate (in action potentials or spikes per second), and the reference value S_0 is often established at half of the maximum response $R_{\max}$ (usually called the semisaturation or half-saturation constant) [4]. The Naka–Rushton function is widely used in neuroscience and represents a nonlinear gain control model that adjusts cell responses and accounts for saturation for large S values [4,6–10].

The reciprocal of Eq. (1) is related with Piéron's law [11,12] and the study of reaction times in modern mental chronometry [13,14]:

$$t = t_{\min} + \gamma S^{-\alpha}, \tag{2}$$

where $t = 1/R$ is the mean reaction time (RT) (in s), $t_{\min} = 1/R_{\max}$ is the asymptotic plateau reached at very high values of S, $\gamma = t_{\min} S_0^{\alpha}$ and S_0 is an estimation of the sensory threshold ($S > S_0$). RT is defined as the time elapsed from stimulus presentation until a response occurs and must be positive [14]. Piéron's law is the counterpart of the reciprocal of the Naka–Rushton function at a macroscopic scale and describes the RT hyperbolic decay as a function of the stimulus strength at suprathreshold conditions. Piéron's law is of great interest in human performance and in sensory–motor transduction such as in sports science, in driving safety [15,16] and in decision making [17–22]. Fractional values of the exponent α characterize each sensory modality [12,14,18,23–26]. Previous works have investigated the theoretical foundations of Piéron's law [19,22,27–31] but it is usually without consideration of the properties of RT variability.

For a fixed experimental condition human RTs are not constant but stochastic. Trial-to-trial RT variability can be correlated over time, with a $1/f$-Fourier spectra or "$1/f$-noise" at low frequencies in most elementary cognitive tasks and it is thought to be mediated by neural activity [32–37]. The analysis of RT distributions is considered a fundamental aspect in RT modeling. Fig. 1A shows an

Abbreviations: RT, Reaction time; pdf, Probability density function; ISI, Interspike interval.

* Tel.: +351 253 604 074; fax: +351 253 604 061.
E-mail address: jmanuel@fisica.uminho.pt.

0375-9601/$ – see front matter
http://dx.doi.org/10.1016/j.physleta.2012.03.025

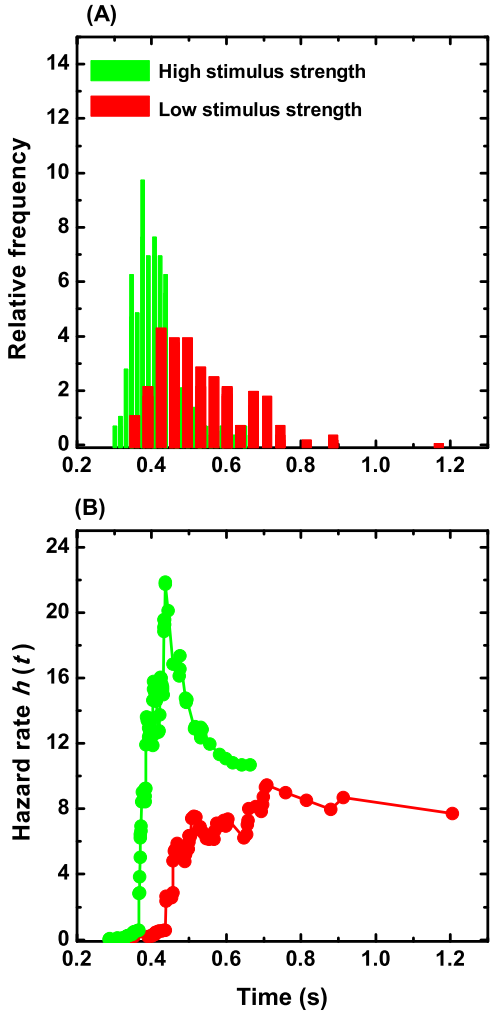

Fig. 1. (Color online.) (A) Example of reaction time histograms to visual signals at low (red bars), and high (green bars) stimulus strengths. (B) For the same experimental data, the corresponding reaction time hazard functions $h(t) = p(t)/[1 - P(t)]$ at low (red circles), and high (green circles) stimulus strengths. $p(t)$ and $P(t)$ indicate the probability density and the cumulative probability function, respectively. See text for details.

example of RT histograms [14] to visual signals of low and high stimulus strengths. Here stimulus strength is the luminance difference between the test stimulus and the background. RT raw data were reanalyzed from [37] and each histogram was based on near 100 RTs. The width of the bins was varied and the sample counts were normalized to obtain a histogram that becomes independent on the bin width [38]. In general the shape of the RT probability density function (pdf) $p(t)$ is skewed and presents extreme values at the right tails especially at low stimulus strength [14,39,40]. The standard deviation also changes with the expected mean value and it is more variable at low stimulus strength [14,41,42].

The hazard function $h(t)$, defined as the quotient between the pdf and the reciprocal of the cumulative distribution function $P(t)$, i.e., $h(t) = p(t)/[1 - P(t)]$ (in events per s), is one common way to represent the dynamics contained in the right tails of the pdfs [14,43]. In RTs the term event indicates the completion of the psychophysical task such as sensory detection and motor execution [14]. Fig. 1B illustrates, for the same experimental data in Fig. 1A, the shape of the RT hazard functions $h(t)$ at low and high stimulus strengths. The hazard functions were calculated using a common procedure in RTs, i.e., the "random smoothing method" [14,37]. The random smoothing method is a nonparametric method and it divides the original RT series in intervals in accordance with the density of observed RTs. The RTs are rank ordered and the degree of smoothing is calculated from the difference of consecutive ranks [14,37]. Under a wide range of experimental conditions, the RT hazard function $h(t)$ increases monotonically until reaches an asymptotic value at low stimulus strength and it exhibits a transition towards a high-tailed peaked form at high stimulus strength [14,37,42,44–46]. Many RT models have been proposed to explain how RT distributions are affected by stimulus strength but a unified theory remains elusive [14,39,40,42,44,47,48]. The presence of long-range correlations such as $1/f$-noise and heavy-tailed distributions may reflect the interplay of a multiplicative process, i.e., the product of random variables in cascade and the RT t may be written as: $t = a \cdot b \cdot c \cdots$ [40,42]. It was proposed that the generic transition as revealed by the RT hazard functions in Fig. 1B may be the result of multiplicative interactions driven by power law dominant and log-normal dominant pdfs at low and high stimulus strengths, respectively [42].

In previous works, I have introduced an analytical RT model based on information theory and a signal-dependent neural noise given by a Langevin equation [31,49]. In this model, the information entropy function H or the H-function defines the internal uncertainty state of a sensory neural network as a function of the time t using the methods of Boltzmann in statistical physics [27,50,51]. It was shown that the time evolution of the H-function determines Piéron's law, the origin of $t_{\min}$ [27,31,49–51], as well as optimal information processing in visual psychophysics [49]. The aim of this work is to examine Piéron's law in a different way, i.e., to infer the stochastic properties of RT distributions using the information-based RT model [27,31,49–51]. The fundamental aspect of the approach is based on the hypothesis that RT fluctuations can be mapped in the randomness generated by the constituents of Piéron's law at each stage. For fixed stimulus intensity, Piéron's law in Eq. (2) represents the predicted mean value and for each RT observation:

$$\text{RT observations} \Rightarrow \text{Piéron's law} + \text{residual fluctuations}. \tag{3}$$

The development of RT fluctuations around the mean value enables us to consider Piéron's law as a stochastic equation to describe the RT dynamics. It is proposed that Eq. (2) can be considered as a one-dimensional random-walk and can be treated as a special case of a more general class of discrete stochastic equations with multiplicative noise repelled from the origin (in our case $t_{\min}$) [52–58]:

$$z_{\tau+1} = b_\tau z_\tau + g_\tau. \tag{4}$$

$z_{\tau+1} = t$, $z_\tau = g_\tau = t_{\min}$ and $b_\tau = (S_0/S)^\alpha$ are stochastic variables, the latter represents a multiplicative noise with pdf, $\Pi(b_\tau)$. The term $g_\tau = t_{\min}$ in Eq. (4) indicates the existence of an origin or "repelling barrier" [53,54,56,58] that prevents RTs collapse to zero when the multiplicative term b_τ shrinks at suprathreshold conditions, $b_\tau = (S_0/S)^\alpha < 1$. Stochastic equations like Eq. (4) are important models for generating power laws in a variety of fields such as in statistical physics and economics, etc. [52–58]. It was demonstrated that in the asymptotic limit ($\tau \to \infty$), if $\langle \ln(b_\tau) \rangle < 0$, Eq. (4) defines a stable process that converges towards the minimum value $t_{\min}$ and leads to a power law pdf. The brackets denote $\langle \ln(b_\tau) \rangle = \int_0^\infty db_\tau \ln(b_\tau) \Pi(b_\tau)$. The predicted power law pdf can be written as follows [53,54,56,58]:

$$\forall (t > t_{\min}), \quad p(t) = C t^{-(1+\mu)}, \tag{5}$$

C is a constant [54,56,58,59]. The exponent μ in Eq. (5) satisfies the following condition [54,56,58]:

$$\langle b_\tau^\mu \rangle = 1. \tag{6}$$

However if $\langle \ln(b_\tau) \rangle > 0$ the multiplicative process diverges from the origin $t_{\min}$ and leads to a log-normal pdf [54,56,58]. In this Letter, I demonstrate that it is possible to examine the stochastic RT dynamics by Piéron's law. The Letter is organized as follows. In Section 2.1, I extend previous works on RT and information theory [27,31,49,50] providing a new analysis of Piéron's law based on geometric series. In Section 2.2, I analyze the RT pdf for $t > t_{\min}$ using Piéron's law to demonstrate that RTs obey the power law distribution in Eq. (5). The relation between the exponents μ and α is also determined. In Section 2.3, I analyze the case for $t < t_{\min}$ to show that the RT pdf is the result of a power law or a log-normal distribution. In Section 3, the implications of power law RTs are discussed in relation to human decision making, the inter-spike time interval distributions in neurons and the production of $1/f$-noise in human cognition. Conclusions are in Section 4.

2. Results

2.1. A derivation of Piéron's law

The information entropy function H as a function of the time t and the stimulus strength S can be written as follows [27,31,50,51]:

$$H(S,t) = \frac{1}{2}\ln\left(1 + \frac{\rho S^{\alpha}}{t}\right), \tag{7}$$

where ρ is a constant. The H-function in Eq. (7) is given in natural units and can be measured in bits dividing Eq. (7) by $\ln(2)$. High values of the H-function indicates high uncertainty and vice versa. The gain of information is related with the drop of uncertainty as a function of time [27,50,51]. The RT model claims that sensory neurons do not process information instantaneously but they always take time to acquire information. Accordingly, the sensory system must gather ΔH bits of information before to react [27,31,49,50]:

$$\Delta H = H(S,t_0) - H(S,t) \geqslant 0. \tag{8}$$

Initially, the H-function is close to zero at $t \cong 0$. After that, uncertainty rises and the encoding time t_0 defines an information entropy state of maximum internal uncertainty, or equivalently maximum loss of information from stimuli and minimum redundancy [27,31,49–51]. In comparison with a popular class of RT models that assume an initial accumulation of information before a decision is made [14,19,22,39], here the sensory system is in an initial state of maximum uncertainty relative to the external stimulus. Sensory perception only starts after this state of maximum uncertainty and it involves a selection from among alternatives [27,50,51,60]. The process of perception diminishes the maximum internal uncertainty as a function of time. There is a drop of uncertainty and the sensory system obtains ΔH bits of information [27,31,49–51]. This information-theoretic measure of perception is especially useful for describing many empirical laws of sensory physiology and psychophysics [27,31,49–51,61,62]. Introducing Eq. (7) in Eq. (8):

$$\begin{aligned}\Delta H &\equiv H(S,t_0) - H(S,t) \\ &= \frac{1}{2}\left[\ln\left(1 + \frac{\rho S^{\alpha}}{t_0}\right) - \ln\left(1 + \frac{\rho S^{\alpha}}{t}\right)\right].\end{aligned} \tag{9}$$

Solving Eq. (9) for the time t [27,50]:

$$t = \frac{t_0 \exp(2\Delta H)}{1 - \frac{t_0[\exp(2\Delta H)-1]}{\rho S^{\alpha}}}. \tag{10}$$

Fig. 2A simulates the RT t in Eq. (10) (in arbitrary units) as a function of the transfer of information ΔH (in bits) ($t_0 = 1$, $\rho S^{\alpha} = 5000$). The RT t increases as the number of bits ΔH increases and the RT model derived in Eqs. (9) and (10) represents a generalization of Hick's law or the ability to select between a number of choices [14,27,63].

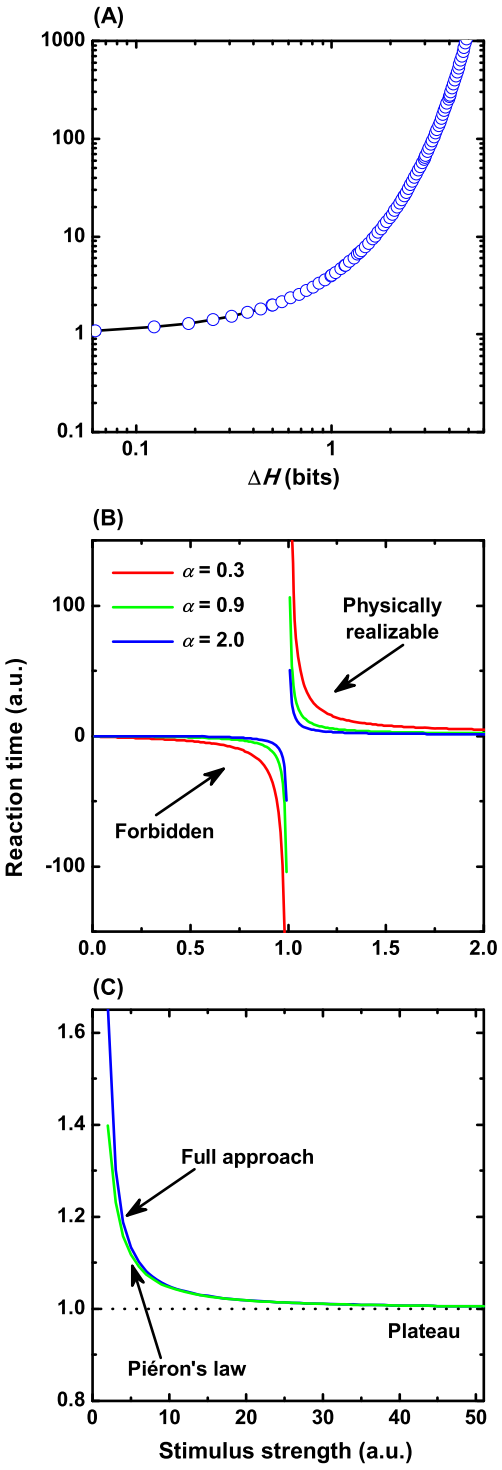

Fig. 2. (Color online.) (A) Double logarithmic plot of the reaction time as a function of the transfer of information ΔH (in bits) ($t_0 = 1$, $\rho S^{\alpha} = 5000$). (B) Linear plot of the reaction time as a function of the stimulus strength as described by Piéron's law for different values of the exponent α ($t_{\min} = 1$, $S_0 = 1$). Those RTs such as $S > S_0$ are physically realizable whereas those RTs for values $S \leqslant S_0$ are forbidden. (C) Linear plot of Piéron's law and the complete approach given in Eq. (12) for the same parameter values ($t_0 = 1$, $S_0 = 1$, $\alpha = 1.33$). The dotted line indicates the asymptotic plateau $t_{\min}$. a.u. = arbitrary units.

There are two different limits to be evaluated. Let the sensory threshold S_0 be the minimum value of S for which RTs are possible. From Eq. (10), the stimulus intensity S can be written as a function of the RT t. In the limit $t \to +\infty$ the variable S tends to the sensory threshold S_0 [27,31,49,50]:

$$\lim_{t\to+\infty}\left(\rho S^{\alpha}\right) \equiv \rho S_0^{\alpha} = t_0\left[\exp(2\Delta H) - 1\right]. \tag{11}$$

Let the asymptotic plateau $t_{\min}$ be the minimum time reached at very high stimulus intensities. In the limit $S \to +\infty$, the RT t in Eq. (10) tends to the asymptotic plateau $t_{\min}$ [27,31,49,50] and using Eq. (11):

$$\lim_{S\to+\infty}(t) \equiv t_{\min} = t_0 \exp(2\Delta H) = t_0\left(1 + \beta S_0^{\alpha}\right), \tag{12}$$

$\beta = \rho/t_0$ is a constant. Therefore, the RT t in Eq. (10) can be expressed as a function of the threshold S_0 and the asymptotic plateau $t_{\min}$ [27,50]:

$$t = \frac{t_{\min}}{1 - (\frac{S_0}{S})^{\alpha}}. \tag{13}$$

Note that the RT model generates a multiplicative process in a recurrent procedure. That is, the time t in Eq. (13) multiplies from the previous one $t_{\min}$ by a factor that depends on the internal threshold S_0. The asymptotic plateau $t_{\min}$ in Eq. (12) also multiplies by its predecessor, i.e., the encoding time t_0 by a factor that depends on the normalized threshold βS_0^{α} and so on. Fig. 2B simulates the RT t in Eq. (13) as a function of the stimulus intensity S for different values of the exponent α ($t_{\min} = 1$, $S_0 = 1$). By definition of RT [14], those RTs such as $S > S_0$ are physically realizable whereas those RTs for $S \leqslant S_0$ are not permitted. Higher values of the exponent ($\alpha > 1$) enhance the RT hyperbolic decay.

A method for extracting Piéron's law from Eq. (13) consists of an infinite geometric series with common ratio $r = (S_0/S)^{\alpha}$. Infinite geometric series are important in the growth of scale-free network models [64] and in the construction of areas and perimeters of classical fractal objects such as the Koch curve [65]. The same approach is used here to map the growth of the sensory neural network in the time domain:

$$t_{\min} + t_{\min}r + t_{\min}r^2 + t_{\min}r^3 + \cdots = \sum_{j=0}^{+\infty} t_{\min}r^j = \frac{t_{\min}}{1-r}. \tag{14}$$

Eq. (14) is a well-known stable process that equals to Eq. (13) because $|r| < 1$ [66,67]. Taking only the first two terms of Eq. (14) Piéron's law in Eq. (2) is obtained. Fig. 2C compares Piéron's law in Eq. (2) with the full approach in Eq. (13) for the same parameter values ($t_0 = 1$, $S_0 = 1$, $\alpha = 1.33$). It is concluded that Eq. (13) captures better the RT hyperbolic decay as a function of the stimulus intensity S at near-threshold conditions and Piéron's law is a very good approximation at suprathreshold conditions ($S > S_0$) [27,31,49,50].

The RT model shows that the asymptotic plateau $t_{\min}$ in Eq. (12) contains at least those latencies require for early sensory processing. In chronological order, RT begins in t_0 as the time needed for encoding the sensory information. After that, the term βS_0^{α} is associated with the formation of a sensory threshold. These results are a direct consequence of the informational principle of RT in Eq. (8) as the time required for the sensory system to gather ΔH bits after efficient encoding [27,31,49–51]. By analogy with Eq. (14), $t_{\min}$ in Eq. (12) can be also represented by an infinite geometric series but now with a common growth ratio, $r' = 1 - \exp(-2\Delta H)$:

$$t_0 + t_0 r' + t_0 r'^2 + t_0 r'^3 + \cdots = \sum_{j=0}^{+\infty} t_0 r'^j = \frac{t_0}{1-r'}. \tag{15}$$

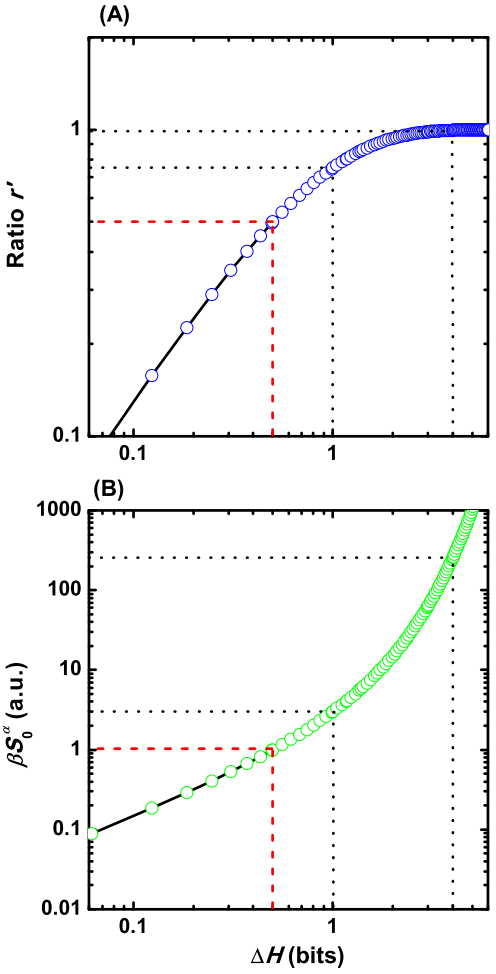

Fig. 3. (Color online.) (A) Double logarithmic plot of the common growth ratio r' of the geometric series of the asymptotic plateau $t_{\min}$ as a function of the transfer of information ΔH (in bits). Black dotted lines indicate $r' = 0.75$ and $r' = 0.99$ at $\Delta H = 1$ bit and $\Delta H = 4$ bits, respectively. The red dashed line indicates the ratio $r'_c = 0.5$ at $\Delta H_c = 0.5$ bits. (B) Double logarithmic plot of the normalized threshold βS_0^{α} as a function of the transfer of information ΔH (in bits). Black dotted lines indicate $\beta S_0^{\alpha} = 3$ and $\beta S_0^{\alpha} = 255$ at $\Delta H = 1$ bit and $\Delta H = 4$ bits, respectively. The red dashed line shows the critical value ratio $\beta S_0^{\alpha} = 1$ at $\Delta H_c = 0.5$ bits. a.u. = arbitrary units.

In comparison with the RT t in Eqs. (13)–(14), the time $t_{\min}$ in Eqs. (12) and (15) can be an unstable process. If the transfer of information ΔH increases, the ratio r' in Eq. (15) will approach to unity and the infinite geometric series will diverge. Fig. 3A represents the ratio r' as a function of the transfer of information ΔH (in bits). The ratio r' increases rapidly and saturates close to unity for high ΔH values. For instance, a transfer of information $\Delta H = 1$ bit corresponds to a ratio $r' = 0.75$ (see black dotted line in Fig. 3A). There should be a lower bound and an upper bound of ΔH. In the latter, category-judgment tasks have concluded that the maximum transmitted information may be around $\Delta H = 2.5$ bits per stimulus (i.e., $2^{2.5}$ or 6 categories), and exceptionally around $\Delta H = 4$ bits per stimulus in some cases (2^4 or 16 categories) [50,61]. $\Delta H = 2.5$ bits and $\Delta H = 4$ bits per stimulus imply a ratio of $r' = 0.96$ and $r' = 0.99$, respectively, the latter very close to unity (see black dotted line in Fig. 3A).

From Eqs. (11)–(12) if ΔH increases the magnitude of the threshold S_0 and $t_{\min}$ will increase too. Fig. 3B represents the normalized threshold βS_0^{α} as a function of ΔH (in bits). For instance, a transfer of information $\Delta H = 1$ bit implies a normalized threshold $\beta S_0^{\alpha} = 3$ in arbitrary units (see black dotted line in Fig. 3B). $\Delta H = 2.5$ bits per stimulus [50,61] implies a normalized threshold

$\beta S_0^\alpha = 31$ in arbitrary units but $\Delta H = 4$ bits per stimulus [50,61] means a normalized threshold $\beta S_0^\alpha = 255$, i.e., 85 times higher than at $\Delta H = 1$ (see black dotted line in Fig. 3B). There is an important condition at $\Delta H_c = 0.5$ bits that provides a ratio $r_c' = 0.5$ or equivalently, a normalized threshold $\beta S_0^\alpha = 1$ in arbitrary units (see red dashed lines in Fig. 3A–B). This value separates in the time domain a stable ($\Delta H < \Delta H_c$, $\beta S_0^\alpha < 1$) from an unstable growth process ($\Delta H > \Delta H_c$, $\beta S_0^\alpha > 1$). This issue will be discussed further later.

2.2. Power law probability distribution functions in reaction times

Pierón's law in Eq. (2) is mapped into the discrete stochastic process in Eq. (4) and the term $\langle \ln(b_\tau)\rangle$ is evaluated for $t > t_{\min}$. The coefficient in Eq. (4) $b_\tau = (S_0/S)^\alpha = k^{-\alpha}$, $\forall k = (S/S_0) > 1$, is a stochastic variable with pdf, $\Pi(b_\tau)$, that goes from near-threshold to very high stimulus strength, $b_\tau \in (1, 0^+)$. By conservation of probability [56,58], $\Pi(b_\tau)\,\mathrm{d}b_\tau = \Pi(k)\,\mathrm{d}k$ and using the fact that b_τ is the inverse of k [58,59]:

$$\Pi(b_\tau) = \frac{\Pi(k_0)}{\alpha} b_\tau^{-(1+\frac{1}{\alpha})}. \tag{16}$$

The constant of proportionality $\Pi(k_0) > 0$ is evaluated near the origin [58,59]. By definition of $\langle \ln(b_\tau)\rangle$ [54,56,58]:

$$\begin{aligned}\langle \ln(b_\tau)\rangle &= \int_0^\infty \mathrm{d}b_\tau \ln(b_\tau)\Pi(b_\tau) \\ &\leqslant \frac{\Pi(k_0)}{\alpha}\int_1^{0^+} b_\tau^{-(1+\frac{1}{\alpha})}\ln(b_\tau)\,\mathrm{d}b_\tau.\end{aligned} \tag{17}$$

The integral at the right-hand side of Eq. (17) can be solved as follows [67]:

$$\begin{aligned}\langle \ln(b_\tau)\rangle &\leqslant \Pi(k_0)\left[\frac{\ln(b_\tau)+\alpha}{b_\tau^{1/\alpha}}\right]_{0^+}^1 \\ &= \Pi(k_0)\left[\alpha - \lim_{b_\tau\to 0^+}\left(\frac{\ln(b_\tau)+\alpha}{b_\tau^{1/\alpha}}\right)\right].\end{aligned} \tag{18}$$

The right-hand side of Eq. (18) is undetermined and l'Hospital's rule is applied to the limit as $b_\tau \to 0^+$ resulting that $\langle \ln(b_\tau)\rangle \leqslant -\infty$ and thus, $\forall t > t_{\min}$ the RT pdf is distributed by a power law as the form indicated in Eq. (5).

It is possible to give an estimation of the exponent μ solving Eq. (6):

$$\langle b_\tau^\mu\rangle = 1 = \int_0^{+\infty} b_\tau^\mu \Pi(b_\tau)\,\mathrm{d}b_\tau \cong \frac{\Pi(k_0)}{\alpha}\int_1^0 b_\tau^{-(1+\frac{1}{\alpha})+\mu}\,\mathrm{d}b_\tau, \tag{19}$$

and the exponent μ depends on the exponent α of Piéron's law:

$$\mu = \frac{1-\Pi(k_0)}{\alpha}. \tag{20}$$

The term $\Pi(k_0)$ can be evaluated using the lowest value $b_{\tau\,\min}$ at which Eq. (16) is valid [59]:

$$\Pi(k_0) = b_{\tau\,\min}^{1/\alpha} = 1/k_{\min}, \tag{21}$$

$\forall k = (S/S_0) > 1$ and $k_{\min}$ is the lowest value where Piéron's law is valid. Therefore the exponent $1+\mu$ in the RT power law pdf in Eq. (5):

$$1 + \mu = 1 + \frac{1-(1/k_{\min})}{\alpha}. \tag{22}$$

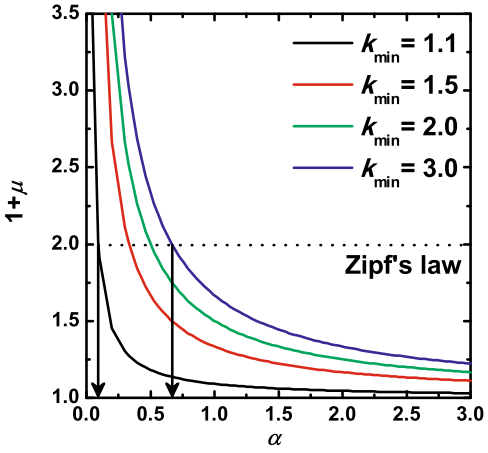

Fig. 4. (Color online.) The exponent $(1+\mu)$ of the power law reaction time distribution as a function the exponent α of Piéron's law for different values of the parameter $k_{\min}$ in Eq. (22). The black dotted line indicates the Zipf's law at $(1+\mu) = 2$. Vertical black arrows indicate $\alpha = 0.1$ and $\alpha = 0.66$ at $k_{\min} = 1.1$ and $k_{\min} = 3$, respectively.

Eq. (22) is very important because it connects the exponent $1+\mu$ from the RT pdf in Eq. (5) with the exponent α of Piéron's law in Eq. (2) and can be verified experimentally $\forall t > t_{\min}$. Fig. 4 simulates the exponent $1+\mu$ as a function of the exponent α for different values of $k_{\min}$.

The value $(1+\mu) = 2$ (dashed black line in Fig. 4) indicates that RT pdfs are distributed in accordance with Zipf's law [59,68]. From Eq. (22), $1+\mu$ decreases as α increases. If $\alpha \in (0.1, 0.66)$ then the exponent $1+\mu$ can obey Zipf's law, the moments are well-defined and the RT distributions have finite mean $(1+\mu) > 2$ and variance $(1+\mu) > 3$ [59]. Interestingly, for $\alpha > 0.66 \Rightarrow (1+\mu) < 2$ and all the RT moments diverge [59].

2.3. Log-normal probability distribution functions in reaction times

The discrete stochastic equation (4) with multiplicative noise can be also applied $\forall t_0 \leqslant t \leqslant t_{\min}$ and from Eq. (12):

$$z'_{\tau+1} = b'_\tau z'_\tau + g'_\tau. \tag{23}$$

Now $z'_{\tau+1} = t_{\min}$, $z'_\tau = g'_\tau = t_0$ and $b'_\tau = \beta S_0^\alpha$ are the new stochastic variables and the new origin or repelling barrier is given by the encoding time t_0. There are two possible cases. If $0 \leqslant \beta S_0^\alpha < 1$ ($0 \leqslant \Delta H < \Delta H_c$), the sensory neural network growths into a stable process driven by a minimum of transfer of information and $t_{\min}$ tends to be close to t_0. Solving the term $\langle \ln(b'_\tau)\rangle$ is similar to the previous section and the RT pdf is distributed in accordance to the RT power law in Eq. (5). However, if $\beta S_0^\alpha > 1$ ($\Delta H > \Delta H_c$), the sensory neural network enters in an unstable process that maximizes the transfer of information and $t_{\min}$ moves away from t_0, thus preventing the consecution of efficient responses (see also Fig. 2A). In this case, $b'_\tau \in [1, +\infty]$ and can be rewritten as: $b'_\tau = \beta S_0^\alpha \equiv x^{-\alpha}$. The pdf, $\Pi(b'_\tau) = \Pi(x_0) b_\tau'^{-(1+1/\alpha)}/\alpha$. x is a stochastic variable and $\Pi(x_0) > 0$ is a reference value evaluated at the origin. The term $\langle \ln(b'_\tau)\rangle$ can be evaluated as follows:

$$\begin{aligned}\langle \ln(b'_\tau)\rangle &= \frac{\Pi(x_0)}{\alpha}\int_1^{+\infty} b_\tau'^{-(1+1/\alpha)}\ln(b'_\tau)\,\mathrm{d}b'_\tau \\ &= -\Pi(x_0)\left[\lim_{b'_\tau\to+\infty}\left(\frac{\ln(b'_\tau)+\alpha}{b_\tau'^{1/\alpha}}\right) - \alpha\right].\end{aligned} \tag{24}$$

The right-hand side of Eq. (24) is undetermined and l'Hospital's rule is applied to the limit as $b_\tau \to +\infty$ resulting that $\langle \ln(b_\tau)\rangle =$

$(\Pi(x_0)\alpha) > 0$ and thus, RTs are distributed in accordance with a log-normal pdf $\forall t_0 \leqslant t \leqslant t_{\min}$ [53,54,56,58].

3. Discussion

The information-based RT model introduced in Eqs. (7)–(15) represents a random multiplicative process and is reminiscent of a kind of renormalization procedure. That is, Piéron's law is shape invariant under transformation of time scales and should converge to the reciprocal of the Naka–Rushton equation in the limit $t \to 0$ [31]. $\forall t > t_{\min}$, the RT model always led to the power law pdf in Eq. (5). However, $\forall t_0 \leqslant t \leqslant t_{\min}$ the existence of an efficient encoder leads to a transition from a multiplicative process that maximizes ΔH until an upper bound between 2.5 and 4 bits [50,61], similar to an *Infomax* procedure [9,69,70] with log-normal pdf, to a process that minimizes ΔH until a lower bound or *Infomin* [49], with power law pdf below the critical condition, $\Delta H_c = 0.5$ bits ($\beta S_0^{\alpha} = 1$). Initially, $\forall t_0 \leqslant t \leqslant t_{\min}$ at low stimulus strength the RT pdfs will exhibit power law dominant dynamics and ($\Delta H < \Delta H_c$, $\beta S_0^{\alpha} < 1$). However, at high stimulus strength the RT pdfs should exhibit log-normal dominant dynamics and ($\Delta H > \Delta H_c$, $\beta S_0^{\alpha} > 1$). This is in agreement with a large body of experimental RT data that have concluded a generic transition from low stimulus strength to high stimulus strength using the RT hazard functions [14,37,40,42,44–46].

The exponent α has been considered the same exponent as in the Steven's law of sensation [27,50], as well as the critical exponent of a phase transition in branching processes in sensory neural networks [71]. The special case of Zipf's law is considered a signature of criticality in biological systems [72]. It is proposed to extend these results and the exponent α of Piéron's law is also related with the transfer of information ΔH at threshold conditions. The stochastic term $b'_{\tau} = \beta S_0^{\alpha}$ enters in Eq. (23) as a multiplicative noise so that fluctuations in βS_0^{α} around the unity can develop power law behavior from log-normal pdfs, in the same way as in generic random multiplicative processes [52–58]. The presence of an efficient encoder by ΔH may be also related with the principle of complexity matching [73] and the free-energy principle in the brain [74] but this issue remains to be determined.

An important result is that the exponent α of Piéron's law governs the right tail of the RT power law pdfs in Eq. (22) and can be measured experimentally. A series of RT experiments may be implemented to span a large range of stimulus intensities such as luminance in vision [12,14,18,50], loudness in audition [14,23,50], the odorant concentration in olfaction [25], etc. Mean RTs could be fitted to Piéron's law to provide an estimation of the exponent α together with the asymptotic plateau $t_{\min}$ in Eq. (2) [14]. RT histograms can be calculated using a method that permits to vary the bin width such as in [38,59]. Those RTs in the right tail of the curve ($\forall t > t_{\min}$) may be useful to provide an estimation of the exponent μ in Eq. (5). Previous psychophysical studies have found that Piéron's law holds for choice RTs (multiple stimulus, one response) as well as for simple RTs (one stimulus, one response), with similar values of the exponent α regardless of task complexity [18]. The exponent α can be close to or lower than unity [17–19] but also close to two or even higher [20]. In accordance with Fig. 4, this suggests a transition from a region with well-defined average and spread for $\alpha \leqslant 0.66$ to a region where the RT moments cannot be defined ($\alpha > 0.66$) [59]. This issue may also explain why the RT standard deviation is not bounded but increases as the mean RT increases in certain experimental conditions [14,35,37,41,42,46]. Interestingly, the asymptotic plateau $t_{\min}$ in choice RTs was higher than in simple RTs [18]. From Eq. (12) this suggests that in decision making longer asymptotic values $t_{\min}$ may arise as a consequence of increasing the encoding time t_0, the transfer of information ΔH or both simultaneously.

The transition of the exponent α from low values compatible with Zipf's law to high values in choice RTs is similar to other multiplicative process in decision making [75] and may share a common origin with gain control mechanisms of neural responses. The results also suggest that the shape of the interspike interval (ISI) distributions (in seconds per spike) may be also analyzed by means of log-normal and power law pdfs due to the renormalization procedure of Piéron's law into the reciprocal of the Naka–Rushton function. Previous works in visual neuroscience have reported that the exponent α in the Naka–Rushton contrast response function is not fixed but it exhibits a hierarchy of values. In luminance processing, α is close to unity early at the retina [3,4,6] and then becomes larger at higher levels in the visual pathway, with values on average around two in the striate cortex [4,6–8] and higher than two at higher cortical areas [4,6–8] and, thus, in the same way as in choice RTs. The existence of a hierarchy of exponents and the presence of multiplicative interactions in RTs may be associated with multifractal phenomena [76], in the same way as in heart beat dynamics [77]. All these issues merit further investigation.

Finally, the RT multiplicative model may also provide a plausible basis of $1/f$-noise in human perception and cognition. It has been proposed that the origin of $1/f$-noise and RT fluctuations may be related in part with the fluctuating threshold, βS_0^{α} [31,37]. From Eq. (11), this is equivalently to assert that the quantity of information ΔH may fluctuate over time and the asymptotic plateau $t_{\min}$ in Eq. (11) can be interpreted as performing a geometric Brownian motion [78]. A similar stochastic model consisting of a fluctuation threshold showing a Brownian diffusion, $1/f$-noise spectra and power law ISI distributions has been proposed before [79].

4. Conclusions

Human RT distributions usually exhibit a transition from power law dominant to log-normal dominant dynamics as the stimulus strength increases. An information-based multiplicative RT model is able to describe the stochastic properties of RT distributions. The RT model predicts that the fractional values of the exponent α of Piéron's law between 0.1 and 0.66 are compatible with the existence of Zipf's law at the right tail of the RT distributions. Finally, the shape invariance of Piéron's law across time scales suggests that the ISI distributions in neurons governed by the Naka–Rushton function may be similar to RTs and may reflect multifractal behavior. These results suggest that RT variability contains important properties of stochastic latency mechanisms that mediate sensory–motor transduction and neural diseases.

Acknowledgements

I thank Dr. José A. Díaz (University of Granada, Spain) for helping me clarify the text and the discussion of the issues. This work was supported by the Fundação para a Ciência e a Tecnologia and by the Center for Physics, University of Minho, Portugal.

References

[1] L. Michaelis, M.L. Menten, Biochem. Z. 49 (1913) 333.
[2] L. Glass, M.C. Mackey, From Clocks to Chaos, Princeton University Press, New Jersey, 1988.
[3] K.I. Naka, W.A.H. Rushton, J. Physiol.-London 185 (1966) 587.
[4] D.G. Albrecht, D.B. Hamilton, J. Neurophysiol. 48 (1982) 217.
[5] V. Torre, J.F. Ashmore, T.D. Lamb, A. Menini, J. Neurosci. 15 (1995) 7757.
[6] G. Sclar, J.H.R. Maunsell, P. Lennie, Vision Res. 30 (1990) 1.
[7] D.J. Heeger, Visual Neurosci. 9 (1992) 181.
[8] D.G. Albrecht, W.S. Geisler, R.A. Frazor, A.M. Crane, J. Neurophysiol. 88 (2002) 888.
[9] A. Gottschalk, Neural Comput. 14 (2002) 527.

[10] V.A. Billock, B.H. Tsou, Psychol. Bull. 137 (2011) 1.
[11] H. Piéron, Année Psychol. 20 (1914) 17.
[12] H. Piéron, The Sensations, Yale University Press, New Haven, CT, 1952.
[13] J.M. Cattell, Brain 8 (1886) 512.
[14] R.D. Luce, Response Times, Oxford University Press, New York, 1986.
[15] Y. He, M. Rea, A. Bierman, J. Bullough, J. Illum. Eng. Soc. 26 (1997) 125.
[16] S. Plainis, I.J. Murray, Ophthalmic Physiol. Opt. 22 (2002) 409.
[17] R. Schweickert, C. Dahn, K. McGuigan, Percept. Psychophys. 44 (1988) 383.
[18] D. Pins, C. Bonnet, Percept. Psychophys. 58 (1996) 390.
[19] J. Palmer, A.C. Huk, M.N. Shadlen, J. Vision 5 (2005) 376.
[20] T. Stafford, L. Ingram, K.N. Gurney, Cogn. Sci. 35 (2011) 1553.
[21] T. Stafford, K.N. Gurney, Front. Psychology 2 (2011) 287.
[22] L. van Maanen, R.P.P.P. Grasman, B.U. Forstmann, E.-J. Wagenmakers, Front. Neurosci. 5 (2012) 143.
[23] R. Chocholle, Année Psychol. 41 (1940) 64.
[24] W.P. Banks, Percept. Psychophys. 13 (1973) 321.
[25] P. Overbosch, R. Dewijk, T.J.R. Dejonge, E.P. Koster, Physiol. Behav. 45 (1989) 615.
[26] C. Bonnet, M.C. Zamora, F. Buratti, M. Guirao, Physiol. Behav. 66 (1999) 549.
[27] K.H. Norwich, C.N.L. Seburn, E. Axelrad, Bull. Math. Biol. 51 (1989) 347.
[28] N. Chater, G.D.A. Brown, Cognition 69 (1999) B17.
[29] T. Stafford, K.N. Gurney, Psychon. Bull. Rev. 11 (2004) 975.
[30] Y.F. Hsu, J. Math. Psychol. 49 (2005) 450.
[31] J.M. Medina, Phys. Rev. E 79 (2009).
[32] D.L. Gilden, T. Thornton, M.W. Mallon, Science 267 (1995) 1837.
[33] D.L. Gilden, Psychol. Rev. 108 (2001) 33.
[34] C.T. Kello, B.C. Beltz, J.G. Holden, G.C. Van Orden, J. Exp. Psychol. Gen. 136 (2007) 551.
[35] J.M. Medina, J.A. Diaz, in: M. Macucci, G. Basso (Eds.), Noise and Fluctuations, AIP Conf. Proc., AIP, Melville, 2009, pp. 553–556.
[36] P. Grigolini, G. Aquino, M. Bologna, M. Lukovic, B.J. West, Physica A 388 (2009) 4192.
[37] J.M. Medina, J.A. Diaz, J. Opt. Soc. Am. A. Opt. Image Sci. Vis. 29 (2012) A82.
[38] L.S. Liebovitch, A.T. Todorov, M. Zochowski, D. Scheurle, L. Colgin, M.A. Wood, K.A. Ellenbogen, J.M. Herre, R.C. Bernstein, Phys. Rev. E 59 (1999) 3312.
[39] P.L. Smith, R. Ratcliff, Trends Neurosci. 27 (2004) 161.
[40] C.T. Kello, G.D.A. Brown, R. Ferrer-i-Cancho, J.G. Holden, K. Linkenkaer-Hansen, T. Rhodes, G.C. Van Orden, Trends Cogn. Sci. 14 (2010) 223.
[41] E.J. Wagenmakers, S. Brown, Psychol. Rev. 114 (2007) 830.
[42] J.G. Holden, G.C. Van Orden, M.T. Turvey, Psychol. Rev. 116 (2009) 318.
[43] R.B. Stein, Biophys. J. 7 (1967) 37.
[44] P.L. Smith, Psychol. Rev. 102 (1991) 567.
[45] J.M. Medina, J.A. Diaz, J. Opt. Soc. Am. A. Opt. Image Sci. Vis. 23 (2006) 993.
[46] J.M. Medina, J.A. Díaz, in: Applications of Optics and Photonics, Proc. SPIE, Braga, 2011, pp. 800131–800139.
[47] J.C. Baird, Sensation and Judgement, Lawrence Erlbaum Associates, Mahwah, NJ, 1997.
[48] R.H.S. Carpenter, B.A.J. Reddi, A.J. Anderson, J. Physiol.-London 587 (2009) 4051.
[49] J.M. Medina, Neural Comput. 23 (2011) 1015.
[50] K.H. Norwich, Information, Sensation, and Perception, Academic Press, San Diego, 1993.
[51] K.H. Norwich, W. Wong, Math. Biosci. 125 (1995) 83.
[52] H. Kesten, Acta Math. 131 (1973) 207.
[53] M. Levy, S. Solomon, Int. J. Mod. Phys. C – Phys. Comput. 7 (1996) 595.
[54] D. Sornette, Phys. Rev. E 57 (1998) 4811.
[55] H. Takayasu, A.H. Sato, M. Takayasu, Phys. Rev. Lett. 79 (1997) 966.
[56] D. Sornette, R. Cont, J. Phys. I 7 (1997) 431.
[57] A.H. Sato, H. Takayasu, Y. Sawada, Phys. Rev. E 61 (2000) 1081.
[58] D. Sornette, Critical Phenomena in Natural Sciences, second ed., Springer-Verlag, Berlin, Heidelberg, 2006.
[59] M.E.J. Newman, Contemp. Phys. 46 (2005) 323.
[60] K.H. Norwich, J. Theor. Biol. 102 (1983) 175.
[61] K.H. Norwich, Percept. Psychophys. 29 (1981) 409.
[62] K.H. Norwich, W. Wong, Percept. Psychophys. 59 (1997) 929.
[63] W.E. Hick, Q. J. Exp. Psychol. 4 (1952) 11.
[64] J. Li, B.H. Wang, P.Q. Jiang, T. Zhou, W.X. Wang, Acta Phys. Sin. 55 (2006) 4051.
[65] H.O. Peitgen, H. Jürgens, D. Saupe, Chaos and Fractals, Springer-Verlag, New York, 1992.
[66] G.E. Andrews, Amer. Math. Monthly 105 (1998) 36.
[67] I.S. Gradshteyn, I.M. Ryzhik, Table of Integrals, Series, and Products, seventh ed., Academic Press, San Diego, California, 2007.
[68] G.K. Zipf, Human Behavior and the Principle of Least Effort, Addison–Wesley, Cambridge, 1949.
[69] R. Linsker, Computer 21 (1988) 105.
[70] R. Linsker, Annu. Rev. Neurosci. 13 (1990) 257.
[71] O. Kinouchi, M. Copelli, Nat. Phys. 2 (2006) 348.
[72] T. Mora, W. Bialek, J. Stat. Phys. 144 (2011) 268.
[73] B.J. West, E.L. Geneston, P. Grigolini, Phys. Rep. 468 (2008) 1.
[74] K. Friston, Nat. Rev. Neurosci. 11 (2010) 127.
[75] B. Blasius, R. Tonjes, Phys. Rev. Lett. 103 (2009).
[76] H.F. Stanley, P. Meakin, Nature 335 (1988) 405.
[77] P.C. Ivanov, L.A.N. Amaral, A.L. Goldberger, S. Havlin, M.G. Rosenblum, Z.R. Struzik, H.E. Stanley, Nature 399 (1999) 461.
[78] S. Karlin, H.M. Taylor, A First Course in Stochastic Processes, second ed., Academic Press, San Francisco, California, 1975.
[79] J. Davidsen, H.G. Schuster, Phys. Rev. E 65 (2002).